Process development for heterotrophic terpene production in *Cupriavidus necator*

Dissertation

Zur

Erlangung des akademischen Grades des Doktors der Ingenieurwissenschaften (Dr.-Ing.)

Dem Promotionszentrum für Ingenieurwissenschaften

am Forschungscampus Mittelhessen

vorgelegt von

Lucas Ernst Becker

M. Sc.

Aus Weilburg

Gießen, den 18.08.2025

Begutachtung durch:

1. **Gutachter: Prof. Dr.-Ing. Dirk Holtmann**
   Institut für Bio- und Lebensmitteltechnik 2 - Elektrobiotechnologie
   Karlsruher Institut für Technologie
   Fritz-Haber-Weg 4, 76131 Karlsruhe
   E-Mail: dirk.holtmann@kit.edu

und

2. **Gutachter: Prof. Dr. Holger Zorn**
   Institut für Lebensmittelchemie und Lebensmittelbiotechnologie
   Justus-Liebig-Universität
   Heinrich-Buff-Ring 17-19, 35392 Gießen
   E-Mail: holger.zorn@uni-giessen.de

"*I did it my way.*"

— Paul Anka, from the song My Way (1969), famously performed by Frank Sinatra.

Für meine Eltern, denen ich diese Arbeit mit Dankbarkeit widme.

Acknowledgments

This has been an exciting, challenging, and rewarding research journey, and I am very grateful to all those who have supported me along the way. My sincere thanks go to the Federal Ministry of Education and Research (BMBF), grant number: 01B1050A (project ProNecator), for providing the funding that made this work possible. I would also like to express my sincere gratitude to my PhD supervisors, Dirk Holtmann and Holger Zorn, who have always believed in me, and who have guided and supported me throughout this process. A sincere thank you to Stephanie Gokorsch for the generous provision of the cell culture laboratory, which made the execution of the immunological experiments possible. Furthermore, I would like to extend my sincere thanks to Gerhilt Donnevert for providing the opportunity and instruction with the α-humulene analysis using GC-MS. Many thanks to Christiane Elseberg and the ZKT team for providing the microscopes and help, which greatly supported my immunological study. Additionally, my deepest thanks go to DECHEMA for providing the *C. necator* strains, which formed the basis of my doctoral thesis.

I am especially grateful to my first supervisor, Dirk Holtmann, for the trust and freedom he granted me throughout my research. His support whenever help was needed, as well as the constructive and successful collaboration on writing the paper, were invaluable to me. I greatly appreciate the space he provided for me to pursue my ideas, along with his valuable input and expertise.

I am deeply thankful to my parents and loved ones, who have been an essential anchor in my life, offering unwavering support and encouragement throughout this journey.

Additionally, special thanks go to my colleagues at THM for the valuable time we spent together and for creating a cooperative, enjoyable, and fun environment. Finally, my sincere thanks go to everyone who has supported me in any way and contributed to the completion of this thesis. Thank you so much!

Content

List of abbreviations

ANOVA	Analysis of variance
BALB/c	Bagg albino house mouse
BMBF	Federal Ministry of Education and Research - Germany
C/N/P ratio	Ratio between carbon, nitrogen and phosphorus
cAMP	Cyclic adenosine monophosphate
CC_{50}	Half-maximal cytotoxicity concentration
CDP-ME	4-Diphosphocytidyl-2-C-methyl-D-erythritol
CDP-MEP	4-Diphosphocytidyl-2-C-methyl-D-erythritol 2-phosphate
CDW	Cell dry weight
CGQ	Cell Growth Quantifier®
Covid-19	Coronavirus disease 2019
DES	Deep eutectic solvents
DMAPP	Dimethylallyl pyrophosphate
DNA	Deoxyribonucleic acid
DoE	Design of Experiments
DXP	1-Deoxy-D-xylulose 5-phosphate
DXS	1-Deoxy-D-xylulose 5-phosphate synthase
eGFP	Enhanced green fluorescent protein
ELISA	Enzyme-linked immunosorbent assay
ERG20	Farnesyl pyrophosphate synthase
FID	Flame ionization detector
fni	Isopentenyl pyrophosphate isomerase
FPP	Farnesyl pyrophosphate
G3P	Glyceraldehyde-3-phosphate
GC-MS	Gas chromatography - mass spectrometry
GR	Glucocorticoid receptor
groESL	*C. necator* chaperones
HC	Hydrocortisone
HeLa	Human immortalized cell line
HMBPP	4-Hydroxy-3-methyl-but-2-enyl pyrophosphate
HMC-1	Human mast cell line 1
HMG-CoA	3-Hydroxy-3-methylglutaryl-CoA
HMGR	3-Hydroxy-3-methylglutaryl-CoA reductase

HMGS	3-Hydroxy-3-methylglutaryl-CoA synthase
HPLC	High performance liquid chromatography
IC_{50}	Half-maximal inhibitory concentration
IKK	IκB kinase
IL-1β	Interleukin-1β
IL-6	Interleukin-6
IPP	Isopentenyl pyrophosphate
IPP	Isopentenylpyrophosphate isomerase
IspA	Farnesyl pyrophosphate synthase
IspG	1-Hydroxy-2-methyl-2-(E)-butenyl 4-pyrophosphate synthase
IspH	1-Hydroxy-2-methyl-2-(E)-butenyl 4-pyrophosphate reductase
ISPR	*In situ* product removal
IκB	Nuclear factor kappa B inhibitor protein
LB	Lysogeny broth
LBP	Lipopolysaccharide-binding serum protein
LogP	Octanol-water partition coefficient
LPS	Lipopolysaccharides
m/z	Mass-to-charge ratio
μ_{max}	Maximum specific growth rate
MEcPP	2-C-methyl-D-erythritol 2,4-cyclopyrophosphate
MEP	2-C-methyl-D-erythritol 4-phosphate
MMasy	Minimal medium according to Anne Sydow
mRNA	Messenger ribonucleic acid
MVA	Mevalonate
MVAD	Mevalonate-5-pyrophosphate decarboxylase
MVAK	Mevalonate kinase
MVAK2	Mevalonate-5-phosphate kinase
MVP	Mevalonate-5-phosphate
MVPP	Mevalonate-5-pyrophosphate
MWD	Multiple wavelength detector
NF-κB	Nuclear factor kappa light chain enhancer of activated B-cells
NSAID	Non-steroidal anti-inflammatory drugs
OD_{600}	Optical density at 600 nm
OFAT	One-factor-at-a-time
PBS	Phosphate buffered saline buffer

PHB	Polyhydroxybutyrate
PI3K	Phosphoinositide 3-kinase
PKA	Protein kinase A
P_{Lac}	Promoter of the lactose operon
PMA	Phorbol 12-myristate 13-acetate
R(c)	Robustness (condition)
RAW	Murine macrophage cell line
rhaBAD	L-rhamnose operon
RhaR	L-rhamnose transcription activator protein
rpm	Rounds per minute
RPMI-1640	Roswell Park Memorial Institute medium
SIM	Single ion monitoring
SOB	Super optimal broth
TBAB	Tetrabutylammonium bromide
TC	Tetracycline
3D	Three-dimensional
THP-1	Human leukemia monocytic cell line
TNF-α	Tumor necrosis factor alpha
UPOs	Unit processing operations
USD	US-Dollar
Vero	Mammalian continuous cell line
VOCs	Volatile organic compounds
$Y_{P/S}$	Yield coefficient, product yield per substrate
$Y_{P/X}$	Yield coefficient, product yield per biomass
$Y_{X/S}$	Yield coefficient, biomass yield per substrate
ZSSI	α-Humulene synthase

List of tables

List of figures

Deutsche Zusammenfassung

Die weltweite Nachfrage nach dem Sesquiterpen α-Humulen wächst kontinuierlich, da es in zahlreichen Bereichen Anwendung findet, darunter in der Lebensmittel-, Duftstoff-, Kosmetik- und Pharmaindustrie. Die Prozessbedingungen der mikrobiellen α-Humulen Produktion mittels *Cupriavidus necator* bieten dabei noch Optimierungspotential, um die enormen Vorteile der biotechnologischen Produktion gegenüber traditionellen Gewinnungsmethoden voll auszuschöpfen. Das Hauptziel dieser Arbeit war daher die Optimierung der heterotrophen α-Humulen Produktion mit *C. necator*, wobei der Fokus auf einer eingehenden Untersuchung und Optimierung verschiedener Prozessparameter lag. In ersten Untersuchungen konnte mittels statistischer Versuchsplanung gezeigt werden, dass im Temperaturbereich von 25 °C bis 28 °C eine erhöhte plasmidbasierte α-Humulen Produktion sowie verbesserte Ausbeutekoeffizienten für Produkt/Substrat und Produkt/Biomasse im Vergleich zur etablierten Standardtemperatur von 30 °C erreicht wurden. Die nachfolgende Optimierung einzelner Prozessparameter führte zu einer gesteigerten Biomassebildung und α-Humulen Produktion. Angepasst wurden dabei die Fruktosekonzentration von 4 g/L auf 8 g/L, die Eisen (II)-sulfat Heptahydrat Konzentration von 0,75 mg/L auf 3,75 mg/L sowie die L-Rhamnose-Induktor Konzentration von 0,2 % auf 2 % (w/v). Zusätzlich wurde die Kultivierungstemperatur in zwei Phasen von 30 °C und 25 °C unterteilt (zuvor konstant 30 °C). Die Kombination der optimierten Einzelparameter führte zu einer 241 %-igen Steigerung des α-Humulen Levels im Vergleich zum nicht optimierten Standardprozess.

Eine anschließende Untersuchung der Robustheit dieser Optimierungspunkte deutete auf einen sehr stabilen Produktionsprozess mit *C. necator* pKR-hum hin. Für die α-Humulen Produktion unter variierenden Prozessparametern wurde ein Wert von -0,155 ± 0,143 festgestellt, während die Biomassebildung mit -0,002 ± 0,002 sogar eine höhere Robutsheit aufwies und nahe dem idealen Robustheitswert von 0 lag. Selbst während einer simulierten Prozessstörung produzierte der Prozess noch 79 % des maximalen α-Humulen Levels im Vergleich zum ungestörten Prozesslauf, mit einem Robustheitswert von -0,045 ± 0,001, was den robusten Charakter des Prozesses unterstrich. Zudem wurde erstmalig ein dosisabhängiger anti-inflammatorischer Effekt von α-Humulen auf Lipopolysaccharid-induzierte humane THP-1 Zellen festgestellt, mit einer maximalen Hemmung der Interleukin-6 Konzentration von 60 % nach Gabe von 100 µM α-Humulen. Diese Ergebnisse tragen erheblich zur Prozessoptimierung der mikrobiellen Terpenproduktion bei. Zudem konnten erste Erkenntnisse gewonnen werden, die α-Humulen als alternativen, naturbasierten und vielversprechenden therapeutischen Ansatz zur Reduktion erhöhter Interleukin-6 Level und chronischer Entzündungen bekräftigen.

Abstract

The global demand for the sesquiterpene α-humulene is steadily increasing due to its wide range of applications in the food, fragrance, cosmetics, and pharmaceutical industries. The process parameters for microbial α-humulene production using *Cupriavidus necator* still offer optimization potential to fully exploit the significant advantages of biotechnological production over traditional production methods. The primary objective of this work was, therefore, the optimization of heterotrophic α-humulene production using *C. necator*, with a focus on in-depth investigation and optimization of various process parameters.

In initial studies, the used statistical experimental design demonstrated that a temperature range of 25 °C to 28 °C resulted in increased plasmid-based α-humulene production, along with improved product/substrate and product/biomass yield coefficients compared to the established standard temperature of 30 °C. Subsequent optimization of individual process parameters led to enhanced biomass formation and α-humulene production. The fructose concentration was increased from 4 g/L to 8 g/L, the iron (II) sulfate heptahydrate concentration from 0.75 mg/L to 3.75 mg/L, and the L-rhamnose inducer concentration from 0.2 % to 2 % (w/v). In addition, the cultivation temperature was divided into two stages at 30 °C and 25 °C, whereas previously it was constant at 30 °C. The combination of these optimized parameters resulted in a 241 % increase in α-humulene production compared to the non-optimized standard process.

A robustness assessment of these optimized parameters indicated a highly stable production process using *C. necator* pKR-hum. For α-humulene production under varying process conditions, a robustness value of -0.155 ± 0.143 was observed, while biomass formation demonstrated even greater robustness with a value of -0.002 ± 0.002, approaching the ideal robustness value of 0. Even under the influence of simulated process disturbances, the process maintained 79 % of the maximum α-humulene level compared to the undisturbed process run, with a robustness value of -0.045 ± 0.001, highlighting the robust properties of the process. Furthermore, for the first time, a dose-dependent anti-inflammatory effect of α-humulene on lipopolysaccharide-induced human THP-1 cells was observed, with a maximum reduction in interleukin-6 levels of 60 % following the administration of 100 µM α-humulene. These findings are expected to significantly contribute to the optimization of microbial-based terpenoid production processes. Additionally, initial insights were obtained that confirm α-humulene's potential as an alternative, nature-based, and promising therapeutic approach for the reduction of elevated interleukin-6 levels and chronic inflammation.

1. General introduction

1.1. Relevance of microbial fermentation

Industrial biotechnology has been developing steadily over the last few decades and represents an important field of research that involves the development of sustainable production methods for valuable chemicals and natural substances [1, 2]. This also includes microbial fermentation processes, which can efficiently produce industrially valuable products in large quantities through the targeted use of microbial cell metabolism. Depending on the desired products and process parameters, different production hosts are used, which can range from animal cell lines to bacteria and archaea. However, the vast majority of industrial processes for the production of valuable products are presently based on bacteria (prokaryotes) and eukaryotic cells such as fungi, yeasts, and algae [1]. The global biotechnology market is substantial, with a valuation of USD 1,070 billion in 2024 and a projected growth to USD 4,143 billion by 2032 [2]. In 2023, the fermentation industry constituted the largest sector within the biotechnology market [2].

Products obtained from microbial fermentation are highly diverse, ranging, for example, from valuable chemicals and alternative biofuels such as isobutanol or 3-methyl-1-butanol [3], to essential pharmaceuticals like insulin [4], and valuable natural substances such as the terpene α-humulene [5]. Microbial fermentation processes are particularly efficient and sustainable, as they convert renewable substrates into valuable compounds. In contrast to conventional chemical syntheses, biocatalysis is enzymatic and therefore often highly product-specific, which reduces by-products, process time, energy costs, and the use of resources [6]. Different types of energy and substrate sources can be used for microbial fermentations and therefore the cultivation method may vary depending on the product and microorganism used. In heterotrophic fermentations, organic carbon sources such as fructose or glucose are added to the culture medium for metabolization [7]. Autotrophic fermentations involve the utilization of inorganic carbon sources like CO_2, often in the absence of organic substrates, to generate the products [8]. Additionally, phototrophic fermentations utilize light energy and are primarily employed for the cultivation of some mircroalgae or cyanobacteria in order to convert CO_2 into biomass and products via photosynthesis [9]. In industrial applications, however, the fermentation types are not fixed and can also be combined depending on system limitations, the specific microorganism used, as well as product and process parameters [9].

To summarize, several advantages of heterotrophic fermentation can be highlighted: In addition to being independent of light energy, which enables continuous production and makes scale-up more feasible compared to phototrophic fermentation [10], it also allows for

the use of a wide variety of organic substrates. This contributes to a more efficient and sustainable production process overall. For example, waste materials such as food waste [11], cooking oil waste [12], or green waste like grass clippings [13] can be sustainably processed and metabolized as carbon sources by versatile microorganisms like *Cupriavidus necator*. Compared to autotrophic fermentation systems, which are also considered sustainable due to CO_2 fixation, heterotrophic systems generally feature simpler reactor designs, and microorganisms like *C. necator* tend to result in higher growth rates [14]. For these reasons, the research focus of this thesis was on optimizing the heterotrophic *C. necator*-based production process of the terpene α-humulene.

1.1.1. α-Humulene - a valuable natural terpene

Terpenes form a broad and heterogeneous natural substance class. With over 80,000 described structures [15], the terpenome, consisting of the terpenes and their subgroups, forms the largest natural product class. Due to their structural diversity, they are involved in a variety of essential functions and metabolic processes. As a result, they are found in a large number of plant and fungal species as well as in some bacteria, insects, and mammals. Moreover, the active functions of terpenes in the organisms are various and range from defensive plant responses against pathogens, such as the release of secondary metabolites like the sesquiterpene (E)-β-caryophyllene in tomato plants against herbivorous insects [16] to the release of anti-microbial terpenes among predatory microorganisms. Furthermore, they are also used for communication and interaction purposes, e.g. limonene as an alarm pheromone in some ant species [17, 18].

The chemical structure of terpenes and their subgroups consists of hydrocarbons, whereby their backbone is always made up of individual isoprene units (C_5 structure), and they are classified into hemiterpenes (C_5), monoterpenes (C_{10}), sesquiterpenes (C_{15}), diterpenes (C_{20}), and even larger structures according to their size [19]. However, it is not free isoprene that is crucial for the terpene synthesis process, but rather the availability of isopentenyl pyrophosphate (IPP) and dimethylallyl pyrophosphate (DMAPP) as activated C_5 building blocks and their subsequent conversion into higher terpenes like α-humulene, see Fig. 1 - A below [19]. In plants, for example, DMAPP can also be enzymatically converted to free isoprene by isoprene synthase [20]. The precursor molecules IPP and DMAPP can be supplied via two different pathways: On the one hand via the methylerythritol phosphate (MEP) pathway, which is mainly found in plants and most prokaryotes, and on the other hand via the mevalonate (MVA) pathway in eukaryotes and some gram-positive prokaryotes and archaea [21]. The structural and functional diversity of terpenes and their subgroups through

functional groups leads to a vast spectrum of interesting properties, not only in nature but also for industrial applications.

One natural terpene that has been used in a variety of industrial processes to date and is also promising for future applications is the sesquiterpene α-humulene (Fig. 1 - B). α-Humulene is naturally found in various plants, including cannabis (*Cannabis sativa*), sage (*Salvia officinalis*), and its namesake, hops (*Humulus lupulus*) [22]. However, its presence is not limited to terrestrial plants; α-humulene has also been identified in marine organisms, such as eukaryotic brown algae (*Padina tetrastromatica*) [23].

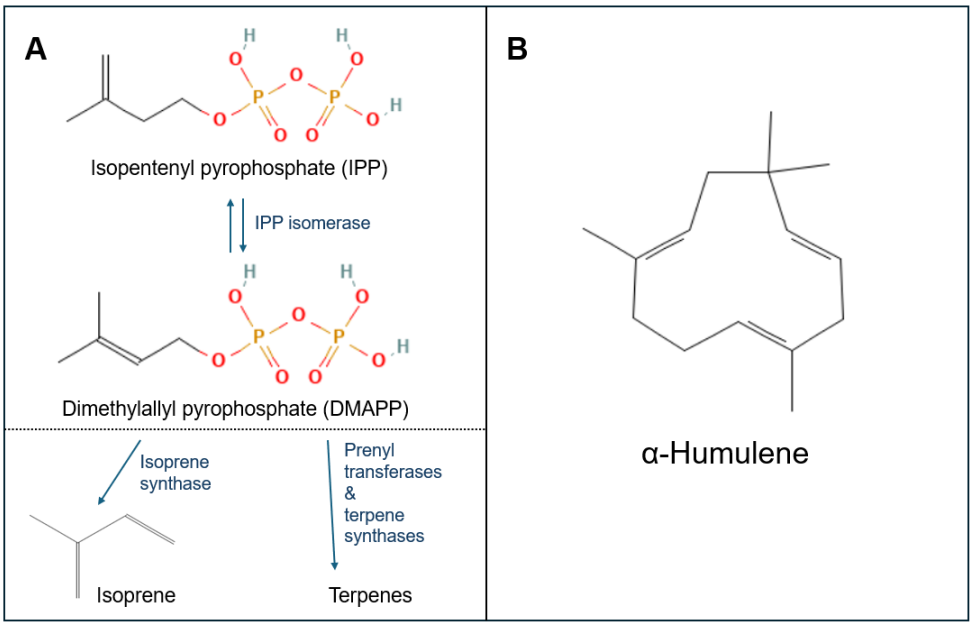

Fig. 1: (A) Isoprene synthesis based on the precursor molecules isopentenyl pyrophosphate (IPP) and dimethylallyl pyrophosphate (DMAPP), with their pyrophosphate groups highlighted in color [24-26]. (B) Chemical structure of the sesquiterpene α-humulene [27]. Own illustration.

The ring-shaped complex sesquiterpene α-humulene, a secondary plant metabolite, has a wide variety of characteristics. Due to its aromatic, anti-microbial [28], anti-biofilm [28], and anti-fungal properties [29], α-humulene protects plants as part of a range of volatile organic compounds (VOCs) from herbivores or pathogenic microbes through stress-induced terpene release on parts like the flowers and leaves [30]. Due to their volative profile, terpenoids are also used to communicate with the plant's environment or to attract pollinators [31]. In addition, α-humulene is involved in stress responses, such as enhancing the resistance of wild tomatoes towards pest infestations like the beet armyworm by modulating biochemical pathways associated with physiological plant status and defense mechanisms [32].

α-Humulene's natural properties are also exploited in the food and beverage industry as a flavoring and aroma agent, as its occurrence in hops, for example, contributes to the taste of beer due to its spicy and bitter taste [33]. Moreover, the aromatic notes of terpenes are used as fragrances in the cosmetics and perfume industry [34], or to provide soothing relief for the skin when applied in anti-inflammatory phytomedical creams like Acheflan® [35]. Essential oil preparations derived from the leaves of medicinal plants, such as *Croton flavens* L., which contain α-humulene, have also been used for a long time as traditional pain-relieving medicines [36]. Furthermore, α-humulene exhibits proven anti-microbial [28], anti-cancer [37, 38], and anti-inflammatory [39, 40] properties, which are being further researched to create innovative pharmaceuticals. Additionally, α-humulene is also used, for example, as an environmentally friendly pesticide or as a component in biological cleaning agents [41]. These versatile properties and areas of application of the sesquiterpene α-humulene, along with its production, make it a subject of considerable interest.

1.1.2. Challenges in α-humulene production

The traditional production of α-humulene is carried out by extraction from plant parts or chemical synthesis, which, however, have considerable drawbacks in terms of efficiency and sustainability. Conventional plant extraction from hops, e.g. using steam distillation, is very time-consuming and only results in small quantities of α-humulene product [42]. However, the industrially produced α-humulene comes mainly from plant extraction, whereby the yield is low, e.g. 6.2 g of α-humulene derived per kg of dried flowers of *Syzygium aromaticum* [43, 44]. Plants must first be grown in a long and energy-intensive process and then chopped and processed further for extraction. In addition, the extract obtained contains a large number of secondary plant metabolites, which requires complex downstream processing in order to obtain the pure target terpene [45]. Due to genetics, heterogeneity of growth, and plant parameters caused by environmental influences, the overall terpene composition and production volume also varies from batch to batch, which complicates industrial processes and leads to variations in performance [46]. In addition, the long growing periods of the plants and the risks of pests and crop failures lead to a very fluctuation-sensitive, unstable, and expensive plant extraction process [47, 48].

In contrast to the plant route, chemical synthesis offers a controllable process with the possibility of producing predetermined amounts of α-humulene, but there are also some drawbacks to consider, such as the use of harmful catalysts and a multi-step cyclization process [49]. The complex chemical synthesis routes require the provision of high temperatures and pressures for their reaction conditions, which is why these processes are

also energy intensive. In addition, expensive, environmentally harmful and fossil-based starting materials are often required [50, 51]. Besides the fossil-based raw materials, unsustainable or toxic waste materials are also formed [50, 51]. Furthermore, productivity is limited due to racemic formation [52], which is why broad industrial application is not attractive when these disadvantages are taken into account [53].

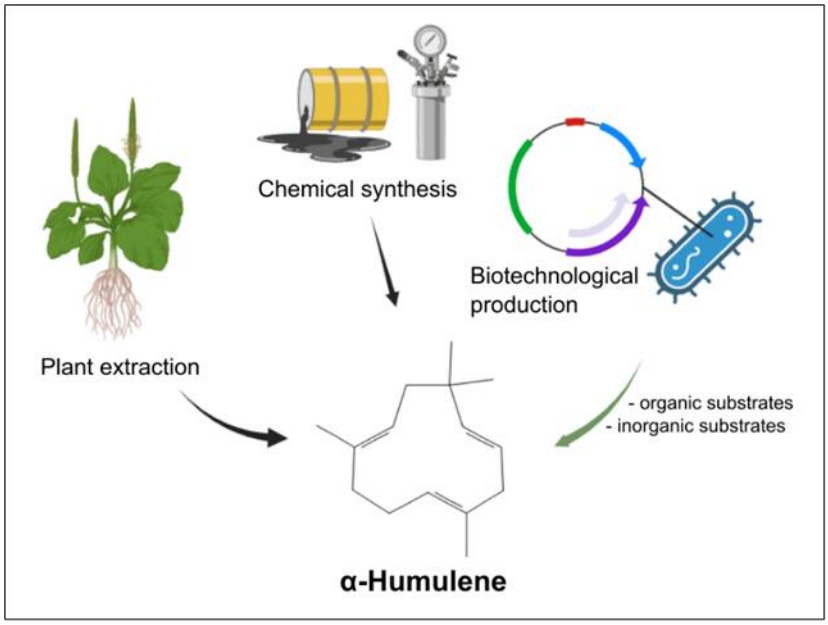

Fig. 2: Possible α-humulene production methods. Created with biorender.com, chemical structure [27].

Compared to the two conventional processes described above, biotechnological production represents a third, sustainable alternative for producing α-humulene using organic or inorganic substrates, as illustrated in the overview of production methods in Fig. 2. For example, production using the bacterial host *C. necator* offers sustainable substrates and mild production conditions, as well as process scalability and efficiency [5]. A controlled biotechnological process environment enables consistent production, and the continuous optimization of fermentation processes has allowed α-humulene yields to be increased further and further, which traditional methods such as plant extraction or chemical synthesis cannot compete with. Nevertheless, the biotechnological production of α-humulene still requires optimization and faces a number of challenges [5]. Complex products like α-humulene often result in low yields during the initial development stages, requiring further research and optimization through metabolic engineering of biosynthetic pathways, genome editing, or general fermentation process optimization [5, 44].

1.2. *C. necator* as a versatile α-humulene production platform

C. necator, formerly *Ralstonia eutropha*, is a gram-negative bacterium of the Burkholderiaceae family, which are classified as β-proteobacteria [54]. *C. necator*, first described by Makkar and Casida as a non-obligate predator of soil bacteria, is a short, rod-shaped bacterium with peritrichous flagella, commonly found in soil and freshwater environments, and was originally isolated from soil near University Park, Pennsylvania, USA [55]. This species-specific epithet (L. n. *necator*) translates to something like “killer”, which is based on the ability of *C. necator* to lyse and utilize other bacteria and fungi, e.g., when there is a deficiency of nutrients in the soil [55, 56]. *C. necator* is a facultative aerobic organism, whereby aerobic conditions and the utilization of oxygen provide the most efficient energy supply. Fermentation or the use of nitrate/nitrite as an alternative electron acceptor represents the less efficient anaerobic energy supply [57]. The metabolism of *C. necator* is facultative chemolithoautrotrophic, which means that it can metabolize organic substrates as well as inorganic substrates as a carbon and energy source. In addition to the heterotrophic utilization of different organic carbon sources, this oxyhydrogen-bacterium can also assimilate inorganic carbon sources like CO_2 by the Calvin-Benson-Bassham cycle and oxidize molecular hydrogen or formic acid as an electron source. [58, 59]

The different cultivation strategies and the use of various carbon sources turn *C. necator* into a versatile and promising biotechnological production strain. The assimilation of CO_2 represents a highly sustainable and environmentally friendly substrate utilization process; moreover, organic substrates such as organic acids [60], fructose [60], or amino acids [61], but also waste materials such as used cooking oil [62], waste glycerol [63], or sugary brewery wastewater [64] can be efficiently utilized heterotrophically by *C. necator*. A central process feature is its native ability to produce and store the biopolymer polyhydroxybutyrate (PHB) under nutrient limitation. This can account for up to 79 % of the *C. necator* cell dry weight heterotrophically [65] or up to 82 % under autrotrophic conditions [66]. Industrial production of these biological polymers offers a sustainable alternative to conventional fossil plastics, for example as bioplastics.

Besides PHB production, a large number of other valuable substance classes such as alcohols (isopropanol [67]), alka(e)nes (e.g., pentadecane [68]), but also terpenes, such as sesquiterpenes β-farnesene [69] and α-humulene [5, 70], are produced by *C. necator* after metabolic engineering. Since native PHB production can consume a large proportion of the available carbon, PHB-deficient strains such as *C. necator* H16 PHB-4 are used to efficiently produce these valuable products. *C. necator* H16 PHB-4 reroutes carbon flux via pyruvate and acetyl-CoA due to the absence of PHB formation, thereby increasing MEP and MVA

pathway-driven production of the terpene precursors IPP and DMAPP [71]. Under additional nutrient limitations such as nitrogen starvation, the natural strain increases PHB formation, while in the PHB-deficient strain, the carbon flux is provided in excess for alternative metabolic routes, including terpene production [5]. To further improve *C. necator*-based α-humulene production, the native MEP pathway has been extended with the heterologous MVA pathway to increase the availability of DMAPP and IPP in the PHB-deficient strain using a plasmid-based approach [5]. This dual pathway system allows for enhanced terpene production by increasing the overall flux towards IPP and DMAPP. Fig. 3 below illustrates both the native MEP and the engineered MVA pathways involved in terpene biosynthesis in *C. necator*.

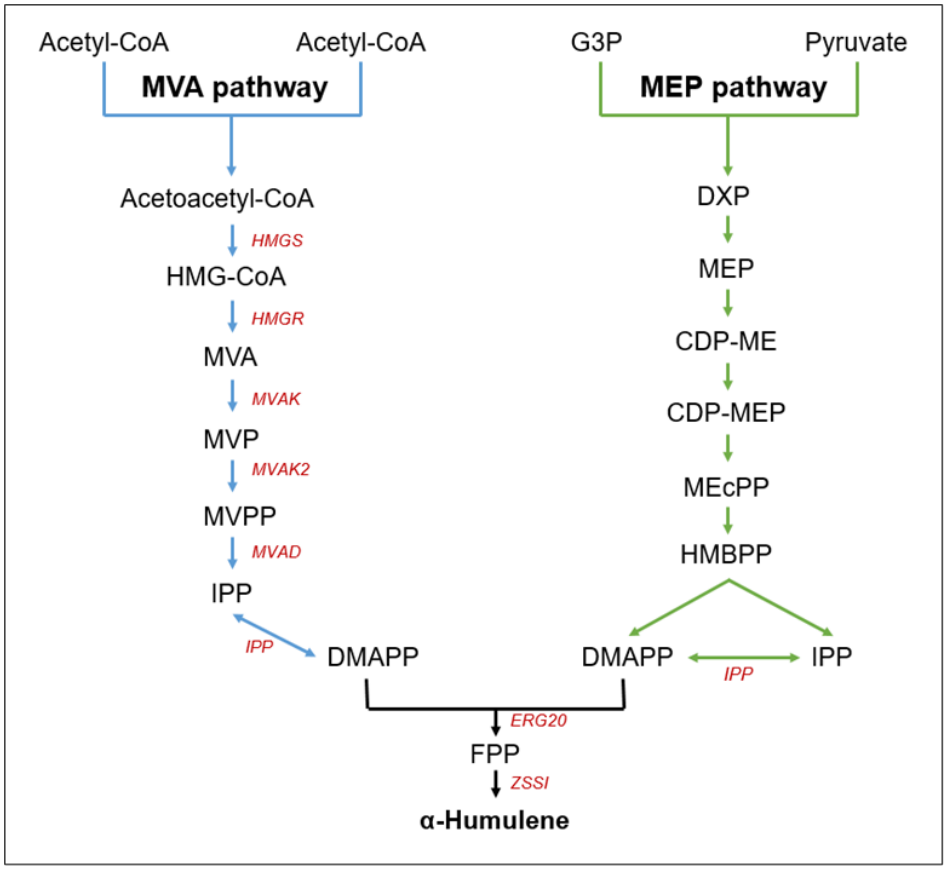

Fig. 3: Simplified schematic representation of the native methylerythritol phosphate (MEP) pathway, in green, and the heterologous mevalonate (MVA) pathway, in blue, in *C. necator* for the biosynthesis of terpenoids such as α-humulene. The MEP pathway is naturally present in *C. necator*, while the MVA pathway was introduced to increase precursor availability and enhance terpene production. Genes encoding the red-marked enzymes have been transformed into *C. necator* as plasmid pKR-hum for optimized α-humulene production, as described by Krieg et al. in [5]. Abbreviations of pathway intermediates and enzymes are provided in the list of abbreviations section. Own illustration, concept inspired by Gomes et al. [72].

For this purpose, the genes for the recombinant MVA pathway derived from *M. xanthus* [73], the farnesyl pyrophosphate synthase *erg20* (derived from *S. cerevisiae*) and the α-humulene synthase *zssI* (derived from *Z. zerumbet*) have been amplified and cloned into a previously designed and stabilized L-rhamnose inducible plasmid [74] to form the α-humulene production plasmid pKR-hum [5]. This co-expression of the MEP and MVA pathway has been shown to increase α-humulene levels in *M. extorquens* [73].

Tab. 1: Microbial α-humulene production – state of the art.

Organism	Substrate (heterotrophic)	Specifications	α-Humulene titer [g/L]	Year / reference
M. extorquens	Methanol	Fed-batch, 2.4 L bioreactor & batch, plasmid-based production	1.650	2015 / Sonntag et al. [73]
C. necator	Fructose	Fed-batch, 1.8 L DASGIP® parallel fermentation system, plasmid-based production using pKR-hum	2.000	2021 / Milker et al. [70]
Y. lipolytica	Glucose	Fed-batch, 5 L parallel bioreactor, peroxisome and genome engineered strain GQ2012	3.200	2021 / Guo et al. [75]
C. tropicalis	Glucose	Fed-batch, 30 L bioreactor & batch, peroxisome and genome engineered strain DC-H21D	4.115	2022 / Zhang et al. [44]
Y. lipolytica	Glucose	Fed-batch, 5 L parallel bioreactor, peroxisome and genome engineered strain GQ3008	21.700	2022 / Guo et al. [76]

The microbial production of α-humulene has been continuously optimized in recent years by scale-up and fed-batch processes, see Tab. 1, whereby up to 2 g/L α-humulene could be produced using a plasmid-based approach in *C. necator* [70]. By exploiting yeasts such as *C. tropicalis* or *Y. lipolytica* through peroxisomal and genomic engineering approaches in larger bioreactors, even higher titers of up to 4.1 [44] or 21.7 g/L α-humulene [76] could be produced. For the case of *C. necator*-based production in septa and shake flasks, these

α-humulene titers are reduced and range from 10 mg/L [13] to 11 mg/L [8] and up to 32 mg/L [77], depending on the media composition, cultivation methods, flask types, and parameters.

1.3. Heterotrophic fermentation and process conditions

Efficient heterotrophic cultivation of *C. necator*, combined with increased α-humulene titers, depends particularly on the optimization of key process parameters to ensure both rapid *C. necator* growth and high production rates. Since *C. necator* is highly versatile due to its ability to utilize various carbon sources, including CO_2 assimilation, and exhibits a high autotrophic redox activity, selecting a suitable fermentation form and appropriate carbon source together with its optimal concentration is crucial [78].

Non-preferred substrates, and concentrations that are excessive or insufficient, can inhibit cell growth and productivity. Additionally, the nutrient composition of the medium, the associated carbon-nitrogen-phosphate (C/N/P) ratio, the cultivation temperature, the shaking speed, and the pH value also play an important role in *C. necator* production [79, 80]. Another factor to be considered is the type of the medium, as a complex medium contains a rich and undefined mixture of nutrients and is often suitable for the growth of a variety of microorganisms and initial experiments. A defined medium, in contrast, has a precisely known nutrient composition adjusted to the organism. A minimal medium is a subtype of a defined medium that contains only the essential nutrients required for growth. Therefore, a minimal medium is ideally suited for tightly controlled and more specific studies, such as enabling rapid production processes in bioelectrochemical *C. necator* systems [81].

Besides the selection of the fermentation types, fermentation parameters and media nutrient compositions, there are other factors to consider, such as the method of product recovery in terpene-producing processes. In addition to the intracellular accumulation of products, which requires cell disruption at the end of the process, terpenes can also be released extracellularly into the culture medium. The secretion and accumulation of terpenes during microbial production processes, like the *C. necator*-based extracellular release of α-humulene, can inhibit cell proliferation and productivity as a result of toxic terpene properties such as hydrophobicity and the potential to increase cell membrane permeability [82, 83]. To counteract these undesirable toxic effects and ensure a continuous process, *in situ* product removal (ISPR) methods such as liquid-liquid solvent extraction or adsorption are often used to efficiently separate terpenes from the fermentation broth [84]. By means of ISPR methods, extracellularly released volatile or toxic products can be bound during fermentation and removed directly from the liquid medium phase, as illustrated schematically in Fig. 4 below.

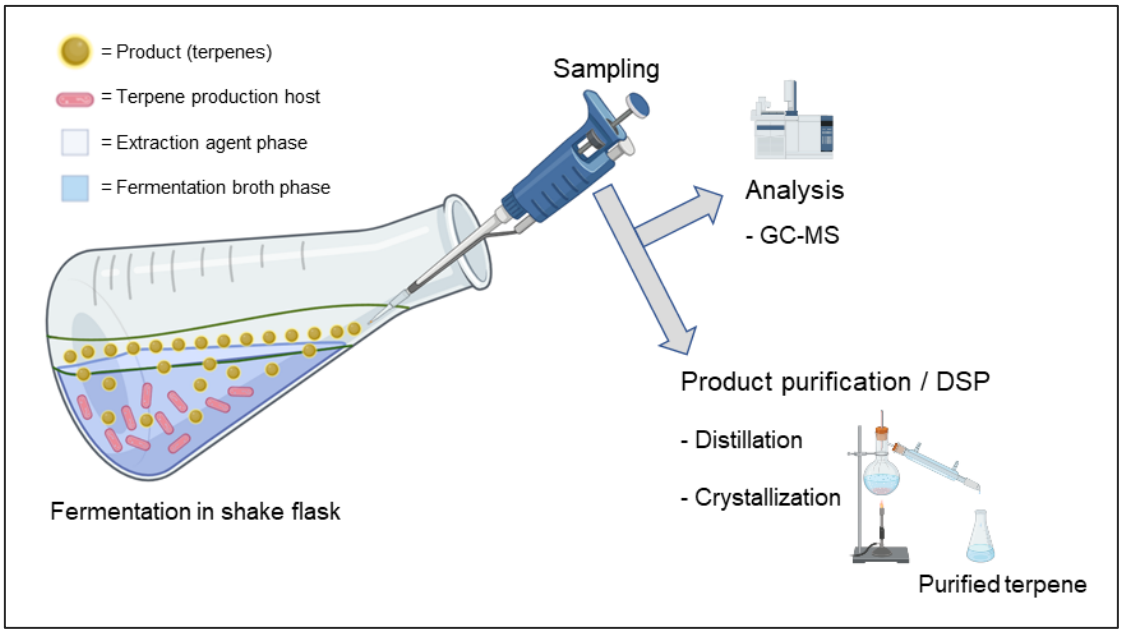

Fig. 4: Schematic representation of *in situ* product removal (ISPR) in shake flasks, as performed in this work, followed by additional downstream processing (DSP) steps for terpene products. This illustrates a potential terpene recovery process. Related to this work: α-humulene (brown particles) released extracellularly by *C. necator* (red bacteria) is captured and enriched *in situ* by the lipophilic extraction agent (upper phase) in a two-phase system consisting of fermentation broth and extraction agent. Created with biorender.com.

The removal step helps to increase process yield and efficiency, counteract toxic product accumulation in the liquid medium phase and is the first step towards product purification and simplified downstream processing [85]. However, an important requirement is the separation of the extraction phase from the media phase in which the cultivation takes place. This separation from the aqueous media phase can be easily ensured by using lipophilic extraction agents, such as higher alkanes like n-dodecane [5]. In addition to the separation from the media phase, the extraction agent should also be biocompatible in order to avoid inhibiting cell growth or product formation. In this context, biocompatibility can be estimated using the logP value, which is a measure of the hydrophobicity of a substance and in the case of *C. necator*-based ISPR should be above the critical logP value range of 3.0 - 4.2 [8].

Another aspect to consider is the extractability of the product by the extraction agent. In the case of *C. necator*-based α-humulene production and release, the lipophilic and volatile sesquiterpene α-humulene binds with the lipophilic n-dodecane phase, which is why the extraction process and overall ISPR proceed efficiently. Additional advantages of ISPR are the maintenance of optimal fermentation conditions as well as the reduction of waste materials and a reduced product purification effort. α-Humulene, for example, can be easily

separated from n-dodecane by distillation or crystallization at the end of the process using different boiling and melting temperatures [70, 86].

Therefore, in addition to adjusting the media compositions and fermentation parameters, the choice of product recovery must also be considered to optimize a production process as efficiently as possible.

1.4. Process optimization of *C. necator*-based α-humulene production

Advances in metabolic engineering and biotechnology in recent years have paved the way for the microbial-based production of terpenes as a sustainable alternative route to chemical synthesis or plant extraction processes. Beyond its previously discussed metabolic flexibility, *C. necator* also exhibits high robustness under industrial conditions and is suitable for genetic engineering, making it a valuable microbial host for biotechnological applications. But despite its flexibility and the associated potential of *C. necator*, achieving industrially acceptable yields of α-humulene using microbial production systems remains a key challenge. To address this, Fig. 5 illustrates the engineered production host used in this work: a PHB-deficient *C. necator* strain harboring the plasmid system pKR-hum, which enables the extracellular release of α-humulene.

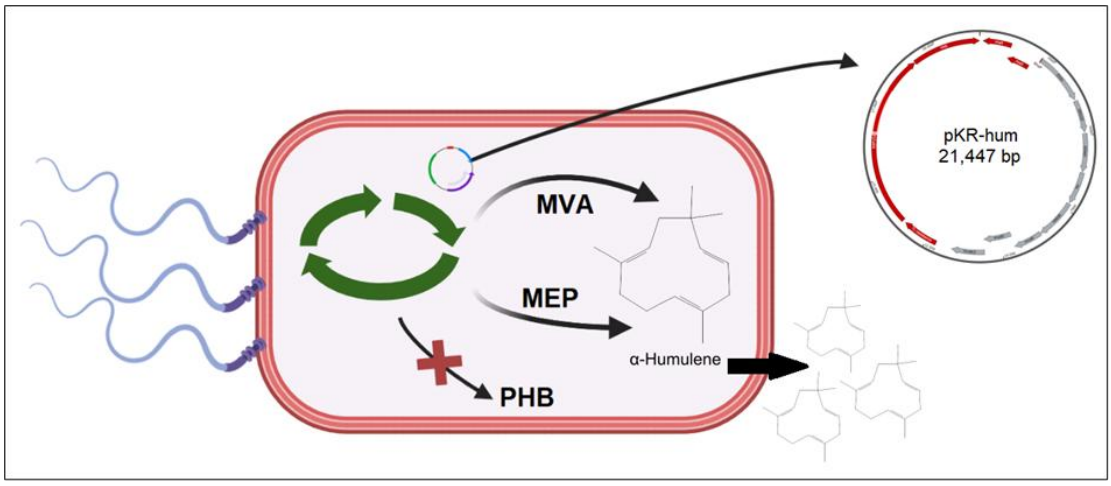

Fig. 5: Schematic representation of the production host: *C. necator*-based α-humulene production via plasmid pKR-hum, transformed into PHB-deficient *C. necator* H16 PHB-4 strain. Production of α-humulene via native MEP and plasmid-based MVA pathway following extracellular release. The illustration features a simplified schematic of the bacterial flagella to highlight *C. necator's* motility. Created with biorender.com, chemical structure [27].

In addition to the necessary α-humulene and farnesyl pyrophosphate synthase, the designed plasmid system pKR-hum also contains the IPP isomerase besides the MVA pathway-related genes from *M. xanthus* [5]. Transformation and pKR-hum plasmid maintenance thus extends the native MEP pathway as a terpene production route and optimizes the carbon flux and the conversion of the precursor molecules to α-humulene. In addition, a PHB-deficient strain *C. necator* H16 PHB-4 has been selected as the production strain. In comparison to the natural strain H16, this strain is not capable of forming PHB due to a 1-nitroso-3-nitro-1-methylguanidine-induced point mutation in the PHB synthase gene *phaC* [87, 88]. This lack of PHB formation thus increases the general carbon availability and reroutes the metabolic flux with regard to enhanced terpene production. While the introduced genetic and molecular biological optimization approaches have been successfully implemented and increased the biosynthetic efficiency of α-humulene production [5, 70], the process parameters and their influence on *C. necator*-based α-humulene production have not been the main focus.

The investigating and fine-tuning of the production parameters is essential for scalable and robust bioprocesses. In this context, process robustness can be described as the capacity of a process to maintain acceptable quality and performance while withstanding variability in inputs [89]. In order to understand and control the robustness of a process, a deep knowledge of the impacts and interactions between variable input and output parameters, such as temperature and media composition on cell growth and product formation, is necessary [90]. In addition to genetic engineering, the optimization of process parameters therefore provides a further approach to increasing productivity. For example, the plasmid-based production of the terpenoid isopentenol in *B. subtilis* could be increased 2.5-fold by optimizing the medium components and the carbon source [91]. Process parameters such as cultivation temperature, iron availability, concentration of carbon sources or the efficiency of plasmid induction are therefore crucial factors that can influence cell growth, metabolic activity and the efficiency of terpene production pathways [92]. Temperature has a major influence on the physiological processes of the *C. necator* production strain and thus on overall metabolic activity and terpene production. Increased cell growth of *C. necator* is observed at 30 °C, whereby deviating cultivation temperatures of 22 - 24 °C slow down the cell growth rate [93].

Additionally, it is important to consider the temperature optima of the enzymes encoded by the heterologous genes, such as the enzymes involved in the MVA pathway or α-humulene synthase. The composition of the growth medium and the availability of trace elements are also crucial factors in this context. Iron in particular plays an essential catalytic role as a prosthetic group or cofactor for many enzymes involved in numerous metabolic processes, thereby directly influencing cell division, cell growth and product formation with its catalytic activity [94]. Insufficient availability of trace elements can therefore lead to a reduced

conversion of precursor molecules, reducing the overall process efficiency. In addition, secondary parameters, such as the induction of the pKR-hum plasmid through L-rhamnose, can also provide a valuable approach for optimization. Regarding the induction parameters, the induction timing and the concentration of the inducer are particularly important [95]. The occurrence of induction at a low biomass concentration, for example, can lead to metabolic stress and insufficient production [95, 96]. Additionally, excessive inducer concentrations result in a metabolic burden on the production cells, while insufficient concentrations fail to adequately activate the plasmid-based biosynthesis [95, 96].

Optimizing process parameters is crucial, as even small changes can significantly influence α-humulene production in *C. necator* and/or cell growth. However, due to the complex interactions between individual process parameters such as temperature, plasmid induction and nutrient availability, the identification of optimal process conditions is challenging. In this context, statistical approaches such as Design of Experiments (DoEs) can help efficiently achieve optimizations and be used to systematically identify synergistic and inhibitory effects between individual parameters.

1.5. Design of Experiment as a method for process optimization

Especially in research and development, a profound understanding of the optimal process parameters and their interactions is required for further process intensification. However, the optimization of processes is often challenging and associated with high material and labor costs, as many experiments have to be conducted to identify optimal parameters [97]. To reduce the number of experiments required, as well as the general costs, the statistical design of experiments is useful [98]. DoE approaches are applied to increase the information obtained from individual experiments and the efficiency of the predictions [98].

The number of experiments conducted is related to the amount of information obtained, which means that the key information content is mostly acquired in the early experiments. This in turn declines as the number of experiments rises. As the project costs increase linearly with the number of experiments, there is an ideal number of experiments to be identified using DoE, providing the optimal ratio of information to project costs [98]. The statistical DoEs can typically be divided into the following three main parts. At the beginning, a screening is carried out to determine the most relevant factors of the production process and their range of investigation [98]. Once these factors are identified, optimization can begin. To minimize interference effects, the experiments and their order are randomized. Optimization is carried out in as few experimental runs as feasible to efficiently investigate the impact of any factor

variation and combination on the target output parameters (responses) [98]. These results are then pooled, analyzed, and modeled in order to generate a significant overview of the individual factor influences and interactions combined with their optimal value range (sweet spot) [98]. In the final part of the statistical DoEs, the robustness of the model generated can optionally be assessed against any factor variations that occur [98, 99].

In contrast to DoE approaches, the conventional one-factor-at-a-time (OFAT) trial and error approach is still widely applied. Factors are tested individually one by one without statistical expertise, and the resulting findings do not involve consideration of any interactions between the factors and only insufficiently reflect the impact of the factor combinations. Additionally, optimal factor values can often be missed due to the fact that the selected and analyzed range of the parameter space is too narrow. The process-related consequences of this incorrect assumption of the OFAT method can be seen in Fig. 6 below.

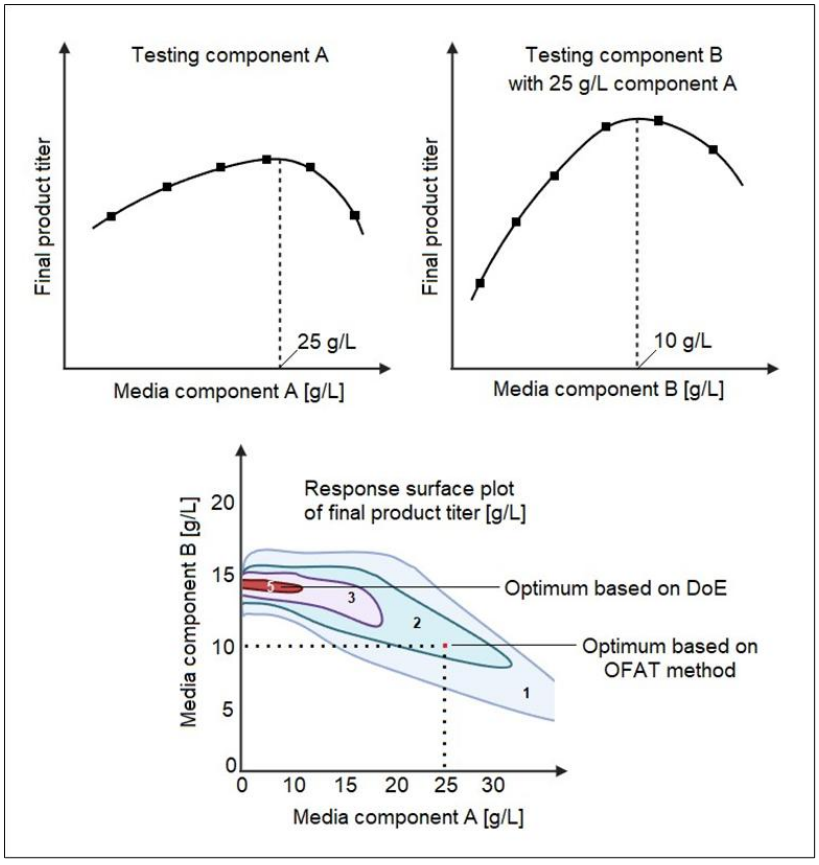

Fig. 6: Procedure of the conventional one-factor-at-a-time (OFAT) method for process optimization and the associated findings vs. optimization using the sweet spot plot of statistical DoEs. Adjusting the concentration of the media components A and B with the aim of optimizing the product titer. Own illustration, concept inspired by Soravia and Orth [100].

The informative value of the OFAT method is limited, as the impact of a factor (in this case media component A) is only combined and analyzed at one value level (concentration of 25 g/L) with the second successively adjusted factor (media component B), see Fig. 6 [101]. Low significance leads to “optimal” concentrations of components A (25 g/L) and B (10 g/L), which, in combination, ultimately result in a lower final product titer of 2 g/L compared to the DoE-based optimum of 5 g/L. The response surface plot thus shows that the optimal concentration of media component A should be below 11 g/L, and that of component B around 14 g/L, indicating that the OFAT approach has therefore not effectively optimized the production process, in contrast to the DoE approach. An in-depth investigation of several complex factors, which may also have unknown interactions, can therefore only be implemented significantly with a DoE approach [100]. Nevertheless, the conventional OFAT method is still helpful, for example, for orienting and rapid preliminary experiments. [98, 100, 101]

1.6. Anti-inflammatory effects of α-humulene and associated investigation

Terpenes such as α-humulene have been shown to exhibit significant anti-inflammatory effects in various experimental models, including the reduction of pro-inflammatory cytokine release in response to bacterial inflammation [38, 39]. This highlights their potential as natural agents for treating a range of inflammation-related conditions, particularly those caused by bacterial inflammation.

A typical bacterial inflammation is often triggered by lipopolysaccharides (LPS) of gram-negative bacteria. They are located in the cell walls and consist of the so-called lipid A, the inner and outer core region, as well as the polysaccharide chain. Structurally diverse lipid A forms the actual endotoxin, which is released when the cell disintegrates. If these endotoxins enter the organism, the sinal transduction of immune cells such as monocytes, activated macrophages, or B-cells shown in Fig. 7 below is induced. [102-104]

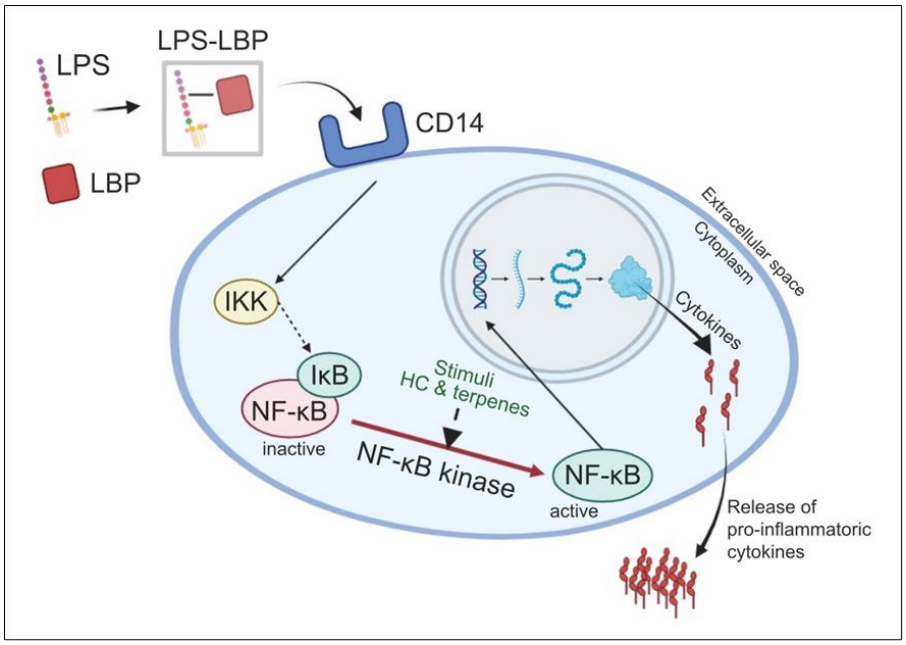

Fig. 7: Simplified model of the inflammatory cascade of a human immune cell induced by lipopolysaccharides (LPS), highlighting the activation of nuclear factor kappa light chain enhancer of activated B-cells (NF-κB) and the extracellular release of pro-inflammatory cytokines. Stimuli such as hydrocortisone (HC) or some terpenes can exert an anti-inflammatory effect by downregulating NF-κB. Own illustration, concept inspired by Grace-Lynn et al. [105]. Created with biorender.com.

In human blood or other systemic fluids, the released LPS binds to the acute phase protein lipopolysaccharide-binding serum protein (LBP). LBP plays a key role in the recognition of LPS and forms the LPS-LBP complex with LPS, which is recognized and bound by immune cells such as monocytes and macrophages that carry the membrane receptor CD14, for example see Ishii et al. [106]. Subsequently, binding of this complex strongly increases cellular sensitivity towards low LPS concentrations in the picomolar range and consequently induces an immune response via interactions with Toll like receptor 4 [107]. This step results in the initiation of complex signaling cascades and interactions that are ultimately related to the activation of the nuclear factor kappa light chain enhancer of activated B-cells (NF-κB). NF-κB transcription factors play a fundamental role in the regulation of the immune response, cell proliferation and cell death [108]. Their presence is largely restricted to the cytoplasm of immune cells through their binding to the nuclear factor kappa B inhibitor proteins (IκB) [109]. Upon contact with extracellular stimulants such as LPS, the IκB kinase (IKK) complex is activated, which in turn tags the IκB proteins for degradation and thus enables the conversion of NF-κB into its active form [109]. Without binding to the IκB proteins, the NF-κB transcription factors can be actively transported into the cell nucleus [109].

Once there, they bind to a wide variety of immunological genes and induce their transcription, which finally results, for example, in the release of inflammatory cytokines [108]. Some of these cytokines are then released extracellularly and can also act as active stimulants for cells, where they stimulate/inhibit immunological processes and thus further intensify or regulate an inflammatory reaction in the organism. [108, 110]

Hydrocortisone (HC) is an established medication for inhibiting inflammatory reactions. HC belongs to the group of glucocorticoids and diffuses into the cell due to its lipophilic properties and binds to the glucocorticoid receptor (GR) in the cytoplasm [111, 112]. This binding activates the GR and forms a dimer, allowing this active complex to enter the cell nucleus of human monocytes, for example, and stimulate the expression of anti-inflammatory cytokine genes such as interleukin-10 [113, 114]. Once there, the complex also reacts, for example, with the RelA (p65) subunit of NF-κB and other co-activators, which blocks the subsequent binding of NF-κB to the DNA [115]. As a result, the expression of pro-inflammatory cytokine genes such as tumor necrosis factor alpha (TNF-α) are inhibited [116]. Another mechanism of action in the cell nucleus is via the activation of the IκB genes by GR binding to their promoter region, whereby more IκB is formed to inactivate the NF-κB [117, 118]. Furthermore, GR is able to decrease the IKK activity in the cytoplasm [119], leaving the IκB bound to NF-κB intact and thus keeping NF-κB in its inactive form. As active stimuli, terpenes or terpenoids are a promising alternative to classical pharmaceuticals from the group of corticosteroids and are also able to inhibit the activation of the NF-κB signaling pathway [120]. However, their mechanism of action is partly substance-specific and often dose-dependent. The monoterpene α-pinene, for example, inhibits NF-κB translocation into the cell nucleus by increasing the expression of IκB genes in LPS-stimulated THP-1 cells [121]. In comparison, the sesquiterpene lactone isodeoxyelephantopin targets the inhibition of the IKK complex in induced human cell lines, thereby indirectly preventing the expression of pro-inflammatory genes through the lack of NF-κB activation by IKK [122].

For an investigation of the NF-κB signaling pathway activation or the subsequent release of pro-inflammatory cytokines, the human leukemia monocytic cell line THP-1 provides an ideal model [123]. In addition to suitable proliferation *in vitro*, THP-1 cells can also be easily differentiated into macrophage-like cells with phorbol 12-myristate 13-acetate (PMA) and then precisely examined for their sensitive inflammatory response after administration of stimuli such as LPS [123, 124]. This experimental approach enables the simulation of the human immune response to LPS and the evaluation of α-humulene's potential anti-inflammatory effects.

1.7. Objectives of the research

In order to meet the increasing global demand for valuable terpenes such as α-humulene, it is necessary to optimize biotechnological production, for example using the versatile *C. necator* strain. Through different cultivation strategies and the versatility of potential substrate sources, this production process offers a highly sustainable and environmentally friendly substrate utilization. The main objective of this thesis was to focus on the optimization of heterotrophic α-humulene production using *C. necator* with regard to the in-depth investigation and optimization of various process parameters. This led to the central research question: Which cultivation and process parameters critically influence heterotrophic α-humulene production in *C. necator*?

To realize these objectives, the production process was first of all identified and orientation studies of the cultivation parameters and their influence on *C. necator* biomass and product formation were conducted. This was followed by a design of experiments investigation and model validation. Furthermore, the ISPR downstream processing was analyzed to identify the most promising solvent. Based on the established use of n-dodecane for ISPR of extracellular α-humulene, the following question was addressed: Which deep eutectic solvents and other promising solvents reported for terpene extraction can serve as biocompatible and effective alternatives to n-dodecane?

Additionally, individual process steps such as composition of the pre- and main culture media, the L-rhamnose inducer concentration and its dosage timing, as well as a process time-dependent cultivation temperature were varied and investigated as a central aspect. In addition, the influence of these steps on biomass and α-humulene formation, both individually and in combination, was examined in order to identify possible potentiations or interactions among these individual steps. This gave rise to another key question: How do individual and combined optimizations of critical process steps affect biomass and α-humulene formation in *C. necator*? Since overall process robustness plays an important role in process optimization, the robustness dependence of the *C. necator*-based production process on the modification of individual process steps, as well as the robustness after a simulated process disturbance, was evaluated with regard to the following question: To what extent do these individual and combined process optimizations affect the robustness of the overall α-humulene production process?

Finally, possible pharmaceutical properties of α-humulene on human immune cells were evaluated. This highlights the broad potential of α-humulene applications and aims to determine whether its proposed anti-inflammatory effects also occur in lipopolysaccharide-induced inflammatory responses in humans.

By combining biotechnological process optimization, evaluation of process robustness and pharmacological investigation of α-humulene, new insights into *C. necator*-based terpene production were gained, which could also be transferred to microbial production processes in general.

In this thesis, each of the research objectives is discussed in a dedicated chapter, organized according to its respective research question. This ensures a focused and consistent presentation of the methods, results, and findings related to each specific research objective.

2. Chapter 1 | Process identification and orientating studies

Material and methods sections 2.3.1 - 2.3.5 and *C. necator* pKR-hum cell dry mass determination result section 2.4.1 of this chapter have been published as follows:

Becker L, Dietz E, Holtmann D. Individual process steps optimization of *Cupriavidus necato*r-catalyzed production of α-humulene. Biochemical Engineering Journal. 2024; 215:109617. doi:10.1016/j.bej.2024.109617. [*1]

Material and methods sections 2.3.7 - 2.3.8 and extraction tests result section 2.4.2 of this chapter have been published as follows:

Sydow A, Becker L, Lombard E, Ulber R, Guillouet SE, Holtmann D. Autotrophic Production of the Sesquiterpene α-Humulene with *Cupriavidus necator* in a Controlled Bioreactor. Bioengineering. 2023; 10:1194. doi:10.3390/bioengineering10101194. [*2]

[*1] Author contributions: E.D.: Investigation. L.B.: Writing – review & editing, Writing – original draft, Visualization, Methodology, Investigation, Data curation. D.H.: Writing – review & editing, Supervision, Project administration, Funding acquisition, Conceptualization.

[*2] Author contributions: Conceptualization, D.H., R.U. and S.E.G.; methodology, all authors; lab investigation (ISPR), L.B.; lab investigation (autotrophic fermentation), A.S. and E.L.; data curation, A.S., L.B. and E.L.; writing - original draft preparation, all authors; writing - review and editing, all authors; supervision, D.H., R.U. and S.E.G.; project administration, D.H.; funding acquisition, D.H.

2.1. Abstract

To meet the growing demand for valuable natural substances such as the sesquiterpene α-humulene, microbial fermentation as an alternative production method must be further optimized. A suitable microbial production method is plasmid-based production employing the versatile production host *C. necator* pKR-hum. To further optimize the production process, external factors, such as the established cultivation parameters, which are still being derived from the literature without adaptation, were investigated and varied. For this purpose, a statistical DoE approach was employed to systematically vary, analyze, and model the shake flask cultivation factors: shaking speed, volume of the extraction agent, and cultivation temperature. The resulting effects on *C. necator* pKR-hum biomass and α-humulene product formation were investigated. It was demonstrated that a modification of the established shaking speed of 180 rpm and the volume of added n-dodecane of 20 % (v/v) in the statistical model had no significant impact on biomass and α-humulene formation. However, a reduction in the established cultivation temperature from 30 °C to a sweet spot of 28 °C exhibited a pronounced quadratic effect with regard to elevated final α-humulene concentrations. Further investigation of these findings may prove beneficial in optimizing production processes based on *C. necator*, with the potential for increased efficiency through the implementation of straightforward adjustments to cultivation parameters.

2.2. Introduction

Continuous process optimization plays an important role in industrial biotechnology in order to meet the growing demand for valuable substances. This includes microbial fermentation processes, such as the *C. necator* pKR-hum-based production of the valuable terpene α-humulene, whose process efficiency, costs, and productivity need to be optimized. *C. necator*, a gram-negative β-proteobacterium, exhibits a broad substrate spectrum and can be cultivated both heterotrophically and autotrophically [125]. Metabolically modified strains of *C. necator* are suitable production hosts and capable of producing a diverse range of valuable compounds, including terpenes such as α-humulene [5]. The valuable sesquiterpene α-humulene, for example, occurs naturally in plants such as hops (*Humulus lupus*) as an essential oil component [126], to which it owes its name. Application areas range from possible pharmaceutical treatments, based on the e.g., anti-microbial [28], anti-cancer [127], anti-fungal [128], or anti-inflammatory [40] effects of α-humulene, to industrial applications. Therefore, α-humulene and its isomers are currently mainly used in the aroma and odor industry [129] and for cosmetic purposes or fragrances [130].

There are many theoretical optimization approaches for a fermentation process, as the entire process can be classically scaled up and/or downstream processing can be improved, for example to capture or extract and purify an extracellularly released product more efficiently [131]. However, microbial production processes are complex and underlie a multitude of factors that interact with each other, often unknown, and can influence biomass formation and the yield of the final product [132]. Furthermore, there are also some bottlenecks to consider when optimizing the process. The microbial production host and its internal metabolic/physiological properties play a major role in this case. These can be optimized or expanded through genome editing [133], adaptive laboratory evolution approaches [134], plasmid-based production [74], and metabolic engineering to increase the yield of the product [78]. However, internal factors such as metabolic and enzymatic properties, as well as plasmid maintenance and copy number, are often predetermined and are more challenging to adjust or optimize compared to external factors. In addition, there is also a certain degree of intrinsic noise due to the internal factors, which can be characterized by susceptibility to variations in product yields and biomass formation [135].

Nevertheless, external process factors such as the media composition, physical parameters and, above all, the production host-specific choice of cultivation parameters such as temperature and shaking speed also have a significant influence on process efficiency [136]. In this context, the choice of cultivation parameters was defined as an optimization point. To date, these have always been adopted from established sources in the literature, where it is described that the plasmid-based production of α-humulene uses the following *C. necator* pKR-hum cultivation parameters: 180 rpm shaking speed with a 25 mm orbital diameter, 30 °C cultivation temperature, and the addition of 20 % (v/v) extraction agent for *in situ* extraction of the extracellularly released product α-humulene [69, 5, 73]. In this context, a statistical DoE to plan and vary the *C. necator* pKR-hum cultivation parameters and to analyze the resulting effects is beneficial. This optimization using a statistical method has advantages over the classical OFAT approach, such as a significant reduction in the number of experiments and the time required, the simultaneous consideration of several process factors and the identification of interactions between these factors [137, 138].

To investigate the cultivation parameters and their influence on *C. necator* pKR-hum biomass and α-humulene product formation, a quadratic response surface design was chosen. This takes into account the model process factors of shaking speed, n-dodecane volume, and cultivation temperature. In order to test the corresponding design range, preliminary orientation and screening experiments were conducted and the most promising solvent for *in situ* α-humulene removal was identified.

The resulting analysis, modeling and knowledge can be used to re-evaluate process factors and provide parameter suggestions that lead to more robust, efficient and optimized production processes based on *C. necator*.

2.3. Materials and methods

In the following chapters, the standard methods and parameters of the *C. necator* pKR-hum fermentation, screening and *in situ* extraction experiments are described. Furthermore, the specifications of the performed DoE approach are indicated. All experimental works, including the results presented in this chapter, were carried out in triplicate.

2.3.1. Heterotrophic cultivation and biomass monitoring of *C. necator* pKR-hum

In order to establish a stock culture and to ensure comparable starting conditions, *C. necator* pKR-hum cryo cultures were prepared at the start of the project and stored at -80 °C for subsequent testing. *C. necator* pKR-hum was cultivated in 50 mL of a lysogeny broth (LB) medium (in a 250 mL Erlenmeyer flask), composition according to Tab. 2 below, supplemented with 15 µg/mL tetracycline (TC) at 30 °C with 180 rpm (Ecotron, 25 mm orbital diameter, Infors HT; Bottmingen, Switzerland). Subsequently, the culture was centrifuged at 5,000 g for 5 min, and sterile glycerol was added for cryopreservation. For this purpose, 750 µL of the culture was mixed with 250 µL of sterile glycerol, resulting in a final concentration of 25 % (v/v) glycerol.

Tab. 2: Composition of the lysogeny broth (LB) preculture medium [77].

Medium component	Medium concentration [g/L]
Yeast extract	5
Tryptone	10
NaCl	5

The standard procedure for all experiments was maintained consistently to ensure reliable results. Initially, 3 mL of LB medium, supplemented with 15 µg/mL TC, was inoculated in a 15 mL sterile tube as a preculture from a cryo culture of the stock culture. Cells were then cultivated for 24 h at 30 °C with 180 rpm. The appropriate amount of biomass needed to inoculate the main culture to a starting OD_{600} of 0.1 was transferred to a sterile reaction tube, centrifuged, and the pellet obtained was resuspended in 20 mL of the main culture medium,

supplemented with 15 µg/mL of TC. The main culture was cultivated (Ecotron, Infors HT; Bottmingen, Switzerland) in 250 mL Erlenmeyer flasks according to the runs defined in the experimental design (see 2.3.10) with variation of the cultivation parameters: cultivation temperature and shaking speed. During the screening experiments (see 2.3.9), the biomass was monitored online in terms of backscattered light intensity measuring every 60 s using the Cell Growth Quantifier® device (CGQ, Scientific Bioprocessing; Pittsburgh, USA). To calibrate and adjust the recorded backscatter values, offline OD_{600} measurements were taken just before the start and immediately after the end of the main cultivation.

2.3.2. Preparation and composition of main culture media

The standard composition of the minimal medium (MMasy) used for all cultivations, according to Sydow et al. [81], is shown in Tab. 3 and Tab. 4. To prepare the minimal medium, stock solutions were prepared with deionized water in the same way as the individual components listed in Tab. 3. After dissolving the media components, all stock solutions, except the trace element stock (Tab. 4), were autoclaved and stored at room temperature. This standard composition of the minimal medium was used in all experiments.

Tab. 3: Standard composition of the minimal medium used (MMasy), stock solutions corresponding to [1)] 10-fold, [2)] 100-fold, and [3)] 20,000-fold final media concentrations [77].

Medium component		Medium concentration [g/L]
Na_2HPO_4	1)	2.895
$NaH_2PO_4 * H_2O$	1)	2.707
K_2SO_4	1)	0.170
$CaSO_4 * 2\ H_2O$	1)	0.097
$MgSO_4 * 7\ H_2O$	2)	0.800
$(NH_4)_2SO_4$	2)	0.934
Trace elements	3)	1:20,000 from stock
D-fructose	2)	4.0

Trace elements were added to the medium at the concentrations given in Tab. 4 below. To prepare the trace element stock solution, all components listed in Tab. 4 were dissolved together in 0.1 M hydrochloric acid at a concentration 20,000 times that of the medium, and then filter-sterilized. The trace element stock solution was then stored at 4 °C until it was added 20,000 times diluted to the minimal medium.

Tab. 4: Trace element composition of the minimal medium used (MMasy) [77].

Trace element component	Medium concentration [µg/L]
$FeSO_4 * 7 H_2O$	750
$MnSO_4 * H_2O$	120
$ZnSO_4 * 7 H_2O$	120
$CuSO_4 * 5 H_2O$	24
$Na_2MoO_4 * 6 H_2O$	90
$NiSO_4 * 6 H_2O$	75
$CoSO_4 * 7 H_2O$	2

2.3.3. Microbial α-humulene production using *C. necator* pKR-hum

C. necator H16 PHB-4 was utilized as the host organism for the production of microbial α-humulene. This PHB-deficient strain was transformed by conjugation with the plasmid pKR-hum [5]. The plasmid pKR-hum contains an L-rhamnose-inducible promoter [74], in addition to the MVA pathway genes, the genes required for the production of α-humulene (*zssI* and *erg20*). A tetracycline resistance gene is present as a marker. The pKR-hum plasmid map is shown in the appendix 7.1, Fig. 27. *C. necator* pKR-hum main cultures were induced at an OD_{600} between 0.50 and 0.70 with a final concentration of 0.2 % (w/v) L-rhamnose to initiate α-humulene production, which was achieved by a hundredfold dilution of a 20 % (w/v) L-rhamnose stock solution prepared in deionized water.

The stock solution was filter-sterilized and stored at -20 °C. Extracellular α-humulene was removed from the culture process through *in situ* product removal. For this purpose, the amount of the suitable and biocompatible extracting agent n-dodecane [8] added to 20 mL of cultivation broth after induction was varied as the third factor in the experimental design. This created a second phase above the cultivation broth, from which samples were taken.

2.3.4. Quantification of fructose using high performance liquid chromatography (HPLC)

The fructose content of filter-sterilized cultivation samples was analyzed by HPLC (1260 Infinity II, Agilent Technologies; Santa Clara, USA) using the Aminex HPX-87H column (Agilent Technologies; Santa Clara, USA). The elution was performed using 5 mM H_2SO_4 at a flow rate of 0.6 mL/min, and the column oven temperature was set at 50 °C.

A multiple wavelength detector (1260 Infinity II Multiple Wavelength Detector, Agilent Technologies; Santa Clara, USA) was used for the detection of fructose at 191 nm. The calibration curve, including the linearity range, as well as an example chromatogram with retention time for fructose HPLC analysis, are provided in the appendix 7.2 (Fig. 28).

2.3.5. Quantification of α-humulene using gas chromatography (GC-MS)

Due to the low water solubility of the product α-humulene in the fermentation broth, *in situ* product removal was performed. For this purpose, the extracellularly released α-humulene was extracted into a n-dodecane phase, which was present in the Erlenmeyer flask during the fermentation process. Since n-dodecane is lipophilic, it forms an upper phase from which samples can be collected and further processed for analysis. 100 µL of the centrifuged (5 min, 1,000 g) n-dodecane upper phase was taken and stored at -20 °C in GC glass vials until measurement. Just prior to measurement, the samples were diluted with 900 µL acetone. In addition to the samples, calibration standards were created using an α-humulene stock solution (83351, PhytoLab; Vestenbergsgreuth, Germany).

The corresponding volumes of pure α-humulene stock solution were diluted in n-dodecane to a final volume of 100 µL and subsequently mixed with acetone at a ratio of 1:10. Samples and standards were prepared by using the same method. As a top standard for the calibration curve, a concentration of 100 mg/L α-humulene was set. The concentration values presented in this work were converted and related to the aqueous culture phase. The detection of α-humulene was performed by gas chromatography and mass spectrometry GC-MS (7890B GC-MS with 5977B GC/MSD, Agilent Technologies; Santa Clara, USA) with an N_2 gas flow of 45 mL/min, air flow of 450 mL/min, and FID of 250 °C. Samples and standards were analyzed using an HP-5ms GC column (Agilent 19091S-433, Agilent Technologies; Santa Clara, USA) with 100 % acetonitrile as the rinsing solvent. The injection volume for the samples was 1 µL. The analysis was carried out using the single ion monitoring method (SIM) at a m/z ratio of 204.2 for α-humulene. The calibration curve, including the linearity range, as well as an example chromatogram with retention time for α-humulene analysis by GC-MS, are provided in the appendix 7.2 (Fig. 29).

2.3.6. Cell dry mass determination

To determine the dry mass of *C. necator* pKR-hum cells, 1 L shake flasks were filled with 200 mL of LB medium, inoculated from a preculture to an OD_{600} = 0.1 and cultivated in triplicate at 180 rpm and 30 °C.

When the OD_{600} increased, 20 mL was removed and centrifuged at 3,000 g for 10 min. The pellet was then resuspended in ultrapure water to an OD_{600} of 1.5, 2.0, 3.0, 3.5 and 4.0 and placed in the moisture analyzer (Kern DBS 60-3; Kern & Sohn GmbH, Balingen, Germany). Once the target conditions were reached (temperature: 120 °C, weight tolerance range: max. 0.055 % for 30 s), the bio dry mass of the cells was measured after complete drying. The resulting cell dry mass values were analyzed for a linear correlation with the previously set OD_{600} values in order to determine the conversion factor.

2.3.7. Solvent selection and testing

In the literature, the recovery of extracellularly released α-humulene from culture broth has been performed by *in situ* product removal (ISPR) with n-dodecane [5, 70]. In order to optimize the ISPR, several alternative solvents were tested. Therefore, different deep eutectic solvents (DES) and other promising solvents used in the literature for terpene extraction were compared with n-dodecane in terms of biocompatibility during cultivation with *C. necator* pKR-hum. Furthermore, the formation of a second liquid phase from the cultivation medium was a criterion to be tested in order to facilitate the removal of the α-humulene-containing solvent after the extraction process.

Two DES systems, namely, tetrabutylammonium bromide (TBAB):1-octanol [139] and D-menthol:lauric acid [140], have been identified as potential alternatives to *in situ* product removal using n-dodecane, based on their applications in the literature and successful terpene extractions. Furthermore, the efficacy of acetophenone [141], methyl butyrate [142] and 1-cyclodextrin [143] as extraction solvents was evaluated.

2.3.8. Preparation of deep eutectic solvents

D-menthol was used as hydrogen bond donor and lauric acid as hydrogen bond acceptor. They were heated together in a molar ratio of 2:1 for 2 h at 50 °C in a closed vessel until the solid components dissolved and a homogeneous liquid was formed [140]. TBAB was heated together with 1-octanol in a molar ratio of 1:2 for 2 h at 80 °C in a closed vessel until a homogeneous liquid was formed [139]. The deep eutectic solvents were then stored at room temperature until use and added to the fermentation broth after inoculation at 20 % (v/v), similarly to the other extraction solvents tested.

2.3.9. Screening experiments

Screening experiments were carried out as preliminary tests to define the limits of factor variation within the experimental approach using the α-humulene-producing *C. necator* pKR-hum strain. In these tests, the implementation of higher shaking speeds and cultivation temperatures within the incubator (Ecotron, Infors HT; Bottmingen, Switzerland) was tested with regard to technical feasibility and *C. necator* pKR-hum biocompatibility as well as growth behavior. To record cell growth, the shake flasks were measured in triplets within the Cell Growth Quantifier® device every 60 s and the resulting backscatter intensity values were calculated via the OD_{600} to the corresponding cell dry mass concentrations.

2.3.10. Analysis and optimization of cultivation process parameters

In order to optimize *C. necator* pKR-hum biomass growth and α-humulene concentration, a DoE approach was applied. For this purpose, the critical cultivation process parameters: shaking speed, *in situ* product removal solvent volume and cultivation temperature were varied as factors within the minimum and maximum design range given in Tab. 5.

Tab. 5: Model process factors and corresponding design range.

Factor	Name	Unit	Minimum	Maximum
1	Shaking speed	rpm	30	330
2	Volume n-dodecane	% (v/v)	3	37
3	Cultivation temperature	°C	28	39

All experiments were designed and analyzed with Design Expert® (software version 12.0.3.0) according to the parameters in Tab. 6 below. A quadratic response surface design with a maximum of 19 randomized runs including 5 center points was selected for the optimization studies. The ANOVA analysis tool of the Design Expert software was used to integrate and analyze the p-values of the models and factors. A value of $p^* < 0.05$ was considered significant.

Tab. 6: Model building parameters used to investigate process intensification.

Parameter	Setting
Software version	Design Expert 12.0.3.0
Study type	Response surface
Design type	Central composite
Design model	Quadratic
Runs	19

The response surface design described above was analyzed for the responses listed in Tab. 7 with their specific work objectives. Factor parameters of the individual design runs and the experimentally determined response data are shown in chapter 2.4.4 Tab. 8.

Tab. 7: Model response information for process intensification.

Response	Name	Unit	Objective
R1	Time until induction	h	minimize
R2	$C_{\alpha\text{-humulene}}$ 24 h after induction	mg/L	maximize
R3	$C_{\alpha\text{-humulene}}$ 48 h after induction	mg/L	maximize
R4	Biomass 24 h after induction	g/L	maximize
R5	Biomass 48 h after induction	g/L	maximize
R6	Yield coefficient $Y_{P/S}$ 48 h after induction	mg/g	maximize
R7	Yield coefficient $Y_{P/X}$ 48 h after induction	mg/g	maximize

2.4. Results and discussion

In the following, the impacts are presented of varying the heterotrophic fermentation parameters shaking speed, extraction volume and cultivation temperature on the biomass growth and α-humulene production of *C. necator* pKR-hum using a DoE approach. For this purpose, preliminary screening experiments were carried out and the most promising solvent for *in situ* product extraction was identified.

2.4.1. *C. necator* pKR-hum cell dry mass determination

To determine the yield coefficients $Y_{X/S}$ and $Y_{P/X}$, the cell dry mass of the *C. necator* pKR-hum strain used was determined. The OD values measured at 600 nm were converted into biomass concentrations using the linear dependency and conversion factor given below (Fig. 8).

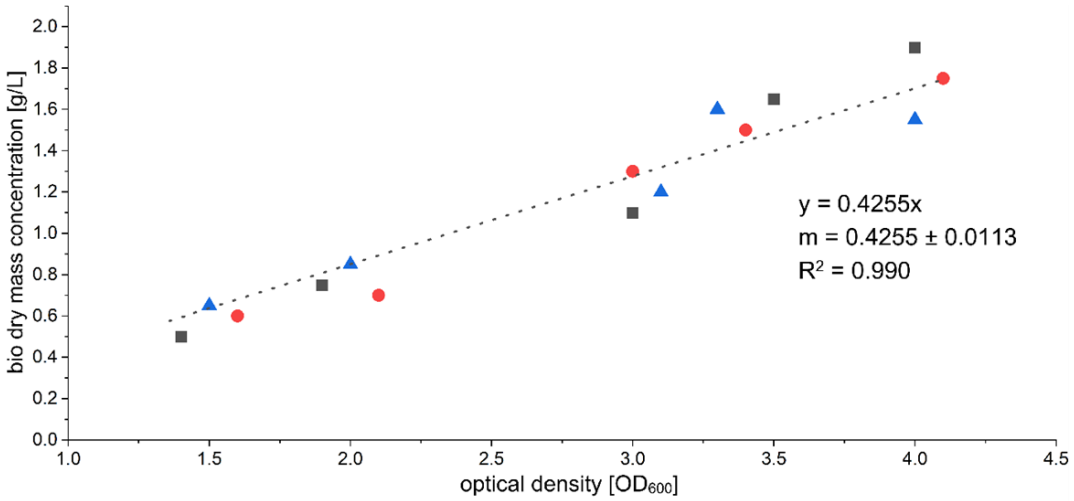

Fig. 8: Determination of cell dry mass concentration based on *C. necator* pKR-hum cultivation samples, linear relationship between optical density (600 nm) and cell dry mass concentration (n = 3). The regression line is annotated with its slope (m) and coefficient of determination (R^2).

Fig. 8 shows the determination of the bio dry mass coefficient for *C. necator* pKR-hum from defined cell suspensions, which can be described by a regression line with a coefficient of determination (R^2). Thus, the following calculation can be made:

$$\text{Biomass } \frac{g_{CDW}}{L} = (m)\ \frac{g}{L} * OD_{600} \qquad (1)$$

Using the previous calculation in formula (1) and based on the slope of the regression line, the conversion of OD_{600} = 1, corresponding to 0.43 g/L biomass, was used for calculations in this work, which is consistent with the literature reference [5]. Refer to the appendix 7.3 (formulas 4 - 6) for details on the calculation of the yield coefficients.

2.4.2. Identification of the most promising solvent for *in situ* product removal

As described in material and methods, various solvents were tested and their suitability as alternatives to n-dodecane was investigated. In the first step, the influence of alternative solvents on the growth of *C. necator* was investigated. As the individual solvents were only compared with each other for their biocompatibility, the cell concentration was subsequently displayed in backscatter intensity (-).

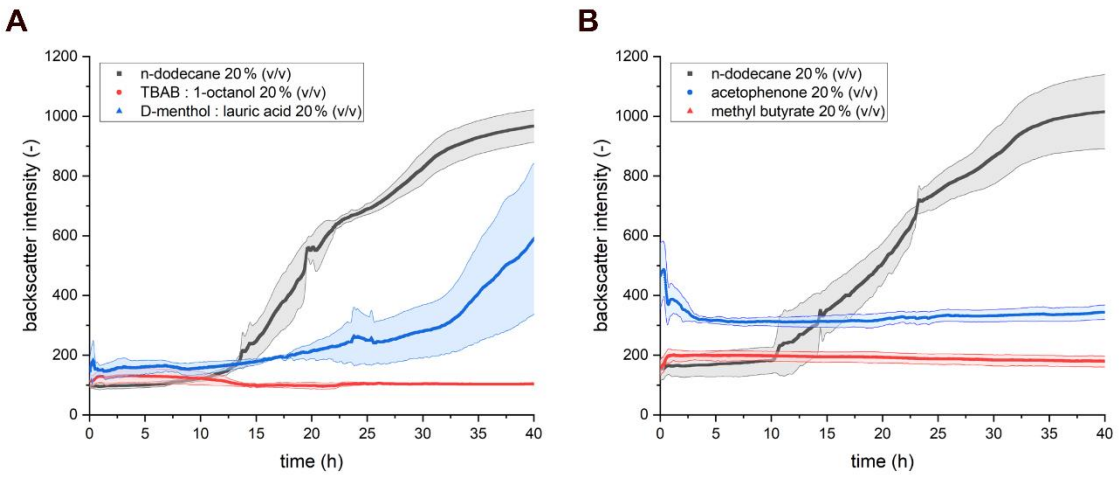

Fig. 9: (A) Heterotrophic growth of *C. necator* pKR-hum in minimal media under the influence of different deep eutectic solvents for *in situ* product removal (n = 3), (B) Heterotrophic growth of *C. necator* pKR-hum in minimal media under the influence of different solvents for *in situ* product removal (n = 3).

The heterotrophic growth of *C. necator* pKR-hum in a minimal medium was reduced by the addition of the deep eutectic solvents compared to n-dodecane (Fig. 9 - A). The addition of 20 % (v/v) of 1:2 molar TBAB:1-octanol resulted in no growth after inoculation. The addition of 20 % (v/v) of the 2:1 molar D-menthol:lauric acid mixture resulted in reduced growth with a prolonged lag phase up to 20 h and a reduced final cell concentration of 300 - 800 backscatter intensity after 40 h compared to 900 - 1050 backscatter intensity with n-dodecane. Nevertheless, successful separation and formation of a second phase above

the minimal medium was observed for both deep eutectic solvents identical to n-dodecane. When 20 % (v/v) of the alternative solvents acetophenone and methyl butyrate were added to the cultivation process, no growth was detected after inoculation compared to the standard extraction solvent n-dodecane (Fig. 9 - B). Both alternative solvents successfully formed a second phase that separated from the minimal medium, with 20 % (v/v) methyl butyrate forming an upper phase identical to 20 % (v/v) n-dodecane and 20 % (v/v) acetophenone forming a phase that appeared at the bottom of the shake flask. In addition, a strong unpleasant odor was detected when acetophenone and methyl butyrate were used as solvents compared to the menthol-containing deep eutectic solvent or n-dodecane. Replacement of n-dodecane with 1-cyclodextrin in the experimental setup was rejected because the addition of the soluble 1-cyclodextrin to the minimal medium did not form an additional second phase, which was used as a decision criterion. The non-biocompatible solvents (TBAB:1-octanol, acetophenone and methyl butyrate) must therefore have an inhibitory effect on the growth of *C. necator*. The question now arose of how biocompatible the addition of n-dodecane actually is.

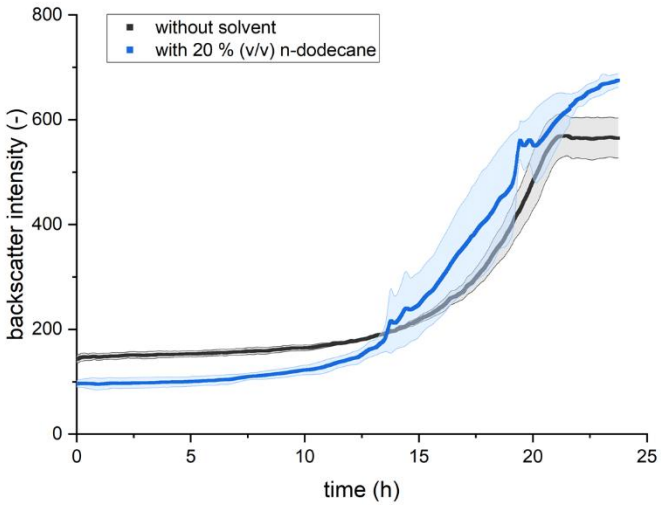

Fig. 10: Heterotrophic growth of *C. necator* pKR-hum in minimal media under the influence of 20 % (v/v) n-dodecane and without solvent (n = 3).

The heterotrophic growth behavior in Fig. 10 shows a similar pattern between the bacterial growth without solvent and the addition of 20 % (v/v) n-dodecane, considering the standard deviation. In both experiments, the length of the lag phase is about 10 h and the cultures in exponential phases behave similarly. The experiment with 20 % (v/v) n-dodecane reaches an increased final backscatter value at 25 h.

However, this increased backscatter intensity value can be attributed to the additional n-dodecane, since an offline OD measurement at 600 nm for both experiments showed a value of 3.0 and 3.1, respectively, at the end of the cultivation. Therefore, the slightly increased backscatter value can be explained by the addition of phase-forming solvents in general.

Biocompatibility of solvents can be assessed on the basis of logP values. LogP is the logarithmic partition coefficient of a target compound in a biphasic system consisting of octanol and water and is a measure of the hydrophobicity of a molecule [144, 145]. The lower the logP, the greater its hydrophilicity and thus its tendency to accumulate in the aqueous phase, where microorganisms such as *C. necator* pKR-hum reside, and interfere with the physiological processes of the cells [146]. A critical logP value, that prevents further metabolic activity, is strongly dependent on the microorganism: e.g., for *E. coli*, the critical logP is reported to be 3.4 [147], whereas *S. cerevisiae* has a critical logP between 4.0 and 5.0 [148, 149]. When comparing the computed logP values, it is noticeable that n-dodecane (6.1), D-menthol (3.0) and lauric acid (4.2) have much higher values than 1-octanol (3.0), acetophenone (1.6) and methyl butyrate (1.3) [150, 151]. Therefore, it can be assumed that the critical logP of *C. necator* is between 3.0 and 4.2.

In terms of the solvent evaluation, it could be shown that the addition of 20 % (v/v) n-dodecane for *in situ* product removal of α-humulene does not reduce *C. necator* pKR-hum growth compared to its absence and is, therefore, a suitable biocompatible solvent. The alternative solvents were all found to be non-biocompatible at the 20 % (v/v) concentration tested, as no bacterial growth occurred upon their addition. Only the deep eutectic solvent tested, consisting of D-menthol:lauric acid 20 % (v/v), showed limited biocompatibility with a longer lag phase and lower final cell concentration. Therefore, n-dodecane can still be considered as the currently most promising solvent for ISPR in *C. necator*-based production processes.

2.4.3. Design of experiment - preliminary screening experiments

To ensure the technical and biological feasibility of varying the cultivation parameters in the planned experimental approach according to the limits in Tab. 5, screening experiments regarding the *C. necator* pKR-hum cultivation temperatures and shaking speeds were carried out (Fig. 11). A biocompatibility test of the third varied factor (n-dodecane volume) was not carried out in this context, as the addition of 20 % (v/v) of this extraction agent has already been successfully tested for the biocompatibility of *in situ* product removal in *C. necator* pKR-hum [8], see chapter 2.4.2.

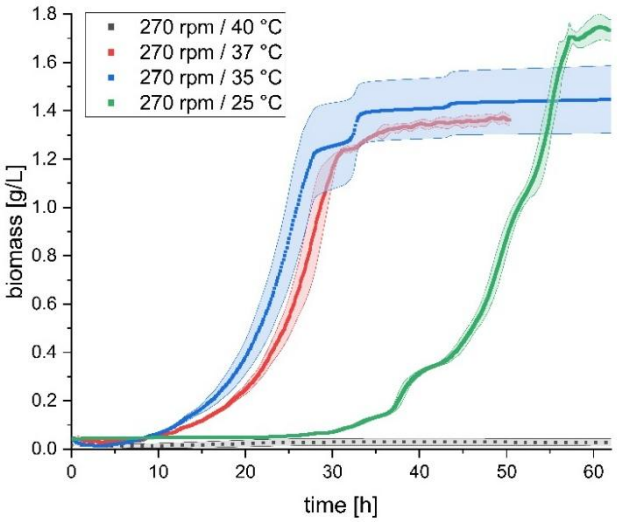

Fig. 11: *C. necator* pKR-hum growth according to different cultivation temperatures between 25 and 40 °C with 270 rpm shaking speed in minimal media, uninduced (n = 3).

The screening experiments were successful, as indicated by the *C. necator* pKR-hum growth behavior shown in Fig. 11 above. A higher shaking speed of 270 rpm combined with cultivation temperatures of 25 - 40 °C was found to be technically feasible and resulted in cell growth of *C. necator* pKR-hum except at 40 °C. However, it can be seen that a low cultivation temperature of 25 °C led to delayed growth behavior with a lag phase of up to 25 h. Higher temperatures of 35 or 37 °C led to a faster growth of the cells with a lag phase of 10 h. A further increase to 40 °C cultivation temperature is technically feasible, but did not result in any cell growth of *C. necator* pKR-hum.

The prolonged growth phase at 25 °C and the lack of growth at 40 °C are caused by deviations from the optimal temperature for *C. necator* pKR-hum growth, which results in microbial adaptation processes to higher or lower temperatures [93]. This leads to longer lag phases, delayed exponential phases and reduced maximum growth rates [152]. In summary, the corresponding design range of the DoE approach shown in chapter 2.3.10 Tab. 5 could be realized in the runs. The final biomasses at cultivation temperatures of 35 and 37 °C, when reaching the stationary phase after 40 h, were 1.3 - 1.5 g/L and in the example of 25 °C after 55 h 1.7 - 1.8 g/L, considering the standard deviations.

2.4.4. Design of experiment – performed experimental approach

The DoE approach with the individual factor combinations from chapter 2.3.10 was planned and tested, see Tab. 8 below. In addition, the corresponding response values were determined for each run. Following Tab. 8, the 3D response surface plots of the model are described.

Tab. 8: Tabular overview of the performed design of experiment work. Divided into 19 runs using varying factors: shaking speed, solvent volume and cultivation temperature (green). Responses analyzed: Time until induction, α-humulene concentration 24 and 48 h after induction, biomass 24 and 48 h after induction and yield coefficients $Y_{P/S}$ and $Y_{P/X}$ 48 h after induction (black). Values not included in the model were crossed out as outliers.

Run	Shaking Speed [rpm]	Volume n-dodecane [% (v/v)]	Cultivation temperature [°C]	Time until induction [h]	$C_{\alpha\text{-humulene}}$ 24 h [mg/L]	$C_{\alpha\text{-humulene}}$ 48 h [mg/L]	Biomass 24 h [g/L]	Biomass 48 h [g/L]	$Y_{P/S}$ 48 h [mg/g]	$Y_{P/X}$ 48 h [mg/g]
1	270	10	30	15.10	2.75	2.87	1.419	1.849	0.68	1.55
2	180	20	34	13.91	0.72	0.71	1.978	2.236	0.17	0.32
3	180	20	28	25.33	0.22	7.28	1.204	1.634	1.84	4.46
4	270	10	37	19.75	0.24	0.30	2.451	2.924	0.07	0.10
5	90	30	37	23.93	0.43	0.21	1.634	1.634	0.05	0.13
6	90	30	30	19.25	2.82	2.02	1.290	1.290	0.47	1.57
7	180	20	34	14.08	0.90	0.74	2.322	2.795	0.19	0.26
8	30	20	34	17.75	1.87	2.53	1.849	1.849	0.60	1.37
9	330	20	34	14.00	3.11	2.87	2.107	2.881	0.69	1.00
10	180	37	34	13.67	1.32	~~1.02~~	2.107	2.623	~~0.25~~	~~0.39~~
11	180	3	34	13.58	0.30	-	2.795	3.053	-	-
12	180	20	34	13.45	0.92	0.93	2.752	2.838	0.23	0.33
13	90	10	30	19.25	2.74	2.70	1.247	1.247	0.63	2.17

Run	Shaking Speed [rpm]	Volume n-dodecane [% (v/v)]	Cultivation temperature [°C]	Time until induction [h]	$C_{\alpha\text{-humulene}}$ 24 h [mg/L]	$C_{\alpha\text{-humulene}}$ 48 h [mg/L]	Biomass 24 h [g/L]	Biomass 48 h [g/L]	$Y_{P/S}$ 48 h [mg/g]	$Y_{P/X}$ 48 h [mg/g]
14	180	20	34	13.83	1.08	1.11	2.623	2.666	0.28	0.42
15	180	20	34	13.99	0.65	0.90	2.107	2.580	0.22	0.35
16	270	30	37	19.75	0.33	0.49	2.322	2.365	0.12	0.21
17	270	30	30	15.10	3.22	3.45	1.290	1.849	0.84	1.86
18	90	10	37	23.93	0.18	0.18	1.849	1.849	0.04	0.10
19	180	20	39	34.75	0.11	0.18	1.892	1.892	0.04	0.10

The 3D response surface plots of the model are shown in the appendix 7.4 Fig. 30. Varying shaking speed and cultivation temperature affected all measured responses in the models (Fig. 30). In particular, cultivation temperature was shown to have a major effect on *C. necator* pKR-hum growth and α-humulene production. A temperature of 33 °C was shown to be optimal in terms of rapid cell growth and reduced process time until induction, reducing this from up to 40 h (39 °C) to 14 h (32 - 33 °C) (Fig. 30 - A). Similar effects were also observed with respect to the final biomass 48 h after induction, where an average temperature of 33 - 34 °C also resulted in the highest measured values of up to 2.7 g/L. Higher and lower cultivation temperatures of 39 and 28 °C, respectively, resulted in a low biomass of 0.8 g/L (Fig. 30 - C).

Complementary to this effect is the behavior of the responses associated with α-humulene production, such as α-humulene concentration 48 h after induction (Fig. 30 - B), yield coefficient $Y_{P/S}$ (Fig. 30 - D) and $Y_{P/X}$ 48 h after induction (Fig. 30 - E). It can be seen that high α-humulene production occurs at lower cultivation temperatures of 28 °C. In the above model, this increase in α-humulene concentration 48 h after induction can be up to 10 mg/L compared to 2 - 3 mg/L α-humulene at higher temperatures of 31 - 32 °C (Fig. 30 - B). The yield coefficient $Y_{P/X}$ 48 h after induction is mainly dependent on the cultivation temperature and can be increased up to 25 mg α-humulene / g biomass by the use of low cultivation temperatures of 25 - 28 °C (Fig. 30 - E). This observation at lower cultivation temperatures of 25 - 28 °C can theoretically be explained by a reduction in the translation and folding stress of proteins, which is temperature-dependent, and due to a resulting reduction in incorrect self-binding and aggregation of proteins [153]. Therefore, it can be hypothesized that the efficiency of the plasmid-supplied enzymes for α-humulene production may have increased due to the lower cultivation temperatures of 25 - 28 °C. Additionally, similar observations were demonstrated by an increase in groESL chaperone activity in *C. necator*, which led to increased heterotrophic isopropanol production [67]. Varying the amount of n-dodecane added or the shaking speed had no significant influence on $Y_{P/X}$ in this model.

2.4.5. Validation of model and process parameters for maximal biomass and α-humulene concentration

To finally ensure the validity of the optimized process parameters from the 3D contour plots, a confirmation run (n = 3) was carried out. The model with its optimal process parameter "sweet spot" (see Tab. 9 below), based on the results obtained from response surface modelling and the maximizing of the final *C. necator* biomass and α-humulene concentration, was verified within the following criteria.

Tab. 9: Optimal process parameters to maximize final α-humulene concentration and biomass, numerical model optimization to predict sweet spot and responses, sweet spot validation limit is set to 10 %.

Factor/Response	Goal (Limit)	Prediction	90 % Limit	110 % Limit	Observed (n = 3)
Shaking speed [rpm]	is in range (100 - 180)	179.998	161.998	197.998	180 ± 2
Volume n-dodecane [% v/v]	is in range (5 - 30)	19.504	17.554	21.454	19.5 ± 0.1
Temperature [°C]	is in range (25 - 33)	28.007	25.206	30.808	28.0 ± 0.2
α-Humulene concentration 48 h after induction [mg/L]	Maximize (2 - 15)	3.812	3.431	4.193	4.18 ± 0.16
Biomass 48 h after induction [g/L]	Maximize (1 - 4)	1.164	1.048	1.280	1.42 ± 0.02
Yield coefficient $Y_{P/X\ 48\ h}$ [mg α-humulene/ g biomass]	Maximize (2 - 15)	3.073	2.766	3.380	2.95 ± 0.15

The sweet spot was predicted based on the factor and response goals described above, then used for cultivation in a final confirmation run (n = 3), during which response values were evaluated. Response values obtained from the “sweet spot” verification are as follows: 4.18 ± 0.16 mg/L α-humulene concentration 48 h after induction, 1.42 ± 0.02 g/L biomass 48 h after induction and 2.95 ± 0.15 mg α-humulene / g biomass yield coefficient $Y_{P/X\ 48\ h}$. The values for the α-humulene concentration and the yield coefficient $Y_{P/X}$ agree with the model predictions of the optimization experiments within their deviation range and indicate verification by the confirmation run (Tab. 9).

Considering the standard deviation, the biomass determined 48 h after induction is 9.3 % above the upper limit of the predicted value range. Optimal process parameters determined for the shaking speed and the volume of n-dodecane added to maximize the final α-humulene and biomass concentration are in good alignment with the established and described literature values of 180 rpm and 20 % (v/v) [5, 73, 70]. Within the framework of this DoE approach, the cultivation temperature of *C. necator* pKR-hum could be lowered from 30 to 28 °C and promisingly adapted with regard to increased α-humulene production.

2.4.6. Conclusions

The process parameters determined by the model were verified by the confirmation run, obtaining a mean final α-humulene concentration of 4.18 mg/L and a *C. necator* pKR-hum biomass of 1.42 g/L, see Tab. 9. Moreover, the results correspond to the expected values of the design optimization and are within the predicted value range. Only the biomass determined 48 h after induction was found to be 9.3 % above the upper limit of the predicted value range.

As shown in Tab. 8, cultivation at 30 °C resulted in an average α-humulene concentration of 2.76 ± 0.59 mg/L 48 h after induction, whereas cultivation at 34 °C led to a lower concentration of 1.40 ± 0.90 mg/L. This demonstrates that cultivation temperature is a critical process parameter affecting α-humulene production. Through the DoE and identification of the sweet spot, lowering the cultivation temperature to 28 °C enabled an increase in α-humulene concentration to 4.18 ± 0.16 mg/L, thereby improving the final α-humulene concentration by 51 % compared to the starting condition at 30 °C.

The cultivation temperature of the established *C. necator* pKR-hum based production process was successfully lowered from 30 to 28 °C. It was demonstrated that within a temperature range of 25 to 28 °C, the statistical model predicts an increased α-humulene production, in conjunction with elevated product/substrate and product/biomass yield coefficients. In this model, lower cultivation temperatures are conducive to greater final α-humulene concentrations; however, they can also delay and reduce the growth behavior of *C. necator* pKR-hum. It is recommended that the reduction in temperature be coordinated with the induction step or the *C. necator* pKR-hum growth phase in order to achieve an optimal balance between biomass and product formation. In future experiments, the temperature should only be lowered from 30 °C once sufficient cell concentrations have been reached in the stationary phase. This allows there to be an optimized process that requires less heat input due to the lower cultivation temperature and at the same time produces more valuable α-humulene.

3. Chapter 2 | Individual process steps optimization of *C. necator*-catalyzed production of α-humulene

This chapter has been published as follows:

Becker L, Dietz E, Holtmann D. Individual process steps optimization of *Cupriavidus necator*-catalyzed production of α-humulene. Biochemical Engineering Journal. 2024; 215:109617. doi:10.1016/j.bej.2024.109617. *

* Author contributions: E.D.: Investigation. L.B.: Writing – review & editing, Writing – original draft, Visualization, Methodology, Investigation, Data curation. D.H.: Writing – review & editing, Supervision, Project administration, Funding acquisition, Conceptualization.

3.1. Abstract

Despite the enormous advantages over traditional plant extraction or chemical synthesis, the microbial production of the valuable sesquiterpene α-humulene using *C. necator* has so far been conducted under non-optimized process conditions. However, optimizing this process would be helpful to meet the growing terpene demand across various application sectors. In this chapter, the established process parameters, including the composition of the minimal medium, the L-rhamnose induction and the process temperature, were varied and optimized using shake flasks. Furthermore, the *C. necator*-based α-humulene production process was divided into two temperature stages. When compared to the initial conditions, these optimizations resulted in an enhanced *C. necator* growth and/or elevated α-humulene levels. The combination of all individual optimizations into an integrated process led to a notable increase in sesquiterpene levels, from 9.5 to 32.4 mg/L, representing a 241 % increase compared to the initial conditions without any optimizations.

3.2. Introduction

The terpenome, which includes terpenes and their subgroups, represents the largest group of natural products, with over 80,000 different structures described [15]. Terpenes exhibit a high degree of structural diversity and are involved in a multitude of essential functions and metabolic processes across a vast array of organisms, spanning from plants to microorganisms and animals [15]. The sesquiterpene α-humulene, also known as α-caryophyllene, constitutes a subgroup of terpenes and is a valuable natural compound found in a multitude of plants and even in some marine eukaryotes [22, 23]. Applications in the fragrance, food, and cosmetic industries [154-156], along with properties such as anti-inflammatory effects [157], lead to increased production demand.

The microbial production of α-humulene offers significant advantages over traditional plant extraction and chemical synthesis with regard to numerous economic drawbacks, including low yields, high downstream processing costs, and a reliance on fossil-based processes [73, 49]. The benefits of a microbial production of α-humulene include economic considerations, controllability, scalability, and the potential for genetic engineering to improve final product levels. *C. necator* serves as an ideal host for α-humulene production through the previously described properties, such as its flexibility in metabolizing various carbon sources [59]. By transforming the PHB-deficient *C. necator* PHB-4 strain with the L-rhamnose-inducible plasmid pKR-hum, the production platform was expanded to include the recombinant MVA pathway from *M. xanthus* [73].

Biotechnological processes can be divided into individual biological steps known as unit processing operations (UPOs). Understanding and controlling these UPOs is a prerequisite for a high-quality and robust manufacturing process [90]. As even small changes in cultivation temperature or media composition can have a major impact on the growth of *C. necator* H16 [158] or on bacterial heterogeneity in general, and thus on the efficiency of product formation, this understanding is very essential. For the first time, these parameters were investigated and varied as well as the published standard conditions for cultivation and induction [5, 74, 13] of *C. necator* pKR-hum with the aim of developing a simple process optimization strategy. In the literature, *C. necator* pKR-hum grown in lysogeny broth medium achieved a α-humulene level of 10 mg/L after 42 h of production in a heterotrophic batch cultivation [13]. In contrast, *C. necator* pKR-hum grown in the minimal medium [81] used in this work produced α-humulene levels of up to 9.4 mg/L after 52 h [5]. Individual process parameters can often interact with or reinforce each other in unknown and complex ways, which can lead to high variations in bacterial growth and potential product formation. Here, the focus was on different parameters to increase the level of α-humulene, including an optimization of the growth media composition, the adaptation of cultivation, and the L-rhamnose induction conditions. In addition to optimizing individual process steps, multiple optimizations were combined into a single process.

3.3. Materials and methods

The following chapters describe the standard methodology and parameters of the fermentation experiments, which were consistently applied unless otherwise stated. Individual process condition changes as a deviation from the standard run, see figure legends. All experimental works, including the results presented in this chapter and the appendix 7.6 - 7.8, were carried out in triplicate.

3.3.1. Heterotrophic cultivation and biomass monitoring of *C. necator* pKR-hum

Heterotrophic cultivation and biomass monitoring were performed following the procedure described in chapter 2.3.1. The appropriate amount of biomass needed to inoculate the main culture to a starting OD_{600} of 0.1 (equivalent to 0.043 g/L biomass, determined by dry mass analysis, see chapter 2.4.1) was transferred to a sterile reaction tube, centrifuged, and the pellet obtained was resuspended in 20 mL of the main culture medium, supplemented with 15 µg/mL of TC.

The main culture was also cultivated at 30 °C with 180 rpm (Ecotron, Infors HT; Bottmingen, Switzerland) in 250 mL Erlenmeyer flasks, unless other cultivation temperatures were stated. During the main cultivations, the biomass was monitored online in terms of backscattered light intensity measuring every 60 s using the Cell Growth Quantifier® device (CGQ, Scientific Bioprocessing; Pittsburgh, USA).

3.3.2. Preparation and composition of preculture and main culture media

The standard composition of the minimal medium (MMasy) used in all the cultivations, according to Sydow et al. [81], is listed in chapter 2.3.2 Tab. 3 and Tab. 4. To prepare the minimal medium, stock solutions were prepared with deionized water in the same way as the individual components listed in Tab. 3. After dissolving the media components, all stock solutions, except the trace element stock (Tab. 4), were autoclaved and stored at room temperature. This standard composition of the minimal medium was used in all experiments, unless other compositions were specified. LB and super optimal broth (SOB) preculture media were prepared according to the standard recipes, see chapter 2.3.1 Tab. 2 and appendix 7.5 Tab. 11.

3.3.3. Microbial α-humulene production using *C. necator* pKR-hum

Microbial α-humulene production was performed using *C. necator* pKR-hum according to the procedure described in chapter 2.3.3. For standard process conditions, *C. necator* pKR-hum main cultures were cultivated as described in chapter 3.3.1 and induced at an OD_{600} between 0.50 and 0.70 (*C. necator* pKR-hum biomass 0.2 - 0.3 g/L) with a final concentration of 0.2 % (w/v) L-rhamnose to initiate α-humulene production, unless otherwise stated, which was achieved by a hundredfold dilution of a 20 % (w/v) L-rhamnose stock solution prepared in deionized water. Extracellular α-humulene was removed from the culture process through *in situ* product removal. To achieve this, 4 mL of n-dodecane was added to 20 mL of cultivation broth as a suitable and biocompatible extraction agent after induction [8], corresponding to 20 % (v/v) pure n-dodecane. This created a second phase above the cultivation broth, from which samples were taken immediately after induction and the addition of n-dodecane, as well as at 8, 24, and 48 h later.

3.3.4. Quantification of fructose using high performance liquid chromatography (HPLC)

Quantification of fructose was carried out following the procedure described in chapter 2.3.4.

3.3.5. Quantification of α-humulene using gas chromatography (GC-MS)

The following section outlines only the modifications, all other procedures were performed as described in chapter 2.3.5. Due to the low water solubility of the product α-humulene in the fermentation broth, *in situ* product removal was performed. For this purpose, the extracellularly released α-humulene was extracted into a 20 % (v/v) n-dodecane phase (4 mL), which was present in the Erlenmeyer flask during the fermentation process.

3.4. Results and discussion

In the following, the effects of changing individual process factors on *C. necator* pKR-hum biomass growth and α-humulene concentration were investigated. For this purpose, process factors such as the composition of the minimal medium, the L-rhamnose induction concentration and timing, as well as the cultivation temperature and preculture medium were individually varied, tested, adapted and combined in a final run.

3.4.1. Optimized sugar concentration in minimal media

The growth of *C. necator* pKR-hum at different fructose concentrations between 2 and 32 g/L in standard minimal medium was recorded in an uninduced (Fig. 12 - A) and an induced culture (Fig. 12 - B). Additionally, the maximum growth rate μ_{max}, the residual fructose content after 24 h, yield coefficients $Y_{X/S}$, $Y_{P/X}$ and $Y_{P/S}$, and α-humulene levels after 16 h of production were determined as growth and production characteristics (Fig. 12 - C). Please refer to the appendix 7.3 (formulas 3 - 6) for details on the calculation of maximum growth rate values and the yield coefficients.

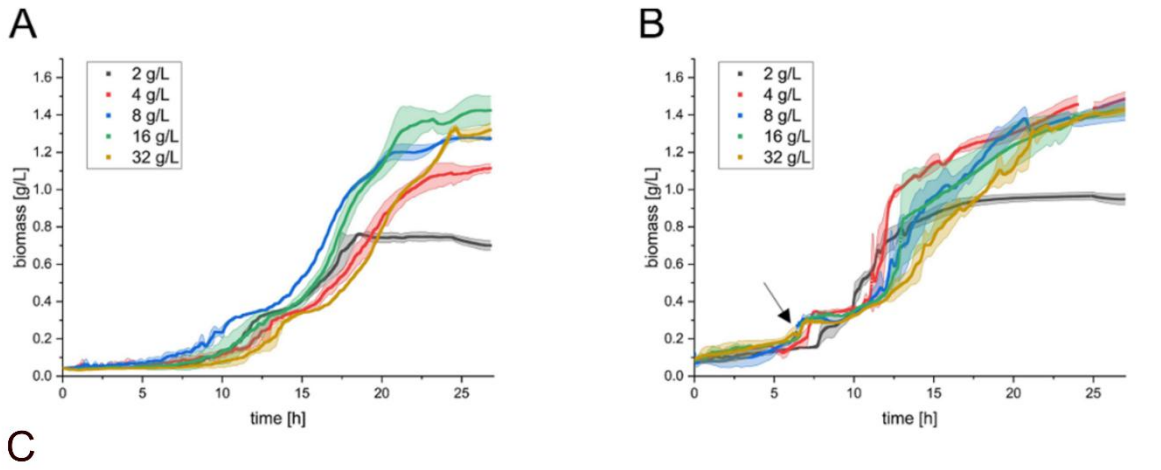

C

$C_{fructose\ initial}$ [g/L]	μ_{max}		$C_{fructose\ 24\ h}$ [g/L]		$Y_{X/S\ 24\ h}$		$Y_{P/X\ 16\ h}$	$Y_{P/S\ 16\ h}$	$C_{\alpha\text{-humulene}\ 16\ h}$ [mg/L]
	no induction	induction	no induction	induction	no induction	induction	induction	induction	induction
2	0.159 ± 0.012	0.230 ± 0.050	0	0	0.351 ± 0.005	0.410 ± 0.033	2.599 ± 0.056	1.067 ± 0.107	2.12 ± 0.12
4	0.147 ± 0.008	0.151 ± 0.013	0.89 ± 0.17	0	0.339 ± 0.041	0.369 ± 0.007	3.201 ± 0.332	1.183 ± 0.140	4.72 ± 0.46
8	0.193 ± 0.012	0.150 ± 0.009	4.91 ± 0.08	4.00 ± 0.60	0.390 ± 0.008	0.349 ± 0.099	3.542 ± 0.469	1.232 ± 0.341	4.57 ± 0.61
16	0.210 ± 0.020	0.155 ± 0.005	12.70 ± 0.30	12.44 ± 0.12	0.405 ± 0.051	0.369 ± 0.029	4.350 ± 0.854	1.623 ± 0.405	5.68 ± 1.16
32	0.177 ± 0.012	0.131 ± 0.009	26.49 ± 0.11	28.26 ± 0.29	0.232 ± 0.013	0.247 ± 0.018	4.578 ± 0.582	1.748 ± 0.094	6.52 ± 0.16

Fig. 12: (A) *C. necator* pKR-hum growth at different fructose concentrations in minimal media, 180 rpm and 30 °C, uninduced (n = 3); (B) *C. necator* pKR-hum growth at different fructose concentrations in minimal media, 180 rpm and 30 °C, induced with 0.2 % (w/v) L-rhamnose at 0.2 - 0.3 g/L biomass and the addition of 20 % (v/v) n-dodecane as an extracting agent, see arrow (n = 3); (C) Performance indicators for the growth of *C. necator* pKR-hum in the uninduced (Fig. 12 - A) and induced (Fig. 12 - B, after 16 h of production) cultures.

Different starting concentrations of fructose in the minimal medium were reflected in the growth behavior of *C. necator* pKR-hum (Fig. 12 - A & B). Adding n-dodecane to extract the α-humulene in the induced state (Fig. 12 - B) influenced and increased the measured backscatter values. A fructose concentration of 2 g/L resulted in an early stationary phase after 18 h with a final biomass of 0.70 and 0.94 g/L in the uninduced (Fig. 12 - A) and induced state (Fig. 12 - B), respectively. The highest fructose concentration of 32 g/L resulted in a late stationary phase and a prolonged exponential phase in both cases. Fructose concentrations of 4, 8, and 16 g/L in the induced state (Fig. 12 - B) performed similarly to the concentrations of 8 and 16 g/L in the uninduced state (Fig. 12 - A).

In summary, a similar *C. necator* pKR-hum growth behavior was monitored at fructose concentrations ranging from 8 to 32 g/L in both the uninduced and induced states.

Initial fructose concentrations of 8 and 16 g/L in the minimal medium proved to be suitable for prolonged cultivation and a sufficient α-humulene production, with final biomasses of up to 1.3 - 1.5 g/L and $Y_{P/X}$ of up to 4.35 ± 0.85 mg α-humulene per g biomass (see Fig. 12 - C).

Lower fructose concentrations, such as 4 g/L, showed no residual fructose content after 24 h process time in the induced state, as the induced formation of the product α-humulene, combined with the plasmid-induced metabolic burden, represents an additional load on the metabolism compared to plasmid-free cells [159]. A fructose concentration of 2 g/L clearly limits growth, with a low final biomass of 0.70 and 0.94 g/L achieved in both the uninduced and induced cultures. Too high levels of fructose in the minimal medium can also negatively affect *C. necator* growth, for example, through osmotic stress or an imbalance in carbon metabolism due to excessive fructose uptake rates. These limitations of cell growth, which were observed at too low (2 g/L) or too high (32 g/L) fructose concentrations, have also been described in the literature, where fructose concentrations between 5 and 25 g/L have proven to be reliable for the cell growth of *C. necator* H16 [158]. In addition to the influence of the fructose concentration on growth and carbon metabolism, secondary factors, such as the availability of inorganic nutrients in the medium described by the C/N/P ratio [64], also exert an effect.

In consideration of the observed growth behavior of *C. necator* pKR-hum and the high yield coefficients, a concentration of 8 g/L fructose was confirmed as suitable in this work. Additionally, residual fructose was observed at the end of the α-humulene production process, indicating that a carbon limitation did not occur over the course of the process. The biomass/substrate yield coefficient $Y_{X/S}$ for fructose is also high at this concentration and indicates efficient biomass formation and fructose utilization (see Fig. 12 - C). With a value of 0.39 in the uninduced state, it is close to the modeled maximum value of 0.53 for fructose in *C. necator* [160], which, however, does not take into account gene expression and other regulatory factors. The biomass curve of the induced cultivation (Fig. 12 - B), which is based on a backscatter signal, shows a sudden increase after the induction point (black arrow). This increase in the backscatter signal, as well as the higher standard deviations, can be explained by the addition of 20 % (v/v) n-dodecane for *in situ* product removal.

In general, the addition of second phase- and droplet-forming solvents, such as n-dodecane to the aqueous cultivation system, could have a disturbing effect on backscattering measurements [161]. With regard to residual fructose contents, and in order to avoid possible limitations, an optimization of the fructose content from 4 g/L to 8 g/L in the minimal medium was implemented. It should be noted that in terms of fructose utilization, a concentration of 4 g/L fructose is the best amount.

3.4.2. Iron supplementation in minimal media

The growth of *C. necator* pKR-hum was measured at various iron (II) chloride tetrahydrate and iron (II) sulfate heptahydrate levels between 1 and 15 times of their standard amount (0.75 mg/L $FeSO_4$ * 7 H_2O [13]) in standard minimal medium in an uninduced culture (Fig. 13). For this purpose, the standard composition of the minimal medium was supplemented with the appropriate concentrations of iron (II) sulfate heptahydrate and iron (II) chloride tetrahydrate.

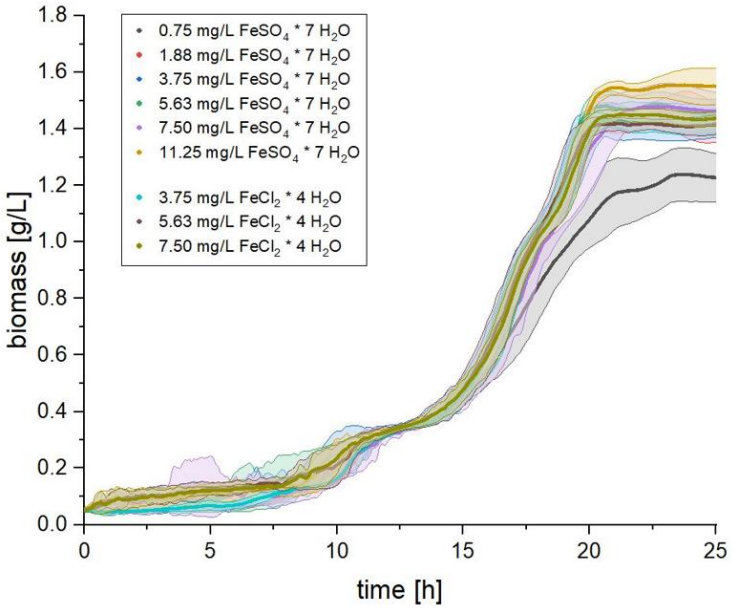

Fig. 13: *C. necator* pKR-hum growth according to different iron (II) sulfate heptahydrate and iron (II) chloride tetrahydrate concentrations in minimal media; 180 rpm and 30 °C, uninduced (n = 3).

The addition of iron salts to the standard minimal medium containing an iron content of 0.75 mg/L iron (II) sulfate heptahydrate (black line) promotes the growth of *C. necator* pKR-hum (Fig. 13). When the iron salt concentration is increased 2.5 - 15 times, the *C. necator* pKR-hum exponential growth phases occur with higher maximum specific growth rates μ_{max} up to 0.26 ± 0.05 h^{-1} and final biomasses of 1.6 g/L. In comparison to the cultivation with a standard minimal medium containing an iron salt content of 0.75 mg/L iron (II) sulfate heptahydrate without iron supplement, a μ_{max} of 0.17 ± 0.01 h^{-1} and final biomasses of 1.3 g/L were achieved. This effect can be observed from a 2.5-fold increase in the iron salt standard level of the minimal medium, and does not differ between the iron (II) sulfate heptahydrate and iron (II) chloride tetrahydrate salts tested.

Given that iron is an essential nutrient for most organisms and is required for numerous enzymatic processes, as prosthetic groups with a catalytic effect or as cofactors, iron is also involved in a multitude of metabolic processes, cell growth, or cell division [94]. However, no difference in growth behavior could be observed when adding iron (II) sulfate heptahydrate or iron (II) chloride tetrahydrate in the same concentrations. Both compounds optimized the growth behavior equally, depending on their concentrations used, indicating that the iron source has no influence. Consequently, the intracellular iron availability can be increased by an extracellular increase in iron level, as only extracellular iron ions are bound and transported into cells by special proteins like transferrin [162]. Siderophores, such as cupriabactin, have also been shown to promote the growth of *C. necator* JMP134 by increasing the rate of intracellular iron uptake [163]. In addition, the promoted growth observed in this work can also be explained by the protective properties of cupriabactin, as it plays a crucial role in the protection against oxidative stress and toxic aromatic compounds. Many of the protective enzymes involved in these degradation processes require iron in their active enzyme structure and increase their activity through a cupriabactin-induced iron uptake into the cytosol. [163, 164]

Gram-negative bacteria, such as *C. necator*, require a minimum iron concentration of 0.017 - 0.101 mg/L [165] for their growth, which means that the standard iron (II) sulfate heptahydrate concentration of 0.75 mg/L (equals 0.15 mg/L iron) in the minimal medium should adequately cover this requirement. However, it was possible to show that a minimal increase in the iron (II) sulfate heptahydrate concentration from 0.75 to 1.88 mg/L is sufficient and results in an increased *C. necator* biomass growth. In order to exclude possible limitations, a 5-fold increase (3.75 mg/L) in established iron (II) sulfate heptahydrate level was added to the minimal medium for optimization in subsequent experiments.

3.4.3. Optimization of the L-rhamnose inducer concentration and dosage time

Subsequently, an investigation was conducted to determine the influence of the L-rhamnose inducer concentration and the induction time on α-humulene production. To this end, the α-humulene production of *C. necator* pKR-hum was analyzed after an induction with different concentrations of 0.2, 1, and 2 % (w/v) L-rhamnose at 0.2 - 0.3 g/L biomass (Fig. 14). Furthermore, the impact of the L-rhamnose induction time on α-humulene production was investigated. Additionally, a potential uptake or consumption of the extracellularly added L-rhamnose over the course of fermentation was evaluated. It was confirmed that *C. necator* pKR-hum does not store or consume L-rhamnose, as the content in the extracellular minimal medium remains constant over the course of fermentation (appendix 7.6, Fig. 31 - B). The results also indicate that the final α-humulene production depends on the L-rhamnose induction time; see appendix 7.6 Fig. 32.

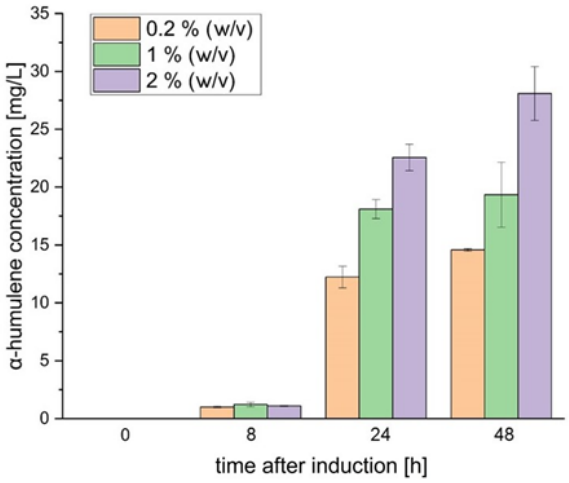

Fig. 14: α-Humulene levels according to different L-rhamnose inducer concentrations in minimal media, at 180 rpm and 30 °C, *C. necator* pKR-hum induced at 0.2 - 0.3 g/L biomass (n = 3).

The corresponding yield coefficients are shown in the appendix 7.6 Fig. 31. Fig. 14 illustrates that an elevated L-rhamnose concentration of 2 % (w/v) enhances the final α-humulene level in comparison to the established standard concentration of 0.2 % by 84 and 93 %, respectively, after 24 and 48 h. An increase from 0.2 % to 1 % (w/v) L-rhamnose concentration (green bar) also results in higher product levels.

The pKR-hum plasmid used in this work, for the heterologous expression of α-humulene, is based on a L-rhamnose-inducible system, which offers a tight regulation of expression at

higher rates compared to other established promoters such as the lactose-inducible P_{Lac} [74]. Varying L-rhamnose levels in *C. necator* pKRrha resulted in a proportional increase in gene expression, as indicated by the increased specific fluorescence of the enhanced green fluorescent protein (eGFP), with 0.20 % (w/v) L-rhamnose (11 mM) yielding the highest gene expression [74]. In later studies, the standard L-rhamnose induction concentration was therefore set at 0.2 % (w/v) [13].

Raising the L-rhamnose concentration from 0.2 % (w/v) to 1 % or 2 % (w/v) resulted in a 33 % or 93 % increase in final α-humulene levels after 48 h. Higher L-rhamnose levels enhance the activation of the transcriptional activator RhaR, triggering rhaSR expression, which leads to RhaS accumulation and the activation of the L-rhamnose operon rhaBAD at the plasmid level [96], ultimately boosting α-humulene synthase gene expression using the plasmid pKR-hum. The L-rhamnose induction time resulted in lower α-humulene levels after induction at early (0 h) and late (17 h and 21 h) growth phases (appendix 7.6, Fig. 32). Early induction impacts further cell growth and energy metabolism, leading to lower levels. Late induction, close to the stationary phase at reduced cell viability and performance, reduces the final product levels as well. The ideal induction time in the initial exponential phase after 11 h was therefore confirmed for *C. necator* pKR-hum. At this point, the induction time is not too early, which can increase metabolic stress, and not too late, because the growth and performance rates of the culture are high and can be utilized for an increased production [95].

3.4.4. Batch process with different cultivation temperature stages

In order to investigate a possible influence of the cultivation temperature on α-humulene levels, the formation of α-humulene by *C. necator* pKR-hum as a function of process temperature was investigated (Fig. 15). All cells were incubated at 30 °C with 180 rpm until induction in the range of 0.2 - 0.3 g/L biomass using 0.2 % (w/v) L-rhamnose. After the induction step, the cultivation temperature was either changed to 25 °C and 20 °C, or kept at 30 °C as the control. These temperatures were maintained until the experiment ended.

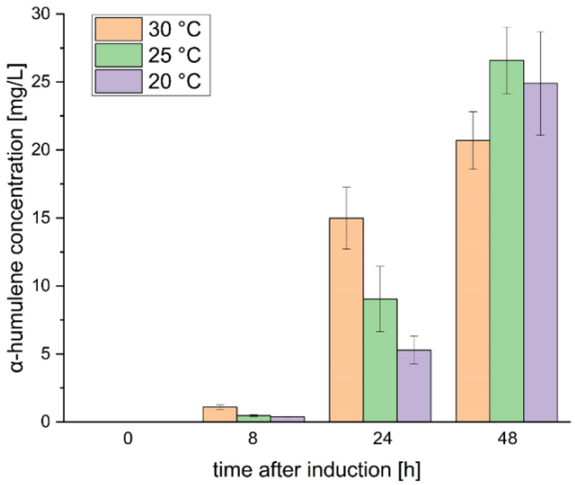

Fig. 15: α-Humulene levels at different cultivation temperatures in minimal media after induction, *C. necator* pKR-hum induced with 0.2 % (w/v) L-rhamnose at 0.2 - 0.3 g/L biomass, at 180 rpm and 30 °C until induction, then switch to the displayed temperature (n = 3).

The α-humulene level over time, depending on the cultivation temperature, is shown above (Fig. 15). It can be concluded that the highest cultivation temperature of 30 °C leads to the greatest α-humulene levels at the measurement points of 8 and 24 h post-induction. However, reducing the cultivation temperature to 25 °C after induction results in a higher final α-humulene level after 48 h compared to the standard temperature of 30 °C. Specifically, the final α-humulene level increases by 28 % at 25 °C and by 20 % at 20 °C compared to the cultivation at 30 °C. The corresponding product yield coefficients $Y_{P/S}$ and $Y_{P/X}$ further support this observation after 48 h, as shown in the appendix 7.7 (Fig. 33).

Although lowering the culture temperature from 30 °C to 25 °C slows down the growth behavior of *C. necator* pKR-hum, with a final biomass in a similar range (following Fig. 16 - B), this reduced cell growth and the subsequent decrease in α-humulene production competes with the benefits of the lower temperature. This explains why, at 8 and 24 h post-induction, the α-humulene level is highest at 30 °C. However, after 48 h, the optimal temperature for production shifts to 25 or 20 °C. Data collected 48 h after induction revealed a significant difference in mean α-humulene levels between 30 and 25 °C, as indicated by an unpaired t-test with Welch's correction. The p-value of 0.064, at a significance level of 0.10, suggests that α-humulene levels are higher at 25 than at 30 °C. This indicates that lower temperatures may enhance production efficiency. During this 48 h period, the cells recover from the temperature-related growth slowdown, and the lower temperatures can now exert their positive effect on α-humulene production.

For an optimization of the overall process, the temperature was therefore lowered from 30 to 25 °C in the final run no earlier than 24 h after induction.

Lowering the cultivation temperature is a common strategy in recombinant protein expression to improve protein folding efficiency and reduce the formation of insoluble aggregates, such as inclusion bodies. In *E. coli*, for example, Sivashanmugam et al. demonstrated that the expression of heterologous proteins can be optimized by decreasing the cultivation temperature from 37 to 23 °C after induction [166]. This effect may have contributed to a higher proportion of active protein in this work. Additionally, Strocchi et al. have shown that in *E. coli*, the activity and production of many chaperones increase at lower cultivation temperatures [167]. For example, in *C. necator*, the increased expression and activity of GroESL chaperones contributed to a higher heterotrophic isopropanol production [67]. In other words, these factors combined lead to a better folding and stability of soluble proteins and enzymes at lower temperatures.

Since this is a case of heterologous gene expression, and the α-humulene synthase is derived from the ginger plant *Zingiber zerumbet* [5], its optimal temperature may also fall within the lower physiological range of sesquiterpene synthases, which is generally reported to be between 20 and 40 °C [168]. Given that a temperature of 25 °C is within this range, it may be more favorable for the activity of the α-humulene synthase compared to 30 °C. The increased chaperone activity, improved protein folding, and reduced aggregate formation at lower cultivation temperatures, along with the likely lower temperature optimum of the terpene synthases used, may explain the increased α-humulene production observed in this work at 25 °C as compared to 30 °C.

3.4.5. Impact of preculture media and cultivation temperature on main culture growth

To investigate the effect of the composition of preculture media on the growth of the main culture, *C. necator* pKR-hum precultures were grown overnight in SOB and LB media. The main cultures were then inoculated to an OD_{600} of 0.1 from SOB or LB precultures, and incubated at 30 °C with 180 rpm (Fig. 16 - A). Additionally, the cultivation temperature of the main cultures was varied after inoculating from LB precultures at 25, 30, 32, or 35 °C, and the cell growth was monitored (Fig. 16 - B).

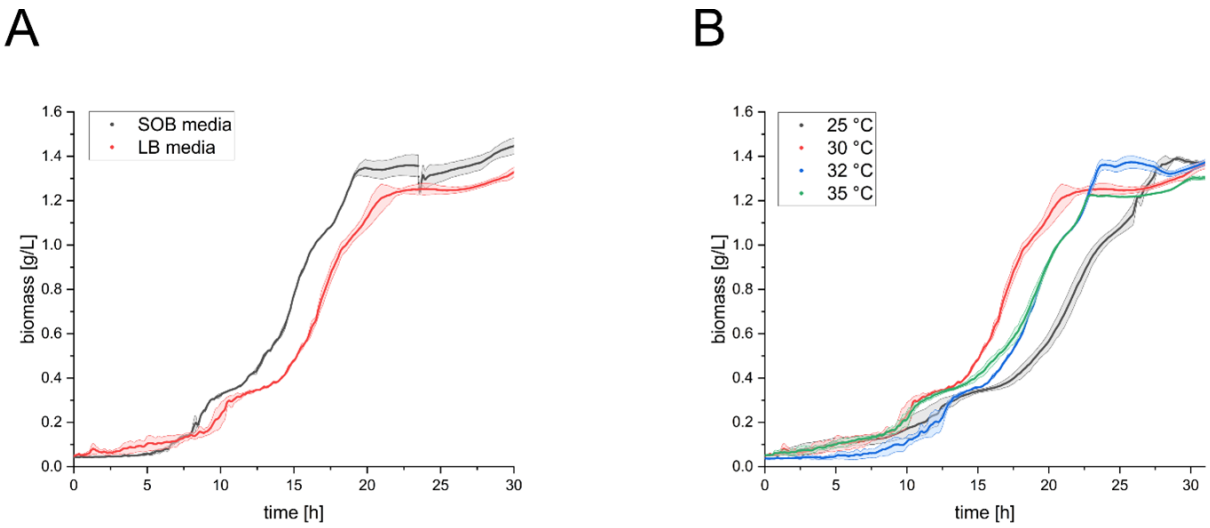

Fig. 16: (A) *C. necator* pKR-hum main culture growth in minimal media following inoculation from lysogeny broth (LB) or super optimal broth (SOB) media precultures, at 180 rpm and 30 °C, uninduced; (B) *C. necator* pKR-hum main culture growth in minimal media at different cultivation temperatures, inoculated from LB precultures, at 180 rpm and uninduced (n = 3).

Using a SOB medium as a preculture has a similar effect on the *C. necator* pKR-hum main culture growth behavior compared to a LB medium (Fig. 16 - A), which is why the LB medium was kept as the standard preculture medium. However, the main culture grown in a minimal medium shows a shorter lag phase when inoculated from the SOB preculture compared to the LB preculture. Additionally, the final biomass of the main culture is higher at 1.42 g/L after inoculation from the SOB preculture, compared to 1.30 g/L from the LB preculture. Changing the cultivation temperature from 30 °C to 25 °C also delays the growth of the *C. necator* pKR-hum main culture in the minimal medium, resulting in a longer exponential phase and in a stationary phase that starts up to 6 h later (Fig. 16 - B). The standard temperature of 30 °C promotes the best cell growth among the tested temperatures. When the temperature is increased to 32 or 35 °C, or lowered to 25 °C, the lag- and exponential phases are extended by up to 2.5 h and 6 h, respectively, compared to 30 °C, although the final biomasses remain similar.

The faster growth and the higher final biomass of the *C. necator* pKR-hum main cultures inoculated from SOB medium precultures may be due to the SOB medium being richer in nutrients, containing extra KCl and $MgSO_4$, as compared to the LB medium. This is supported by literature, indicating that magnesium, sulfate, and potassium are important for promoting the growth of *C. necator* [169]. The different cultivation temperatures tested lead to longer lag phases and lower maximum growth rates, this could be observed in *C. necator* when the temperature deviated from the optimal level of 30 °C [93]. The lag phase is prolonged by

microbial adaptation processes to lower or higher temperatures, delaying the start of the exponential phase [152]. However, at the end of the cultivation process, the final biomass reached similar levels of 1.30 - 1.35 g/L across the tested temperature range of 25 - 35 °C.

3.4.6. Combined optimization throughout the whole process vs. standard conditions

After optimizing several single steps throughout the production of α-humulene, the key question was how these combined effects would influence the overall process performance. The standard parameters were extended, based on the following insights. Minimal medium optimizations included (i) an increase of fructose from 4 to 8 g/L and (ii) the addition of 3.75 mg/L iron (II) sulfate heptahydrate. For induction step optimizations, (iii) the concentration of L-rhamnose was increased from 0.2 % to 2 % (w/v), and (iv) the cultivation temperature was reduced to 25 and 20 °C, 24 h after the induction step, from an initial temperature of 30 °C. An induction time of 11 h after inoculation (induction step) was set during the initial exponential phase, with biomass ranging from 0.2 to 0.3 g/L, as adopted from standard parameters. α-Humulene levels were measured under both standard and optimized conditions at 25 and 20 °C (Fig. 17).

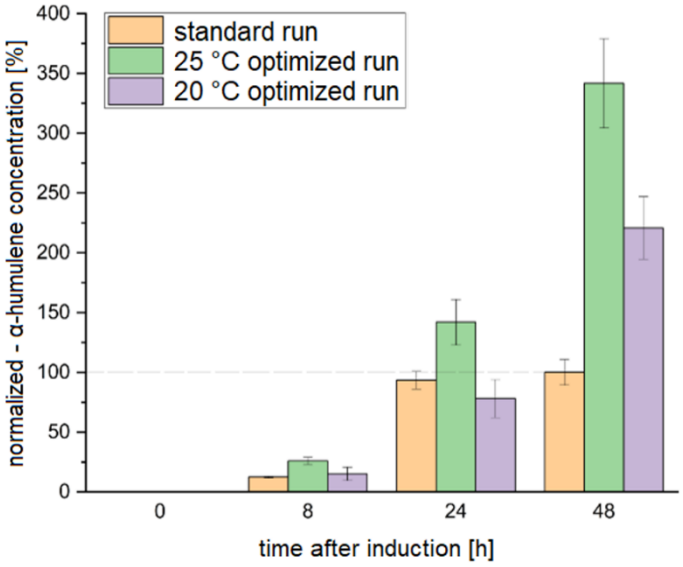

Fig. 17: α-Humulene levels according to standard and optimized conditions and temperatures (n = 3); *C. necator* pKR-hum, at 180 rpm and 30 °C, standard process induced with 0.2 % (w/v) L-rhamnose at 0.2 - 0.3 g/L biomass, optimized process induced with 2 % (w/v) L-rhamnose at 0.2 - 0.3 g/L biomass and switched to 25 and 20 °C cultivation temperature 24 h after induction, α-humulene levels normalized to the 48 h standard run, set as 100 %.

Fig. 17 illustrates that maintaining a continuous cultivation temperature of 30 °C, along with the established standard parameters (standard run), results in considerably lower α-humulene levels than in the optimized run at 25 °C at the measurement times of 8, 24, and 48 h after induction. Notably, all α-humulene levels were normalized to the 48 h level of the standard run, which was considered as 100 %. With the optimized process conditions, final α-humulene levels increased by 241 % at 25 °C, and by 121 % at 20 °C, after 48 h, compared to the levels achieved under standard conditions at 30 °C after 48 h. These values are normalized for illustration in Fig. 17. The corresponding figure, showing absolute α-humulene levels, can be found in the appendix 7.8 (Fig. 34). Corresponding growth measurements indicate that a cultivation with optimized parameters shortens the lag phase, yielding similar final biomass concentrations between 1.50 and 1.55 g/L compared to the established standard conditions. The data are provided in the appendix 7.8 (Fig. 35). Increasing the fructose minimal medium content, the iron (II) sulfate heptahydrate minimal medium content, the L-rhamnose induction level, and dividing the batch process into two cultivation temperature stages (30 and 25 °C), led to an optimization of the overall process performance compared to the established standard process parameters.

3.5. Conclusions

The aim of this work was to optimize the microbial α-humulene production in order to increase the biomass and the terpene production of *C. necator* pKR-hum. The analysis and the variation of the process parameters were successful. The optimized parameters leading to an increased biomass and an increased α-humulene production are a fructose concentration of 8 g/L, an iron (II) sulfate heptahydrate concentration of 3.75 mg/L, a L-rhamnose concentration of 2 % (w/v), and a splitting of the whole process into two cultivation temperature stages of 30 and 25 °C. Combining the optimized individual parameters led to an increased α-humulene level of 241 % compared to the non-optimized process. With this work, it was shown that it is possible to optimize the *C. necator*-based α-humulene production process by adjusting the standard parameters.

4. Chapter 3 | Robustness of the *C. necator*-catalyzed production of α-humulene

This chapter has been published as follows:

Becker L, Dietz E, Holtmann D. Robustness of the *Cupriavidus necator*-Catalyzed Production of α-Humulene. Bioengineering. 2025; 12.3:323. doi:10.3390/bioengineering12030323. *

* Author contributions: E.D.: Investigation. L.B.: Writing – review & editing, Writing – original draft, Methodology, Investigation, Data curation, Formal analysis, Conceptualization. D.H.: Writing – review & editing, Supervision, Project administration, Funding acquisition, Conceptualization.

4.1. Abstract

The increasing global demand for natural substances such as the sesquiterpene α-humulene makes optimizing microbial production essential. A production process using the versatile host *C. necator* was improved by adjusting the minimal media and process parameters as described in the previous chapters. In this context, microbial and process robustness were examined as key factors for maintaining consistent performance. Established process improvements and the impact of common or individual precultures were analyzed and quantified for their effect on the robustness of product and biomass formation. A robust α-humulene production process with even more consistent biomass formation using *C. necator* pKR-hum can be reported. Even with a simulated process disturbance, 79 % of the maximum α-humulene level was still produced. Overall, the analysis of the results shows that the α-humulene production process using *C. necator* pKR-hum is highly robust, demonstrating its resilience to process disturbances and suitability for industrial applications.

4.2. Introduction

The microbial production of complex, bio-based compounds has gained significant attention due to its efficiency and versatility, and it is increasingly being adopted in industrial manufacturing processes. Beyond its established applications in areas such as the food industry, α-humulene is also attracting growing interest due to its potential anti-microbial [170] and anti-cancer [171] properties in pharmaceutical development. However, robustness plays a critical role in the microbial production of α-humulene, particularly in the context of fermentation and process intensification. Ensuring process robustness is therefore a key consideration when optimizing α-humulene production. Process robustness is defined by Olsson et al. as the ‘ability of a system to maintain unchanged performance when one or more perturbations occur’ [172]. Additionally, microbial robustness must be considered in relation to the production host, which ideally maintains consistent biomass and product formation rates despite process disturbances or changes [173].

A production method that is robust at both the process and microbial cell levels is essential for the efficient bioproduction of valuable natural substances. Understanding this is key to subsequent bioprocess intensification. Therefore, the robustness of microbial α-humulene production can be enhanced by adjusting or optimizing individual process parameters. To better understand how these factors influence the process robustness of α-humulene production using *C. necator* pKR-hum, the different process conditions that were shown to affect biomass formation and α-humulene production were investigated.

These conditions include optimizations that increased α-humulene production and biomass formation, as described in chapters 3.4 and 3.5. Key parameters tested include the concentration of iron (II) sulfate heptahydrate in the minimal medium, the concentration of the inducer L-rhamnose, and the process cultivation temperature. A 5-fold increase in the established iron (II) sulfate heptahydrate concentration (to 3.75 mg/L) led to increased *C. necator* biomass growth [77]. Additionally, increasing the L-rhamnose inducer concentration from 0.2 % to 2 % (w/v), along with decreasing the cultivation temperature 24 h after the induction step, resulted in higher α-humulene levels [77]. In addition to examining the effects of the implementation of individual process conditions on robustness against standard parameters, the potential impact of inoculating the main cultures from either common or individual precultures was also tested.

The robustness of α-humulene production and biomass formation (n = 6) in *C. necator* pKR-hum across various conditions was calculated according to formula (2), adopted from Trivellin et al. [174]:

$$R = -\frac{\sigma^2}{\bar{x}} \qquad (2)$$

When calculating robustness, both positive and negative deviations from the mean value ($\bar{x}$) affect the robustness value (R) due to the variance (σ^2). An R value of 0 indicates ideal robustness. However, the robustness value alone does not directly reflect process performance, although value ranges can be compared with each other. For example, Torello Pianale et al. showed that the glycerol yield (g/g) of *S. cerevisiae* CEN.PK113-7D and PE2 can be described with robustness values of -0.8 and -0.5, respectively, while the cell mass yield (g/g) for these strains was calculated as -0.6 and -0.4 [175]. These results suggest that cell mass formation is a more robust sub-process with fewer fluctuations than glycerol production in both strains.

This work quantitatively assesses how key process parameters affect the robustness of α-humulene production in *C. necator* pKR-hum. By comparing their effects, along with preculture handling, on the robustness of α-humulene and biomass formation, insights are provided for optimizing microbial processes in industrial applications. Understanding these factors is crucial for developing robust, scalable production systems for α-humulene and other valuable bio-based compounds using the versatile *C. necator* strain.

4.3. Materials and methods

The materials and methods used in this chapter were partially adopted from chapter 3.3. The following sections describe the standard methodology and parameters for the fermentation experiments, which were consistently applied unless stated otherwise. Individual process condition changes as deviations from the standard run are noted in the Figure legends.

The 2-phase temperature run included two cultivation temperature stages: 30 °C until 24 h after induction, followed by a switch to 25 °C. The final combination of all individually modified conditions was tested with 8 g/L D-fructose in addition to the standard 4 g/L as the substrate source. Additional robustness tests, simulating process disturbances with a 12 h shaking pause after the induction step, were performed to assess the robustness of the bacterial production host, *C. necator* pKR-hum.

4.3.1. Heterotrophic cultivation of *C. necator* pKR-hum

Heterotrophic cultivation and biomass monitoring were performed following the procedure described in chapter 2.3.1. *C. necator* pKR-hum main cultures (20 mL of minimal medium in 250 mL Erlenmeyer flasks) were inoculated from either a common preculture (100 mL Erlenmeyer flask containing 10 mL of LB medium + TC) or from individual precultures (15 mL tubes with 3 mL of LB medium + TC) to investigate potential influences of preculture handling. The amount of biomass equivalent to an OD_{600} of 0.1 (0.043 g/L) was taken from the precultures, centrifuged, resuspended in 20 mL of the main culture medium with TC, and cultivated at 30 °C with 180 rpm.

4.3.2. Preculture and main culture media

The standard composition of the minimal medium (MMasy) used in all the cultivations, based on Sydow et al. [81], is listed in chapter 2.3.2 Tab. 3 and Tab. 4. Stock solutions of the components were individually prepared with deionized water. After dissolving the components, all stock solutions, except for the trace element stock, were autoclaved and stored at room temperature. This minimal medium composition was used for all experiments unless stated otherwise due to additional supplementation with $FeSO_4 * 7\ H_2O$. The LB preculture media were prepared following standard recipes, see chapter 2.3.1 Tab. 2.

4.3.3. *C. necator* pKR-hum based α-humulene production

Microbial α-humulene production was performed using *C. necator* pKR-hum according to the procedure described in chapter 2.3.3. Main cultures were induced at an OD_{600} of 0.50 - 0.70 (biomass 0.2 - 0.3 g/L) with 0.2 % (w/v) L-rhamnose (unless otherwise specified). To facilitate *in situ* product removal of the extracellularly released α-humulene, 20 % (v/v) pure n-dodecane was added to the shake flasks immediately after the induction step [8]. A second phase formed above the cultivation broth, from which a control sample was taken directly after the addition of n-dodecane and then a further sample was taken after 48 h.

4.3.4. α-Humulene quantification

The following section outlines only the modification, all other procedures were performed as described in chapter 2.3.5. The extracellularly released α-humulene was extracted into a 20 % (v/v) n-dodecane phase (4 mL), which was present in the Erlenmeyer flask during the fermentation process.

4.4. Results and discussion

Subsequently, the robustness of α-humulene production using *C. necator* pKR-hum was evaluated, focusing on the influence of changes in previously established individual process factors. Factors such as the composition of the minimal medium, L-rhamnose induction concentration, and cultivation temperature were adopted from chapters 3.4 and 3.5, and the resulting robustness was assessed. Additionally, the effect of a simulated process disturbance on the robustness of the production host *C. necator* pKR-hum was investigated.

4.4.1. Effect of preculture handling on robustness of α-humulene production

A growth curve of the production strain *C. necator* pKR-hum was initially recorded in minimal medium under standard process parameters, as seen in Fig. 18.

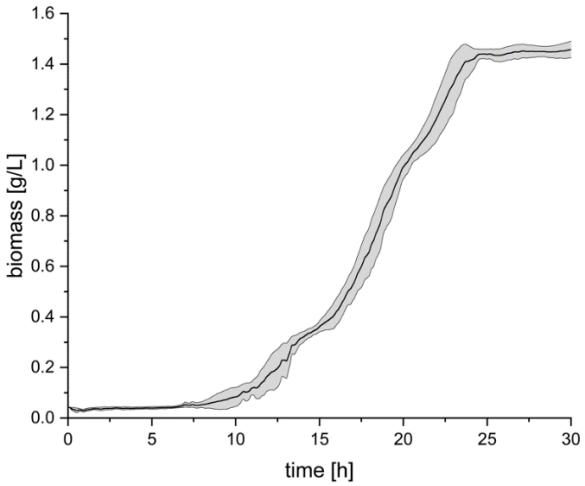

Fig. 18: *C. necator* pKR-hum main culture growth in the minimal medium according to standard process conditions, with the standard media composition as described in chapter 4.3.2, uninduced, at 30 °C with 180 rpm (n = 3).

Considering the growth curve in Fig. 18 above, it can be deduced that the *C. necator* pKR-hum strain shows, as expected, rapid growth after the lag phase, reaching a stationary phase after 25 h at a biomass concentration of 1.45 g/L. This growth behavior was consistent across the tested flasks, with a small standard deviation (n = 3). In the following experiments, the effect of inoculating from a common LB medium preculture versus individual LB precultures (n = 6 each) on α-humulene production and robustness under varying process conditions using *C. necator* pKR-hum was investigated.

First, the influence of inoculating the main cultures from either a common LB preculture or individual LB precultures on final α-humulene levels and robustness was tested under standard conditions.

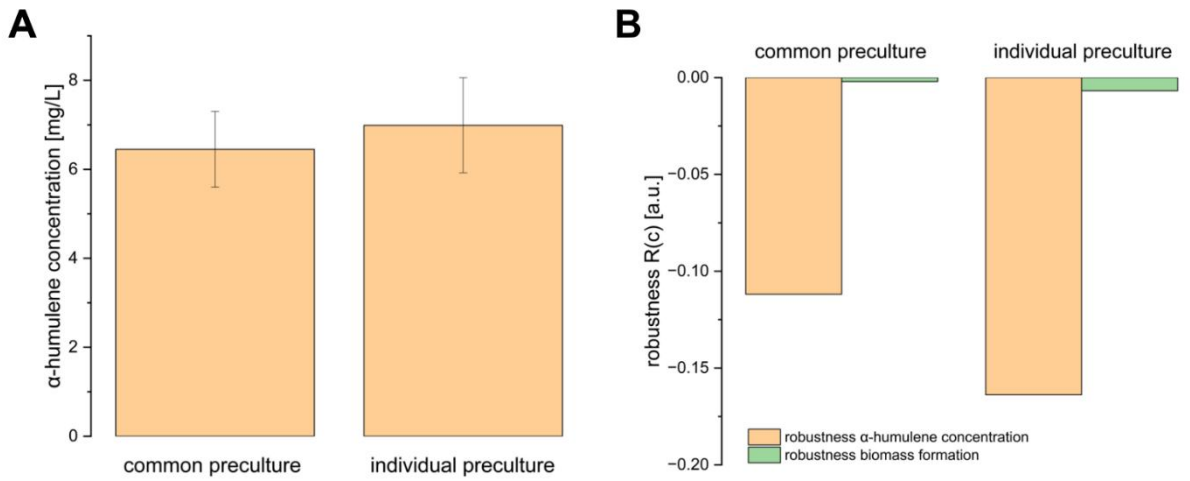

Fig. 19: (A) α-Humulene level and (B) robustness of α-humulene production and biomass formation in *C. necator* pKR-hum, measured 48 h after induction, based on the standard process conditions: cultures were supplemented with 0.75 mg/L iron (II) sulfate heptahydrate and 4 g/L fructose, in accordance with the standard media composition, incubated at 30 °C with 180 rpm, and induced with 0.2 % (w/v) L-rhamnose at 0.2 - 0.3 g/L biomass. Comparison between main cultures inoculated either from a common LB preculture or from individual LB precultures (n = 6).

It is shown that, considering the standard deviations, there are no differences in the final α-humulene levels after 48 h of production between the cultures inoculated from a common LB preculture and individual LB precultures (Fig. 19 - A).

The robustness of α-humulene production and biomass formation, whether inoculated from a common LB preculture or individual LB precultures, falls within a low robustness value range (Fig. 19 - B), close to the ideal value of 0, with a maximum value of -0.16. This indicates a robust process under standard process conditions. However, the robustness values are lower and more robust when inoculating from a common LB preculture. Additionally, *C. necator* pKR-hum biomass formation is much more robust than α-humulene production, with robustness values of -0.002 and -0.007 compared to -0.11 and -0.16, respectively.

One possible explanation for this is the defined minimal medium used, which allows the biomass formation to adapt more consistently to the defined external conditions. In contrast, α-humulene production may fluctuate more between individual runs, potentially due to bacterial heterogeneities, such as varying gene expression cascades, metabolic burdens, or plasmid instability in the isogenic production cells [176, 90].

4.4.2. Robustness of α-humulene production under varying process conditions

Next, the standard parameters were extended with previously optimized and established conditions, either individually or in combination. *C. necator*-based α-humulene production was compared, and their influence on final α-humulene levels and robustness was tested.

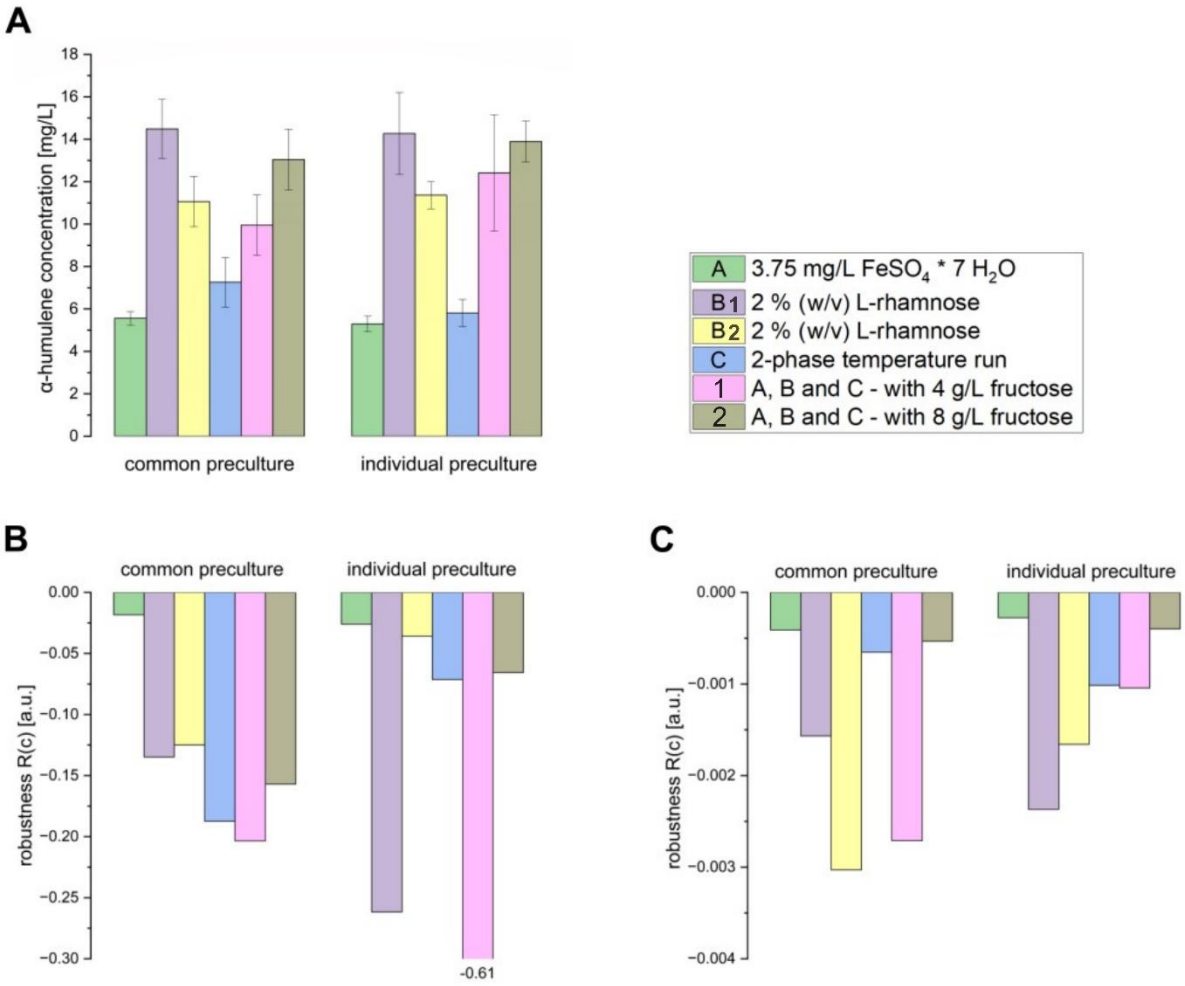

Fig. 20: (A) α-Humulene level, (B) robustness of α-humulene production, and (C) robustness of biomass formation in *C. necator* pKR-hum 48 h after induction, based on the standard conditions listed below, each further extended with subsequent individual adjustments to process conditions: standard conditions with modification A - 5-fold increase in the concentration of iron (II) sulfate heptahydrate (from 0.75 to 3.75 mg/L), standard conditions with modification B_1 - increasing the L-rhamnose inducer concentration from 0.2 to 2 % (w/v), standard conditions with modification B_2 - repetition of B_1, standard conditions with modification C - 2-phase cultivation temperature, standard conditions with modifications 1 - combination of individual process conditions A, B and C with 4 g/L fructose, standard conditions with modifications 2 - combination of individual process conditions A, B and C with 8 g/L fructose. The standard conditions are detailed in the following text. Comparison between main cultures inoculated either from a common LB preculture or from individual LB precultures (n = 6).

As standard conditions, the cultures were supplemented with 0.75 mg/L iron (II) sulfate heptahydrate and 4 g/L fructose, in accordance with the standard media composition, incubated at 30 °C with 180 rpm, and induced with 0.2 % (w/v) L-rhamnose at 0.2 - 0.3 g/L biomass. The 2-phase temperature run consisted of the following steps: 30 °C until 24 h after the induction step, followed by a decrease in the cultivation temperature to 25 °C.

Fig. 20 - A shows that the specific process conditions of 2 % (w/v) L-rhamnose, a two-stage cultivation temperature, and the addition of 8 g/L fructose increased the final α-humulene levels after 48 h, despite the standard deviations. No differences in final α-humulene levels after 48 h of production were observed between cultures inoculated from either a common LB preculture or individual LB precultures. The robustness of both α-humulene production (Fig. 20 - B) and biomass formation (Fig. 20 - C) remained within a low robustness value range, regardless of whether inoculation was from a common LB preculture or individual LB precultures. This indicates robust implemented process conditions, regardless of preculture handling and inoculation. Moreover, this robustness towards both preculture handling variants also demonstrates the flexible and adaptable properties of the *C. necator* production strain, which are particularly in demand in industry and can reduce overall process complexity. However, the composition of the main medium can cause greater variation in α-humulene production by *C. necator*, with 2 mg/L α-humulene in grass juice medium and 10 mg/L α-humulene in LB medium being detected 42 h after induction [13].

Robustness towards variations in preculture handling is not always guaranteed and is often strain-specific. For example, in *E. coli*, population heterogeneities and fluctuating growth behavior as a result of variations in preculture conditions have been demonstrated by Hoang et al. [177]. Additionally, it can be seen that the robustness values of biomass formation lie in a much lower value range, suggesting more stable robustness than α-humulene production. Indicating that essential and vital biological processes such as biomass formation in *C. necator* are more robust to external fluctuations and parameter variations than specific metabolic processes such as α-humulene production. Similar observations in *E. coli* were reported by Ishii et al., where enzyme levels were actively regulated to stabilize the metabolic status of the growth rate and thus the biomass formation for more robustness in the presence of fluctuations [178]. Overall, the analysis of these results indicates highly robust product and biomass formation in *C. necator* pKR-hum, even under varying external process conditions such as the minimal medium composition or cultivation temperature.

4.4.3. Robustness of α-humulene production following a simulated process disturbance

Subsequently, the question arose as to how a simulated process disturbance would affect the robustness and final α-humulene level of the production process. To investigate this, a run combining conditions A, B, and C (3.75 mg/L $FeSO_4$ * 7 H_2O, 2 % (w/v) L-rhamnose, and a two-stage cultivation temperature with 8 g/L fructose) was simulated with a process disturbance. Therefore, the shaking was paused for 12 h following the induction step, with the culture held at 30 °C during this period.

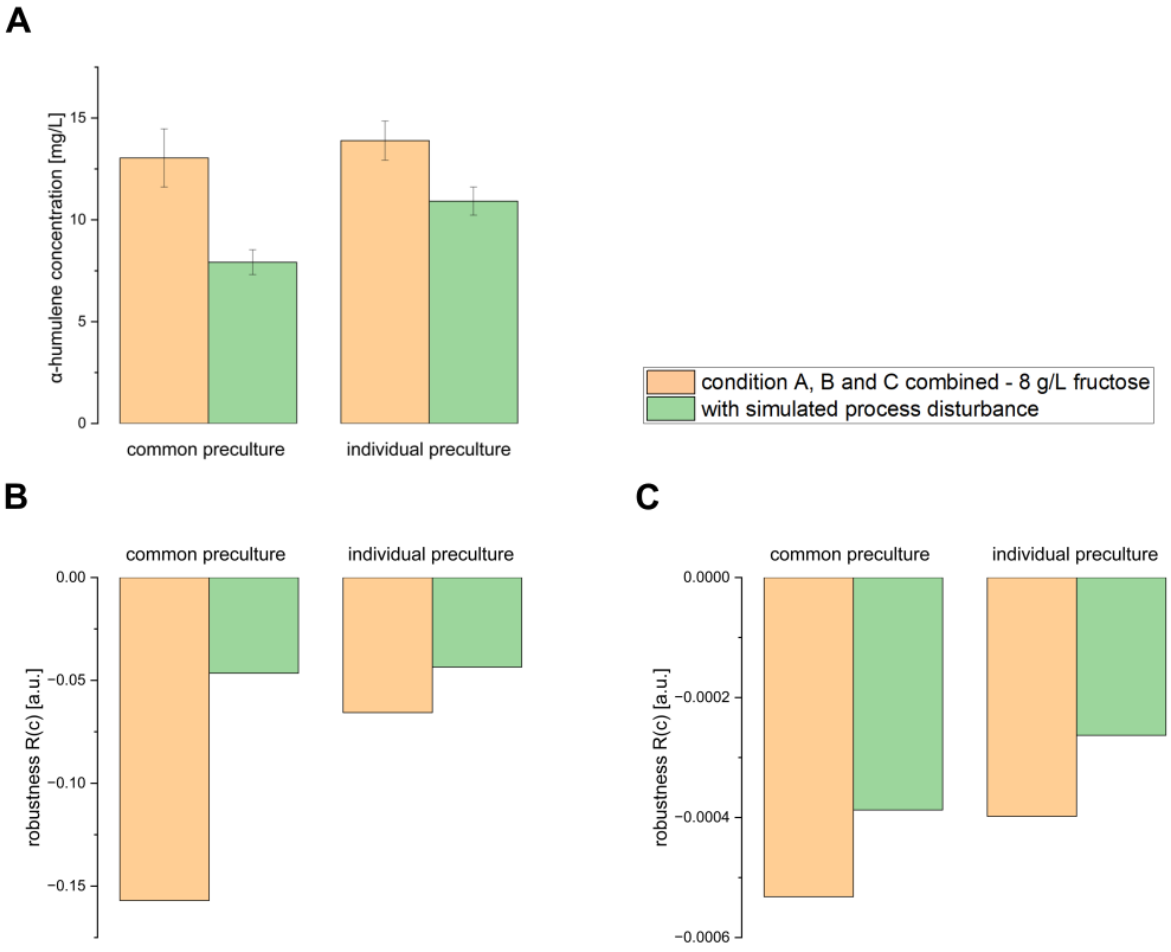

Fig. 21: (A) α-Humulene level, (B) robustness of α-humulene production, and (C) robustness of biomass formation in *C. necator* pKR-hum 48 h after induction. The combined run included the following conditions: 3.75 mg/L $FeSO_4$ * 7 H_2O, 2 % (w/v) L-rhamnose, a 2-phase cultivation temperature, and 8 g/L fructose. The run was conducted both with and without a simulated process interruption, where shaking was paused for 12 h after the induction step while temperature control remained active. Cultures were induced at 0.2 - 0.3 g/L biomass. Comparison between main cultures inoculated either from a common LB preculture or from individual LB precultures (n = 6).

Fig. 21 - A shows that there were no differences in the final α-humulene levels after 48 h of production when inoculations were performed from either a common LB preculture or individual LB precultures, considering standard deviations (with 8 g/L fructose in the combined run). A simulated process disturbance, created by interrupting shaking for 12 h after the induction step, reduced the final α-humulene levels after 48 h in both cases, regardless of how the precultures were handled. Still, the main cultures inoculated from individual LB precultures produced 79 % of the maximum α-humulene level.

The robustness values for α-humulene production (Fig. 21 - B) and biomass formation (Fig. 21 - C) were low for both common and individual LB preculture inoculations, suggesting robust process conditions in the combined condition run with 8 g/L fructose. While both inoculation methods produced similar robustness values, inoculation from individual precultures resulted in slightly lower robustness values. Similarly to previous experiments, Fig. 21 - B, C show that the biomass formation robustness values are lower than those for α-humulene production when testing the combined-condition run, indicating the highly robust biomass formation of *C. necator* pKR-hum.

The simulated process disturbance did not negatively impact the robustness of the production process, as the robustness values remained low, even with the process disturbance, indicating robust and continuous production by *C. necator* pKR-hum. Compared to the run without the simulated process disturbance, the final α-humulene levels reached 61 % and 79 % of the maximum after inoculation from common and individual precultures, respectively. This observed robustness and the relatively high final α-humulene levels despite the process disturbances may be attributed to the known metabolic adaptability of *C. necator*, which enables the organism to sustain productivity under suboptimal conditions such as reduced oxygen availability. An additional, but more speculative, explanation could involve a stress-induced increase in flagella formation in response to nutrient and oxygen limitations due to the lack of shaking. The increase in flagella formation could enable better motility and nutrient uptake in the unshaken culture, which, however, also consumes additional energy and could therefore have reduced α-humulene production. In the literature, a comparable mechanism has been described by Parker et al. in poorly motile *E. coli* BW25113 cells, which became motile overnight after a shaking-free incubation in liquid medium as a result of stress-induced motility gene expression [179].

4.5. Conclusions

This work demonstrates that the α-humulene production process using *C. necator* pKR-hum with recently optimized parameters is highly robust. The robustness value for α-humulene levels under varying process conditions is -0.155 ± 0.143, while it is -0.002 ± 0.002 for the biomass formation. Even with a simulated process disturbance, the process still produces 79 % of the maximum α-humulene level compared to the undisturbed run, with a corresponding robustness value of -0.045 ± 0.001. The analysis of these results indicates that the *C. necator*-based production process for α-humulene is robust to external fluctuations, which is crucial for large-scale industrial applications where such fluctuations may occur. Additionally, the lower robustness values for biomass formation as compared to α-humulene production also suggest that biomass formation is a more fundamental mechanism in *C. necator*. Contrary to this, the α-humulene biosynthesis route seems to be more sensitive to fluctuations, possibly due to the additional metabolic load involved in terpene production. Moreover, the α-humulene production process demonstrated robustness to inoculation from both common and individual precultures.

Overall, the quantification of robustness, along with these insights into both process and microbial robustness, contributes to a better understanding of the process for future industrial applications and supports the development of efficient terpene production processes.

5. Chapter 4 | Pharmaceutical α-humulene effects

Except for the *in vitro* toxicity evaluation material and methods chapter 5.3.5 and the corresponding results chapter 5.4.5, this chapter has been published as follows:

Becker L, Holtmann D. Anti-inflammatory effects of α-humulene on the release of pro-inflammatory cytokines in lipopolysaccharide-induced THP-1 cells. Cell Biochem Biophys. 2024; 82:839–47. doi:10.1007/s12013-024-01235-7. *

* Author contributions: Conceptualization, L.B. and D.H.; methodology, L.B.; lab investigation, L.B.; data curation, L.B.; writing - original draft preparation, L.B.; writing - review and editing, L.B. and D.H.; supervision, D.H.; project administration, D.H.; funding acquisition, D.H.

5.1. Abstract

While acute inflammation is an essential physical response to harmful external influences, the transition to chronic inflammation is problematic and associated with the development and worsening of many deadly diseases. Until now, established pharmaceutical agents have had many side effects when used for long periods. In this work, a possible anti-inflammatory effect of the sesquiterpene α-humulene on lipopolysaccharide (LPS) induction was tested. Herein, human THP-1-derived macrophages were used and their pro-inflammatory interleukin-6 (IL-6), tumor necrosis factor alpha (TNF-α), and interleukin-1β (IL-1β) cytokine release was measured by means of enzyme-linked immunosorbent assay. A dose-dependent effect of α-humulene on IL-6 release was observed at 0.5 and 100 µM α-humulene, with a maximum IL-6 inhibition of 60 % compared to the LPS reference value after the addition of 100 µM α-humulene. TNF-α as well as IL-1β cytokine concentrations were not reduced by the addition of 0.5 and 100 µM α-humulene. This work suggests that α-humulene has potential as a promising natural alternative to established pharmaceuticals for the treatment of elevated IL-6 levels and chronic inflammation in humans.

5.2. Introduction

Natural plant-derived terpenes, such as α-humulene, have gained increasing attention for their anti-inflammatory properties and offer promising therapeutic approaches to regulate inflammatory responses [38, 39]. Inflammation can be divided into two types: acute inflammation and persistent chronic inflammation. Acute inflammation is an important physical repair mechanism and a life-sustaining response to extrinsic influences, such as injuries and viral or bacterial infections [180]. For acute inflammatory reactions, common anti-inflammatory drugs from the group of corticosteroids or non-steroidal anti-inflammatory drugs (NSAID) such as aspirin or ibuprofen can be used [181].

Chronic inflammation, however, exceeds the benefits of acute inflammation due, to its continuous stimulation of the organism, and can lead to a wide range of physical and mental diseases, from diabetes and Alzheimer's to cancer [180, 182, 183]. Diseases that are considered to be the consequence of chronic inflammation currently account for more than 50 % of the world's deaths [184, 185]. A long-term use of NSAID for the treatment of chronic inflammation, though, can cause many undesirable side effects, suppresses the patient's immune system, and damages the liver and kidney, thus worsening symptoms and overall physical health [186]. In the transition from acute to chronic inflammation, the sustained increased release of pro-inflammatory cytokines and the resulting sustained imbalance with

anti-inflammatory cytokines play an important role [187]. Thus, there is an urgent need for new anti-inflammatory agents with fewer side effects that counteract the release of pro-inflammatory cytokine. Therefore, drugs based on plant extracts or their pharmacologically active ingredients could be a promising alternative, which allow for longer medication periods and results in fewer side effects compared to classic anti-inflammatory pharmaceuticals.

Plant extracts have been used in traditional medicine for thousands of years, and studies are increasingly demonstrating their anti-inflammatory effects [188]. Due to the composition of various active secondary plant compounds, such as terpenes, essential oils can cause a remodulation and influence the nuclear factor kappa-light-chain-enhancer of activated B cells (NF-κB) signaling pathway, which is significantly involved in the inflammatory cascade through the transcription and release of pro-inflammatory cytokines, such as TNF-α, IL-1, IL-6, and IL-8 [189, 190]. The anti-inflammatory effect of plant components could also be observed after administering lipopolysaccharides (LPS) in the murine microglial cell line BV-2. Here, thyme essential oil or its major monoterpene components, linalool, geraniol, and thujanol, reduced LPS-induced IL-6 and TNF-α release [191]. In this context, the administration of bacterial LPS, which are bacterial toxins and trigger signaling cascades of inflammatory responses, initiates the bacterial inflammatory process [192]. This work focuses on the sesquiterpene α-humulene, which, along with its isomer β-caryophyllene, is found in many plants around the world. The compound is named after its main source, the hop plant *H. lupulus* [193, 194].

In addition to its aroma and odor properties, α-humulene has promising pharmacological effects, including anti-inflammatory, anti-microbial, anti-biofilm, and anti-fungal. It also has anti-cancer properties, such as chemosensitizing and growth inhibition [28, 171, 195, 196]. To demonstrate the potential anti-inflammatory effects of α-humulene and its transfer to human cells, the human leukemia monocytic cell line THP-1 was chosen as a comparative model. This immortal monocyte cell line shows proliferation *in vitro* and is, therefore, suitable for immunological studies, unlike isolated human blood cells. Stimulation of human leukemia cells with phorbol 12-myristate 13-acetate (PMA) induces their differentiation into macrophage-like cells, which serve as an *in vitro* model for certain aspects of the immune response upon contact with pathogens [197]. In particular, PMA activates protein kinase C, which regulates signal transduction into the target cell through phosphorylation and triggers cell differentiation via p21 target gene activation [198]. As a result, the cells become adherent and stop their proliferation [199]. The functional and morphological properties such as shape, structure, cell surface characteristics or differentiation markers are similar to those of primary macrophages. Thus, they represent a suitable model to investigate human LPS-induced

inflammation and pro-inflammatory cytokine release, as well as *in vivo* phytopharmaceutical effects, similar to the previously mentioned α-humulene effects [123, 200].

5.3. Materials and methods

The following chapters describe the methodology and parameters of the cell culture experiments, which were applied unless otherwise specified. All chemical components were purchased from Sigma-Aldrich (St. Louis, Missouri, USA) unless otherwise stated.

5.3.1. THP-1 cell culture and differentiation

THP-1 cells were purchased from the German Collection of Microorganisms and Cell Cultures (ACC 16, Leibniz Institute DSMZ; Brunswick, Germany) and cultivated in a humidified incubator (ICO 150, Memmert; Schwabach, Germany) at 37 °C and 5 % CO_2 in T-flasks. The cells were maintained at a cell concentration of 5 * 10^5 cells/mL and sub-cultivated every 2 - 3 days by addition, or medium exchange after centrifugation (90 g, 10 min), of fresh and pre-warmed RPMI-1640 medium, which was composed of the following components: RPMI-1640 supplemented with 2 mM L-glutamine (art. no. R8758), 10 % (v/v) heat-inactivated fetal bovine serum (art. no. F9665), and 10 U/mL penicillin-streptomycin solution (art. no. P0781). The THP-1 cell count was determined using a Neubauer improved counting chamber (0640010, depth 0.1 mm, 0.0025 mm^2 Bright-Line; Paul Marienfeld, Lauda-Königshofen, Germany). Furthermore, cell viability was monitored using a trypan blue staining assay (art. no. 93595). Cell counting and trypan blue staining was only performed during the growth phase of the THP-1 cells to allow appropriate sub-cultivation of the suspension cells prior to differentiation and the start of the work. When the total cell number reached 12 * 10^6 cells, the THP-1 cells were centrifuged and the pellet was resuspended in 24 mL of a fresh RPMI-1640 medium containing 100 nM PMA (art. no. P8139) to induce monocyte-macrophage differentiation. For this purpose, the PMA stock used was previously dissolved in dimethyl sulfoxide (art. no. D2650) and diluted in 1x phosphate buffered saline buffer (PBS, art. no. D1408). Subsequently, 1 mL of this cell suspension (5 * 10^5 cells/mL) was added to each well of a 24-well tissue plate and incubated for a differentiation time of 48 h.

5.3.2. Stimulation of activated macrophages

After 48 h of PMA differentiation, non-attached cells and the medium containing PMA were removed to enhance further differentiation, the adherent macrophage-like cell layer was

washed twice with 1x PBS, and 500 µL of fresh complete medium was added. LPS from *E. coli* (art. no. L4391), dissolved in 1x PBS, were applied at a final concentration of 5 ng/mL into the associated wells to initiate the inflammatory cell response. After 2 h, the α-humulene stimuli (art. no. PHL83351), as well as hydrocortisone (HC, art. no. H6909) as positive controls, and alcohol (96 % EtOH) as negative controls, were added according to Tab. 10. The α-humulene was previously diluted in 96 % EtOH, and all stimuli were added to a total volume of 10 µL in the specific wells. Following 24 h of stimuli exposure during incubation at 37 °C and 5 % CO_2, the supernatants from each well were collected, vortexed, aliquoted, and frozen at -80 °C until cytokine analysis.

Tab. 10: Overview of tested stimuli with their concentrations, PMA differentiated THP-1 cells, performed in 24-well tissue plates.

Basis	**Stimuli**					
5 ng/mL LPS	0.5 µM HC	0.25 µM HC	0.5 µM α-humulene	100 µM α-humulene	1,000 µM α-humulene	2 % (v/v) 96 % EtOH
no LPS	0.5 µM HC	0.5 µM α-humulene	100 µM α-humulene	1,000 µM α-humulene	2 % (v/v) 96 % EtOH	N/A

5.3.3. Analysis of pro-inflammatory cytokines TNF-α, IL-6, and IL-1β by enzyme-linked immunosorbent assay (ELISA)

Quantitative analysis of the cytokines TNF-α, IL-6, and IL-1β was performed using the ELISA Ready-SET-Go!™ kits (art. no. TNF-α - 15521127, IL-6 - 15531037, and IL-1β - 15541087) obtained from Thermo Fisher Scientific (Waltham, Massachusetts, USA). All assays were performed according to the manufacturer's protocol using 1 M H_2SO_4 (art. no. 1.60313) as a stop solution. Finally, the plates were analyzed with the microplate reader Infinite 200Pro (Tecan, Männedorf, Switzerland) according to the following parameters: mode absorption, measuring wavelength 450 nm, reference wavelength 570 nm, bandwidth 9 ms, number of flashes 20, rest time 0 ms, plate geometry: Costar 96 flat bottom transparent, and temperature 22 - 25 °C using software version Tecan i-control 1.10.4.0.

5.3.4. Light microscopic imaging of THP-1 cells in suspension and after PMA differentiation into macrophages

THP-1 cell counting and viability tests were performed using 100x magnification light microscope (type 11090137002; Leica Microsystems CMS GmbH, Wetzlar, Germany). Verification of the PMA differentiation achieved in the 24-well plate, as well as the generation of images of macrophage-like cells, were also performed by light microscopy (DMi1 and type DMI6000 B; Leica Microsystems CMS GmbH, Wetzlar, Germany) using Leica Application Suite 4.12.0.

5.3.5. *In vitro* toxicity evaluation of α-humulene on differentiated THP-1 cells

THP-1 cell cultivation and differentiation were performed analogously to chapter 5.3.1, but using 6-well tissue culture plates instead of 24-well plates. Following 48 h of PMA-induced differentiation, the PMA-containing medium and non-attached cells were removed as described in chapter 5.3.2. The adherent macrophage-like cell layer was washed twice, and 1 mL of fresh complete medium was added. Subsequently, either no α-humulene (positive control, addition of 10 µL of 96 % EtOH) or 0.5, 100, 250, 500, and 1,000 µM α-humulene (from stock solution, α-humulene diluted in 96 % EtOH) was added in a volume of 10 µL to the corresponding wells. After 24 h of α-humulene exposure, the medium was removed and replaced with 1 mL of fresh complete medium. The CellTiter-Blue® Cell Viability Assay reagent (G8080; Promega Corporation, Madison, Wisconsin, USA) was then added to the wells according to the manufacturer's protocol. Following incubation, the supernatant was removed, and fluorescence was measured at 560_{Ex} / 590_{Em} nm using fluorescence spectroscopy. The signal is proportional to the number of viable or metabolically active cells.

5.3.6. Statistical analysis

The absorbance values determined by ELISA were subtracted from their reference wavelengths and used as surrogate parameters to determine the final cytokine concentrations. All experiments were performed in triplicate (n = 3), and data are presented as mean ± standard deviation. GraphPad Prism 9.0.0 software was used to present results and test for significance. A one-way analysis of variance (ANOVA) followed by Dunnett's test for multiple comparisons (95 % confidence interval) was performed. Differences between stimuli and/or controls were considered significant at a level of $p \leq 0.05$ for all tests.

5.4. Results and discussion

Subsequently, the PMA-induced differentiation of THP-1 cells was examined by light microscopy and the influence of stimuli on the pro-inflammatory cytokine release of TNF-α, IL-6 and IL-1β was tested. In addition, a α-humulene toxicity evaluation on THP-1 cells was performed.

5.4.1. Light microscopic imaging of PMA differentiated THP-1 cells

The PMA-induced differentiation of THP-1 cells into macrophage-like cells was examined and confirmed by light microscopy (Fig. 22). Furthermore, the effect of 0.5, 100, and 1,000 µM α-humulene concentrations in combination with the application of 5 ng/mL LPS on the morphological characteristics of PMA-differentiated THP-1 cells was investigated (Fig. 22 - A - D).

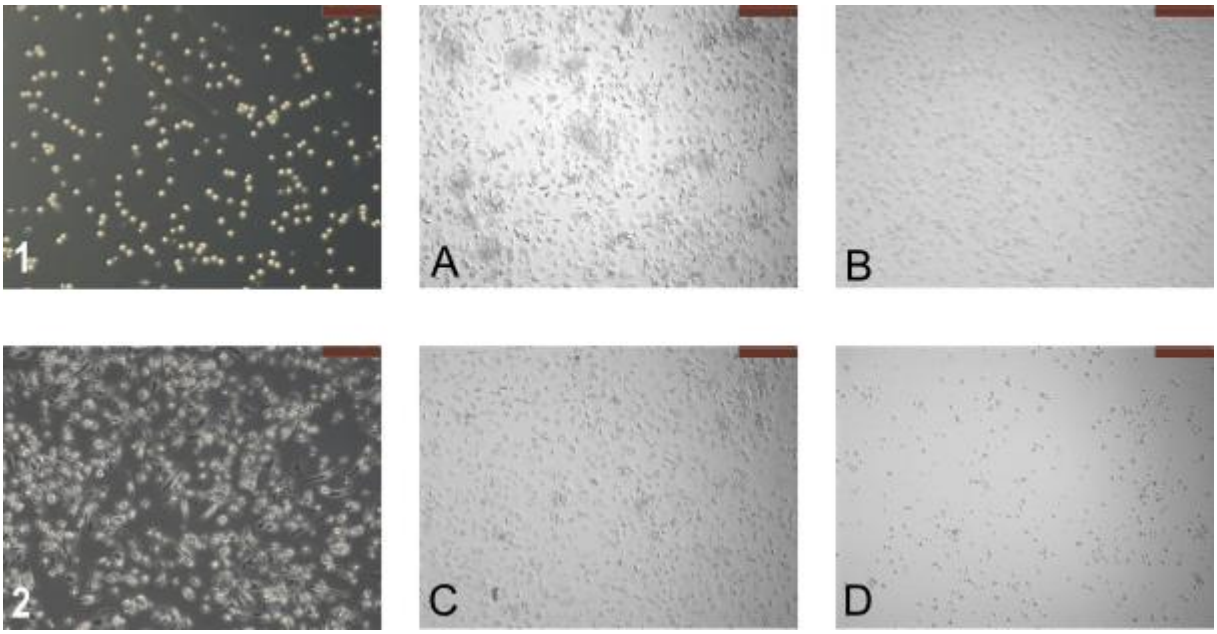

Fig. 22: Light microscopic images of THP-1 cells and adherent macrophage-like cells after PMA differentiation of THP-1 cells and addition of stimuli, differentiation with 100 nM PMA & 48 h exposure time in 24-well plates. (1) THP-1 monocytes in cell suspension. (2) Macrophage-like cells after differentiation of THP-1 cells with PMA. (A) Macrophage-like cells after 24 h exposure to 5 ng/mL LPS (B) Macrophage-like cells after 24 h exposure to 5 ng/mL LPS + 0.5 µM α-humulene (C) Macrophage-like cells after 24 h exposure to 5 ng/mL LPS + 100 µM α-humulene (D) Macrophage-like cells after 24 h exposure to 5 ng/mL LPS + 1,000 µM α-humulene. The scale bar equals 200 µm.

Exposure to 100 nM PMA for 48 h changed the morphology of THP-1 suspension cells from previously round and non-adherent to plastic-adherent and macrophage-like (Fig. 22 - 1 and 2). This phenotype was not affected by the addition of 5 ng/mL LPS or the further 0.5 and 100 µM α-humulene addition for 24 h, respectively (Fig. 22 - A - C).

However, after the addition of 1,000 µM α-humulene, it was observed that the adherent cells were disrupted after an exposure time of 24 h, the medium became turbid and small droplets formed. After addition of 1,000 µM α-humulene following LPS induction, no more adherent macrophage-like cells were found at the bottom of the 24-well plate, only cell fragments were visible as dark dots (Fig. 22 - D). In summary, THP-1 derived macrophage-like adherent cells were generated by differentiation using PMA, which disintegrated after the addition of 1,000 µM α-humulene.

5.4.2. TNF-α cytokine release in PMA differentiated THP-1 cells after the addition of stimuli

To confirm a possible anti-inflammatory effect after the addition of α-humulene stimuli to PMA-differentiated THP-1 cells, the released cytokine concentrations of TNF-α, IL-6, and IL-1β were analyzed from the cell supernatant by ELISA. The resulting TNF-α concentrations were compared and normalized on the mean value after the addition of 5 ng/mL LPS to the differentiated cells. This allows a direct comparison of anti-inflammatory effects by specific stimuli addition on LPS-induced cytokine release. The following graph (Fig. 23) demonstrates the calculated TNF-α mean values after stimuli exposure and their statistical significance.

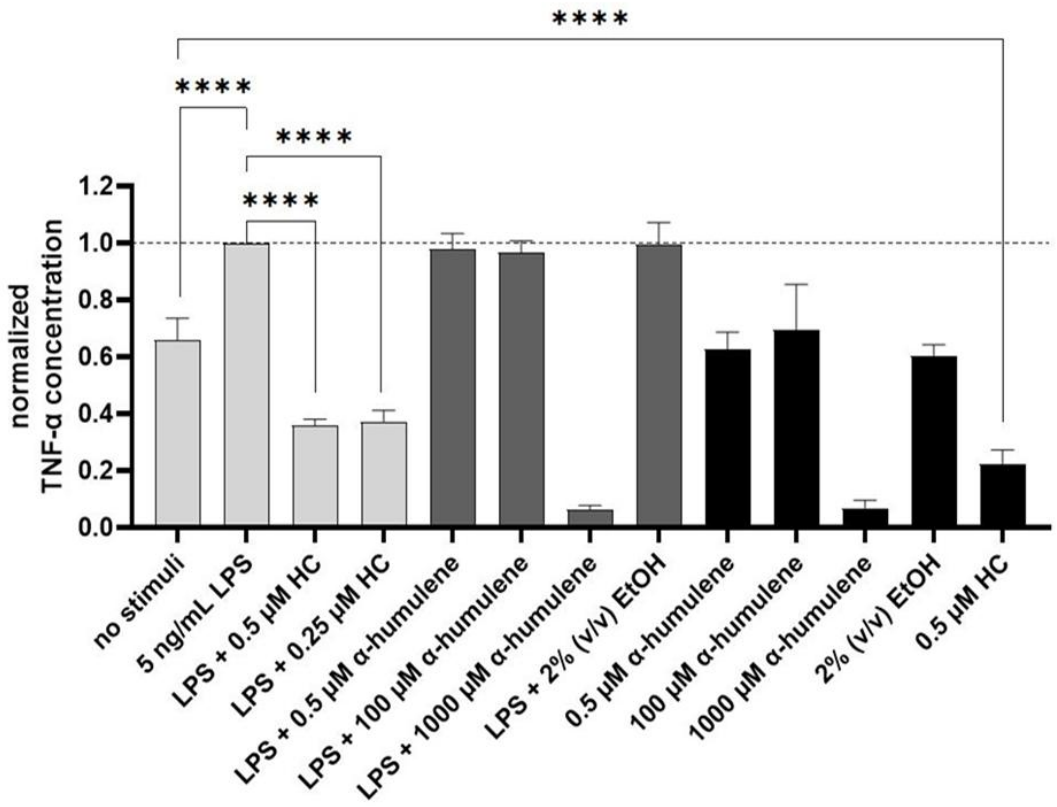

Fig. 23: TNF-α concentration normalized on LPS addition after stimulation of PMA-differentiated THP-1 cells, 24 h exposure, statistical analysis using one-way ANOVA (n = 3), **** $p \leq 0.0001$. An overview of the tested stimuli is provided in Tab. 10.

TNF-α release was significantly increased (**** $p \leq 0.0001$) by the addition of 5 ng/mL LPS to the previously PMA-differentiated THP-1 cells (Fig. 23). The addition of 0.5 or 0.25 µM HC as a positive control significantly decreased (**** $p \leq 0.0001$) the TNF-α cytokine released concentration. Addition of 0.5 - 1,000 µM α-humulene did not decrease the TNF-α release in comparison.

Moreover, after the LPS induction and treatment with 1,000 µM α-humulene, only 6 % of the normalized TNF-α concentration (reference sample: LPS induction without additional stimuli – 2,689 pg/mL TNF-α) was detected in the sample supernatant. In summary, TNF-α release was reduced by the addition of the positive control HC (0.5 and 0.25 µM), but the addition of 0.5 or 100 µM α-humulene did not result in a significant TNF-α reduction.

5.4.3. IL-6 cytokine release in PMA differentiated THP-1 cells after the addition of stimuli

Identical to the previous TNF-α investigation, the IL-6 cytokine concentration was also determined in the cell supernatant by ELISA. Here, IL-6 concentrations, after the addition of different stimuli, were compared with respect to the normalized value (addition of 5 ng/mL LPS). The following graph (Fig. 24) shows the calculated IL-6 levels after exposure to the stimuli and their statistical significance.

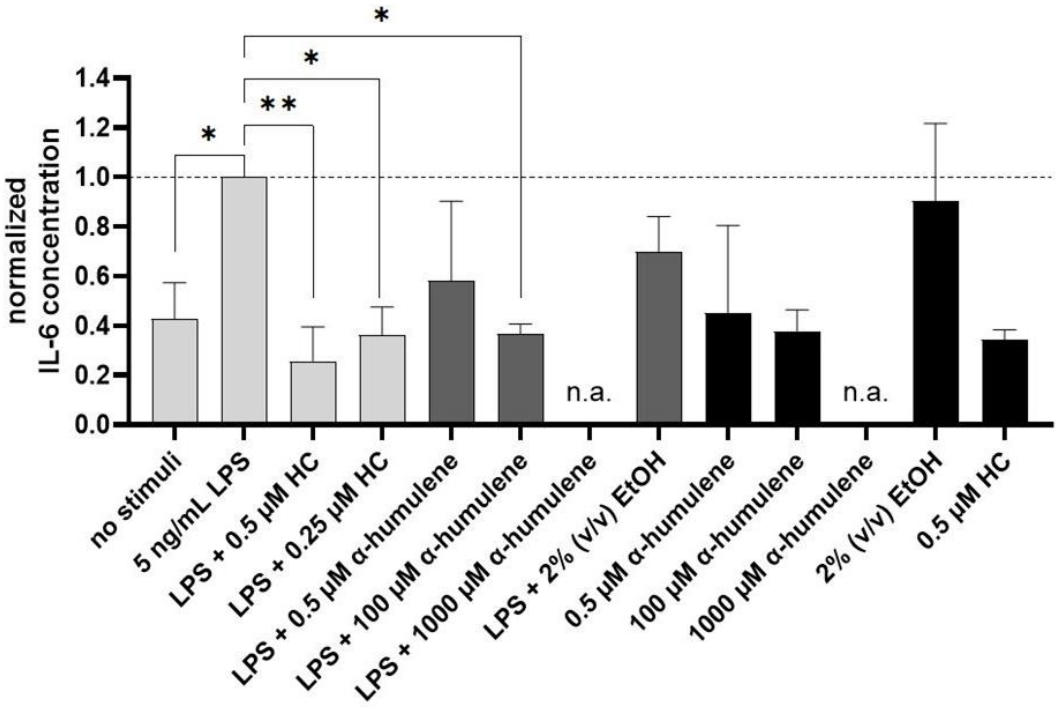

Fig. 24: IL-6 concentration normalized on LPS addition after stimulation of PMA-differentiated THP-1 cells, 24 h exposure, statistical analysis using one-way ANOVA (n = 3), ** $p \leq 0.01$. An overview of the tested stimuli is provided in Tab. 10.

IL-6 release was significantly increased (* $p \leq 0.05$) by the addition of 5 ng/mL LPS to the previously PMA-differentiated THP-1 cells (Fig. 24). The addition of 0.5 (** $p \leq 0.01$) or 0.25 µM HC (* $p \leq 0.05$) as a positive control significantly decreased the IL-6 cytokine concentration released. Addition of 0.5 µM α-humulene did not significantly decrease IL-6 release in comparison, whereas the IL-6 cytokine concentrations after treatment with 1,000 µM α-humulene could not be detected and were below the detection limit (n.a.). In addition, after the LPS induction and treatment with 100 µM α-humulene, IL-6

concentration could be significantly reduced (* $p \leq 0.05$) to 37 ± 4 % of the normalized reference value (LPS induction without additional stimuli - 20 pg/mL IL-6). Overall, IL-6 release was reduced in a dose-dependent manner by addition of the positive control HC (0.5 and 0.25 µM), and addition of 100 µM α-humulene led to a significant IL-6 reduction.

5.4.4. IL-1β cytokine release in PMA-differentiated THP-1 cells after the addition of stimuli

As a third pro-inflammatory cytokine, levels of IL-1β release were determined identically as described before by ELISA. The IL-1β concentrations after the addition of different stimuli were compared with respect to the normalized value (5 ng/mL LPS addition). The graph below (Fig. 25) shows the IL-1β values after the exposure to stimuli and the statistical significance.

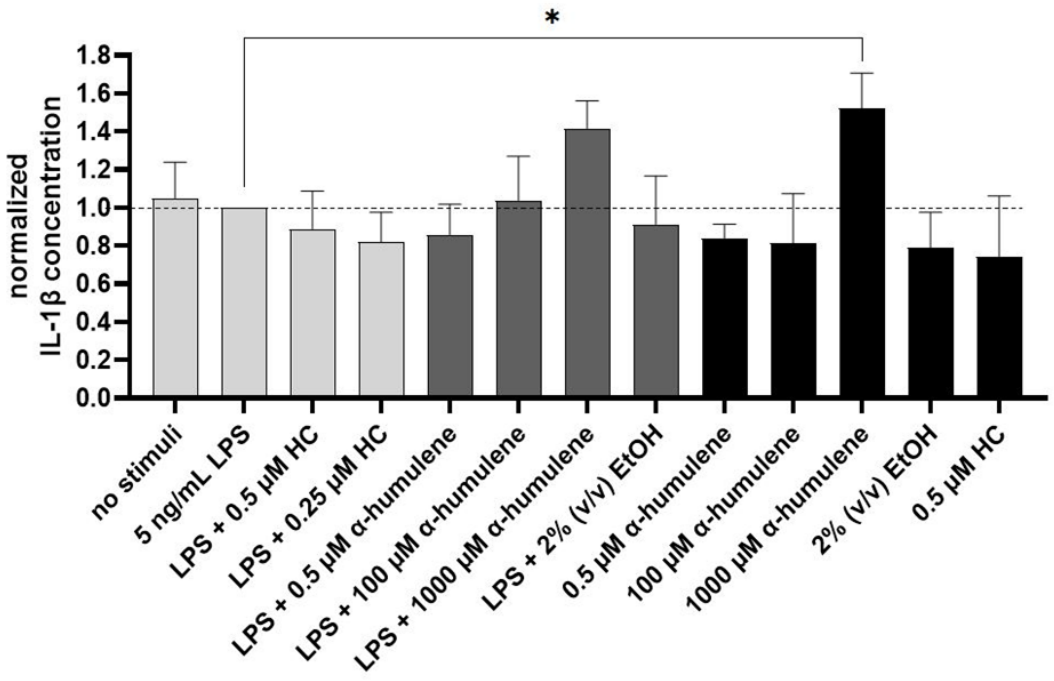

Fig. 25: IL-1β concentration normalized on LPS addition after stimulation of PMA-differentiated THP-1 cells, 24 h exposure, statistical analysis using one-way ANOVA (n = 3), * $p \leq 0.05$. An overview of the tested stimuli is provided in Tab. 10.

No significant increase in IL-1β cytokine release was detected by the addition of 5 ng/mL LPS to the previously PMA-differentiated THP-1 cells (Fig. 25). The addition of 0.5 or 0.25 µM HC as a positive control hardly reduced the LPS-induced IL-1β release compared to the previous cytokines. All stimuli additions resulted in IL-1β concentrations at the normalized reference level considering their standard deviations.

However, it can be seen that the addition of 1,000 µM α-humulene resulted in a significantly higher IL-1β release (* $p \leq 0.05$) compared to the normalized reference value (LPS induction without additional stimuli - 174 pg/mL IL-1β) or the control without stimuli. In summary, IL-1β release was not significantly altered by the addition of the stimuli tested compared with the control value (addition of 5 ng/mL LPS). However, the addition of 1,000 µM α-humulene significantly increased the release of IL-1β, while the addition of 1,000 µM α-humulene resulted in lower to undetectable TNF-α and IL-6 cytokine concentrations.

5.4.5. α-Humulene toxicity evaluation on THP-1 cells

After PMA-induced differentiation of THP-1 cells into macrophage-like cells and subsequent exposure to 0, 0.5, 100, 250, 500, and 1,000 µM α-humulene for 24 h, cell viability was analyzed. The lower graph (Fig. 26) presents cell viability after 24 h of exposure as a function of the added α-humulene concentration.

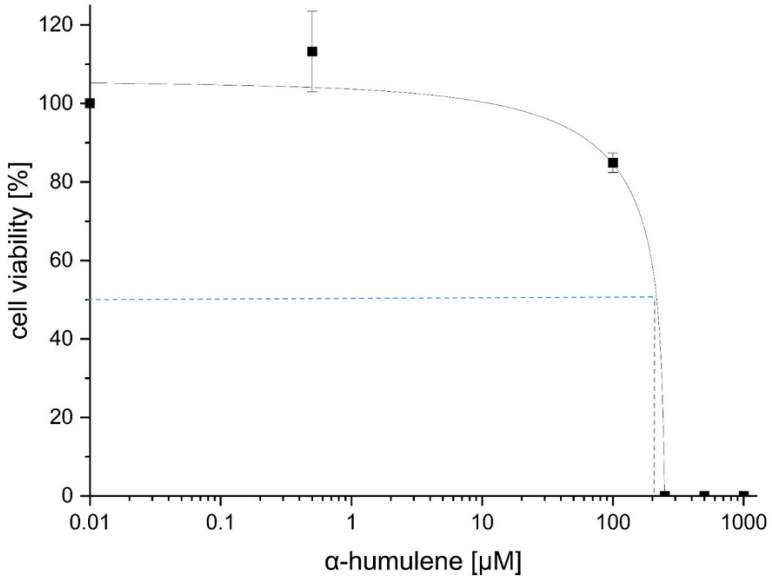

Fig. 26: Viability of differentiated THP-1 cells after 24 h of exposure to 0, 0.5, 100, 250, 500, and 1,000 µM α-humulene. The blue dashed line indicates the graphically interpolated CC_{50} value, estimated by identifying the intersection of the dose-response curve with the 50 % cell viability level. Data are presented as mean ± standard deviation (n = 3).

The addition of α-humulene for 24 h to previously differentiated THP-1 cells demonstrated a dose-dependent effect on cell viability (Fig. 26). The reference controls without α-humulene,

as well as samples treated with 0.5 µM α-humulene, showed cell viability values around 100 %, considering their standard deviations, indicating no inhibitory effect on cell viability. In contrast, exposure to 100 and 250 µM α-humulene reduced cell viability to 84.9 ± 2.5 % and 0 %, respectively, after an exposure time of 24 h. Graphical interpolation of the CC_{50} value (Fig. 26, blue dashed line), representing the concentration at which cell viability reaches 50 %, indicates a value of approximately 210 µM α-humulene.

These findings suggest, until date, for the first time that α-humulene may reduce LPS-induced release of the pro-inflammatory cytokine IL-6 in a dose-dependent manner. Of particular interest is the fact that the work was carried out using the human monocyte cell line THP-1, which has been differentiated into activated macrophages, allowing direct translation of the findings to human inflammatory responses, in contrast to many animal cell models. The addition of 5 ng/mL LPS to PMA-differentiated THP-1 monocytes resulted in significantly increased TNF-α and IL-6 cytokine concentrations. Since LPS belongs to the class of pathogen-associated molecular patterns, it is immunologically active and binds to surface structures such as pattern recognition receptors. These LPS-binding proteins can now transport the binding complex to the membrane-bound CD14 surface protein, found on monocytes and macrophages. After further interactions with several membrane receptors, it is assumed that toll-like receptors 4 bind this complex and transmit the signal intracellularly via dimerization with the help of the mediator protein MD-2. There, it leads to the activation of the NF-κB signaling pathway and an increased release of various cytokines by further, partly unknown, mechanisms. This cytokine conglomerate also includes the pro-inflammatory cytokines TNF-α, IL-6, and IL-1β tested in this work. [201, 202]

This increased LPS-induced TNF-α and IL-6 cytokine release, which was significant in the results, could be inhibited in a dose-dependent manner by the addition of 0.5 and 0.25 µM HC, respectively. HC was used in this work as a pharmacologically established and effective positive control, which initiates an anti-inflammatory effect by counteracting the LPS-induced activation of the NF-κB pathway to a certain extent [203]. In doing so, HC induces transcription of the NF-κB cytoplasmic inhibitor protein gene IκB, which decreases the quantity of NF-κB by binding and deactivation in the cytoplasm and preventing NF-κB from entering the nucleus [204]. An anti-inflammatory effect was also successfully observed after the addition of 100 µM α-humulene, which showed a significant decrease of LPS-induced IL-6 release by 60 % that can be compared to the anti-inflammatory effect of a 0.25 µM HC dosage in this work. The addition of 0.5 µM α-humulene after LPS induction also decreased IL-6 release, to a lesser extent, suggesting a dose-dependent pattern of effect.

How α-humulene affects the inflammatory cascade and has an anti-inflammatory effect has not been studied in detail. Medeiros et al. have demonstrated a decrease in NF-κB activation and reduced neutrophil migration in the tissue of LPS-inflamed rat paws after α-humulene addition [205].

Giving α-humulene to the inflamed lung tissue of female BALB/c mice also decreased NF-κB activation and activator protein 1 [157]. Furthermore, a decrease of IL-6 mRNA expression levels and histamine levels, via control of intracellular calcium and cyclic adenosine monophosphate (cAMP) levels, in PMA-stimulated human mast cells HMC-1 cells was observed by adding α-humulene [206]. In paw oedema of rats previously inflamed by carrageenan injection, anti-inflammatory effects and a down-regulation of prostaglandin E2 by α-humulene addition were also demonstrated by Fernandes et al. [39].

These effects of α-humulene described in the literature may all interact to produce the IL-6 inhibition shown in this work. NF-κB and activator protein 1 signaling play major roles in the initiation of inflammation in human cells through their transcriptional activities, and weakening the binding affinity of their transcription factors to cytokine receptors leads to additional anti-inflammatory effects [207]. Thus, this reduced activity by α-humulene successively decreases IL-6 release in the PMA-stimulated THP-1 cells used, as it has also been shown by Chun et al. after administration of epimagnolin A by attenuated IL-6 promoter activity [208]. Since histamine additionally upregulates IL-6 release in M1 macrophages [209], histamine levels lowered by α-humulene, as previously described, thus directly influences IL-6 release in the demonstrated dose-dependent manner. The modulator of the immune response, prostaglandin E2, induces IL-6 expression in humans via cAMP/PKA and PI3K-dependent pathways and its NF-κB activation coupled with NF-κB subunit p65 binding to the IL-6 promoter [210]. Since lower prostaglandin E2 levels and the control of intracellular cAMP levels inhibit IL-6 synthesis [210, 211], α-humulene effectively decreases IL-6 synthesis.

Other sesquiterpenoids have also been shown to have anti-inflammatory properties via LPS-induced IL-6 cytokine release: zerumbone - IC_{50} of 2.5 µM in THP-1 derived macrophages [212], popolohuanones G-I - 73.1 % inhibitory activity at 10 µM in THP-1 cells [213], chlorojanerin - IC_{50} of 1.8 ± 0.7 µM in THP-1 cells [214], estafiatin - IC_{50} of 3 µM in THP-1 cells [215]. Some monoterpenes may also have anti-inflammatory effects. Here, it was shown by Juergens et al., that the administration of 10 µM 1,8-cineol, which is successfully used as a drug component against human respiratory diseases [216], reduced LPS-induced IL-6 secretion in isolated human monocytes by 76 ± 10 % [217]. In LPS-stimulated RAW 264.7 cells, administration of 0.04 % D-limonene (2,470 µM) reduced IL-6 secretion by 80 % in a dose-dependent manner [218].

Moreover, toxic effects were also observed after the addition of an excessive α-humulene concentration (1,000 µM). Toxicity studies showed a cytotoxic concentration that reduces cell viability by 50 % (CC_{50} value) of two *Salvia officinalis* sage extracts, which are rich in α-humulene, on differentiated THP-1 macrophages between 66.70 ± 5.41 and 80.24 ± 7.58 µg/mL, respectively, after 24 h exposure [219]. Furthermore, a CC_{50} value of 109.7 ± 2.3 µg/mL and 29.0 ± 0.3 µg/mL, respectively, was demonstrated when lineage Vero and HeLa cells were stimulated with α-humulene for 72 h [220]. The CC_{50} values reported in literature confirm the assumption that cytotoxic effects and cell lysis occur at high α-humulene concentrations. This was observed by light microscopy following the addition of α-humulene at a concentration of 1,000 µM (equivalent to 204 µg/mL) and in the cell viability assay at concentrations above 100 µM. A concentration of 1,000 µM clearly exceeds the previously reported CC_{50} values. The graphically interpolated CC_{50} value of 210 µM α-humulene (after 24 h of exposure) falls within the same concentration range as the literature-reported CC_{50} values for Vero and HeLa cells (after 72 h of exposure), considering the longer α-humulene exposure durations in those studies. The CC_{50} value of 210 µM α-humulene indicates that the concentrations used in the cytokine assays (0.5 and 100 µM) were within a biocompatible range.

By addition of 1,000 µM α-humulene and the early-stage macrophage cell lysis, hardly any TNF-α or IL-6 cytokines were expressed and released via their cascade, which explains the low or undetectable TNF-α or IL-6 cytokine concentrations. The release of IL-1β, on the other hand, was increased by addition of 1,000 µM α-humulene above the normalized LPS reference value in this work. This initially contradictory finding, can be explained by the intracellular uptake and storage of IL-1β in activated macrophages, whose function is to activate and release small IL-1β amounts during an inflammatory reaction [221]. Thus, as a consequence of cell disintegration by toxic amounts of α-humulene (as shown in this work with 1,000 µM α-humulene), there may be an uncontrolled release of the intracellularly stored IL-1β, resulting in high IL-1β titres as shown in the results [222, 223]. The reduction of pro-inflammatory IL-6 levels by α-humulene shown in this work has enormous immunoregulatory benefits for the human organism. This is because IL-6 titres play a key role in molecular signaling and are significantly involved in the initiation of acute phase reactions in inflammatory processes [224].

Furthermore, elevated IL-6 levels also negatively influence the ongoing clinical process, as titres above 24 pg/mL have been shown to induce hypoxemia in Covid-19 patients [225]. In addition, chronically elevated IL-6 levels are associated with the formation and growth of several tumors such as breast cancer [226], making IL-6 a cancer marker, leading to a great need for novel IL-6-lowering cancer immunotherapy approaches [227, 228].

5.5. Conclusions

In conclusion, the addition of 0.5 and 100 µM α-humulene exerted anti-inflammatory effects on LPS-induced IL-6 release in differentiated THP-1 cells, while α-humulene did not affect the release of TNF-α and IL-1ß at these concentrations in this work. Thus, these findings could be transferred to the human organism to provide α-humulene as an alternative, natural-based, gentle and promising therapeutic approach against elevated IL-6 levels and chronic inflammation. This underscores the need for further research on the application of α-humulene. Future studies should aim to clarify the underlying molecular mechanisms and evaluate the therapeutic potential of α-humulene in *in vivo* approaches to confirm its efficacy and safety for clinical applications. Additionally, the potential effects of α-humulene on the release of anti-inflammatory cytokines should be investigated to fully understand its immunomodulatory properties.

6. Final conclusion and outlook

This work systematically optimized the heterotrophic production of α-humulene using *C. necator*, with the primary aim of maximizing product level and establishing a robust production process. This is achieved by targeted investigation and optimization of key process parameters. Based on the central research question: “Which cultivation and process parameters critically influence heterotrophic α-humulene production in *C. necator*?“ - this work demonstrated that targeted optimization of cultivation conditions, particularly temperature, and the adaptation of specific media components, significantly impacted α-humulene formation and can considerably increase its production. In addition, another key research question that was remarkably addressed was: “How do individual and combined optimizations of critical process steps affect biomass and α-humulene formation in *C. necator*?“ - The findings indicate that individual process steps optimizations, such as adjustments to temperature, media components, and inducer concentration have strongly enhanced their individual effects on α-humulene production when combined. Thus, this led to the question: “How does the implementation of these process step optimizations impact the robustness of the production process?“ To address this, its influence on production robustness was evaluated, and for the first time, it was quantitatively demonstrated that the *C. necator*-based α-humulene production process remains highly robust, even under simulated process disturbance. Having identified the key parameters for optimal and robust production, the final stage of the research explored the potential therapeutic effects of α-humulene in humans. In this context, it was demonstrated for the first time that the anti-inflammatory effects proposed for α-humulene also occur in lipopolysaccharide-induced inflammatory responses by reducing LPS-induced IL-6 release in differentiated THP-1 cells.

First, a statistical experimental design was successfully conducted to evaluate the cultivation parameters. Results indicated that *C. necator* pKR-hum produced higher levels of α-humulene when cultivated at a lower temperature range of 25 - 28 °C, compared to the standard 30 °C. This reinforces the importance of process parameters as a key factor in optimizing microbial terpenoid production. This observation aligns with previous studies suggesting that lower temperatures can enhance product stability and enzyme activity across different microbial hosts, particularly for terpenoids production. For example, Qin et al. found that *S. cerevisiae* produced and effluxed terpenes such as glycyrrhetinic acid, β-caryophyllene, and α-amyrin more efficiently at 22 °C than at 30 °C [229]. This was attributed to improved protein folding, reduced aggregation, and increased activity of heat-sensitive enzymes [229]. Notably, β-caryophyllene, which is an isomer of α-humulene, was also extracted extracellularly using ISPR in this study.

After three days, the production of β-caryophyllene increased by 23.8 % when the cultivation temperature of *S. cerevisiae* was lowered to 22 °C instead of 30 °C [229]. Here, a notable parallel can be drawn between yeast and *C. necator* pKR-hum, as both rely on the MVA pathway. Although a decrease in temperature enhances the MVA pathway flux in yeast [229], the plasmid-based *C. necator* pKR-hum may likewise experience similar mechanism. In this work, reducing the cultivation temperature from 30 °C to 25 °C and 20 °C led to increases in α-humulene production by 28 % and 20 %, respectively after 2 days.

This highlights the beneficial effect of moderate cooling on sesquiterpenes biosynthesis across different microbial hosts. The MEP pathway also exhibits increased flux in bacterial production systems at lower cultivation temperatures, thereby inducing higher production. Here, another study found that reducing cultivation temperature from 30 °C to 25 °C increased isopentenol production in genetically modified *B. subtilis* [230].

Since 1-deoxy-D-xylulose 5-phosphate synthase (*DXS*) is a rate-limiting enzyme of the bacterial MEP pathway, this effect is likely caused by improved folding, solubility, and activity of *DXS* at lower temperatures, which increases the levels of intermediate 1-deoxy-D-xylulose 5-phosphate (DXP) [231]. In *E. coli*, Zhou et al. demonstrated that reducing the cultivation temperature to 20 °C enhanced the production and solubility of MEP pathway enzymes, such as *DXS*, 1-hydroxy-2-methyl-2-(E)-butenyl 4-pyrophosphate synthase (*IspG*), 1-hydroxy-2-methyl-2-(E)-butenyl 4-pyrophosphate reductase (*IspH*), and farnesyl pyrophosphate synthase (*IspA*), which functions downstream to convert IPP and DMAPP into farnesyl pyrophosphate (FPP) [232]. This further promotes terpene production and increases the availability of IPP and DMAPP. A similar MEP pathway mechanism may account for the increased α-humulene production observed in this work by improved efficiency of downstream enzymes. Thus, by extending the native MEP pathway with plasmid-based MVA pathway genes in *C. necator*, α-humulene production benefited from both pathways due to the lowered cultivation temperatures. Lowering the temperature increases the final α-humulene level and, reduces the heat energy input, which can reduce process costs.

Based on these findings, additional process parameters were specifically optimized, including the concentrations of individual media components and the L-rhamnose inducer concentration. In addition, the cultivation process was divided into two different temperature stages. These two stages were the use of 30 °C until sufficient biomass was reached, and the subsequent switch to 25 °C implemented 24 h after induction. This two-stage temperature separation ensures sufficient biomass formation during early cultivation, followed by enhanced terpenoid production by reducing the temperature below 30 °C [233, 234]. A similar effect was observed by Kim et al. in *E. coli*, where reducing the cultivation temperature from

37 °C to 25 °C during the exponential growth phase led to a 20 % increase in the final plasmid-based lycopene concentration [235]. Notably, this temperature-dependent relative lycopene increase can be compared to the α-humulene production observed in this work (20 % and 28 %, respectively), as both systems rely on plasmid-based gene expression and the utilization of the isoprenoid precursors IPP and DMAPP. This highlights the effectiveness of temperature shifts in decoupling bacterial growth from terpene production.

In summary, the following implementations led to increased biomass formation and α-humulene production: Increasing the fructose concentration from 4 g/L to 8 g/L. Increasing the iron (II) sulfate heptahydrate concentration from 0.75 mg/L to 3.75 mg/L. Increasing the L-rhamnose inducer concentration from 0.2 % (w/v) to 2 % (w/v). Splitting the cultivation temperature from only 30 °C to 30 °C and 25 °C stages. These observed improvements in the production process result from a combination of individual optimization steps. For example, the increase in iron (II) sulfate heptahydrate concentration in the minimal medium from 0.75 to 3.75 mg/L with sufficient fructose supply indicates a possible link between the higher iron availability and terpene biosynthesis. This is probably because the terminal MEP pathway enzymes (*IspG* and *IspH*) depend on iron-sulfur clusters [236, 237]. In addition, Sydow et al. reported that protein expression driven by the L-rhamnose inducible promoter system in *C. necator* saturates at 11 mM L-rhamnose, corresponding to approximately 0.2 % (w/v) [74]. In contrast, this work observed a substantial increase in α-humulene production, up to 93 %, when the L-rhamnose inducer concentration was elevated to 2 % (w/v). Thus, this indicates that plasmid-based expression and promoter were not yet saturated at previously assumed conditions. This finding aligns with Kim et al. who demonstrated that certain L-rhamnose promoter variants in *E. coli* possess extended dynamic range, allowing expression to continue rising even at 2 % (w/v) L-rhamnose without reaching their saturation point [238]. Consequently, this indicates that L-rhamnose inducible promoter systems, especially mutant variants, can enable higher gene expression, while L-rhamnose concentrations above 2 % (w/v) can further increase product concentrations across different microbial hosts [238]. However, factors such as substrate toxicity, osmotic stress, metabolic stress, and solubility limitations must be considered. Future research should focus on optimizing promoter performance by enhancing promoter strength through site-directed mutagenesis and creating promoter library to further increase expression and α-humulene production [238, 239].

In particular, a noteworthy finding is the combination of the optimized individual parameters, resulting in a 241 % increase in the final α-humulene level compared to the non-optimized standard process. Thus, these substantial improvements suggest that the positive effects of each optimized parameter were potentiated when combined. Also, this demonstrates that

optimization of the standard process parameters and fine adjustment of the cultivation temperature offers enormous potential for enhancing terpene production. Similar findings were reported by Yang et al. in *E. coli* [240]. In their study, they demonstrated that lowering the cultivation temperature from 37 °C to 30 °C increased plasmid-based α-pinene production from 0.165 mg/L to 1.31 mg/L [240]. By subsequently adjusting the inducer concentration at 30 °C, the production increased further to 1.77 mg/L, which corresponds to a 35 % increase [240]. Combining both parameters potentiated the individual effects. Further adjustment of the nitrogen source increased α-pinene production to 5.44 mg/L, thereby highlighting the potentiating effects of combined optimizations while indicating that the optimization of the nitrogen source and concentration could offer further potential for terpene production in *C. necator* [240]. Similar observations were reported by Milker and Holtmann for β-farnesene production using *C. necator*, where a fed-batch strategy with combined fructose and nitrogen feed increased growth-dependent production, thereby highlighting fed-batch cultivation as a promising optimization tool for future α-humulene process development in the context of this work [69]. One effective strategy could be to feed the 8 g/L fructose concentration, identified as sufficient in this work, in a fed-batch approach, while varying the ammonium sulfate concentration over the 48 h production period following induction.

Furthermore, this work evaluated for the first time that the *C. necator*-based production process of α-humulene is very robust. Thus, the impact of the previously implemented parameter optimizations on the process robustness was assessed. Although specific studies addressed aspects of robustness in microbial production, an in-depth quantitative assessment of robustness in terpenoid-based production systems, particularly in bacteria, has been lacking. The experimental and quantitative approach to assess robustness in this work, adapted from Trivellin et al., has been rarely applied because past literature often assumed that biological robustness cannot be realistically and mathematically quantified [174, 241]. In this work, the robustness values determined were approximately equivalent to the ideal value of 0, thereby indicating that *C. necator* biomass formation is even more robust than α-humulene product formation. Using the same experimental and quantitative approach, Torello Pianale et al. observed a similar phenomenon in *S. cerevisiae* PE2 with respect to glycerol production [175]. However, a robustness value of -0.4 was reported for cell mass yield (g/g) [175]. Thus, the robustness value receded the -0.007 quantified in this work, thereby underlining *C. necator* as a highly robust and suitable production host. However, direct comparison of the robustness to other systems is limited due to differences in organism and process conditions [175]. In this context, it is particular noteworthy that a simulated process disturbance yielded 79 % of the maximum final α-humulene level compared to the undisturbed run. As similar experiments to simulate industrial process disturbances remain

unconducted with *C. necator*, this work is the first to quantitatively demonstrate its remarkable robustness and suitability for industrial applications. In this context, it is well known that production hosts often show high sensitivity to process changes such as temperature, shaking rate, or nutrient distribution [242]. For example, Elahi et al. demonstrated that the staphylococcal enterotoxin type A production of *S. aureus* decreased from 2,000 ng/mL in shaken to 200 ng/mL in stationary cultures, thereby corresponding to only 10 % of the maximum product level achieved, compared to 79 % in this work [243]. This effect becomes more obvious when compared to *E. coli*, as reducing the shaking speed from 100 rpm to 50 rpm during production decreased the specific activity of surface-displayed lipase A from *C. antarctica* to only 13 % of its initial level [244]. While *C. necator* has often been described as a flexible organism [245, 246], this work provides experimental evidence of its robustness and resilience under process conditions and underlines its suitability as a production host for industrial applications.

Finally, immunological tests with α-humulene were successfully conducted, showing for the first time that administration of 0.5 or 100 µM α-humulene resulted in an anti-inflammatory effect on LPS-induced IL-6 release in differentiated THP-1 cells. According to a comparable study, α-pinene lipid nanoparticles decreased relative IL-6 mRNA levels and NF-κB expression in LPS-induced THP-1 cells within a similar concentration range of approximately 147 µM, suggesting that they can influence IL-6 release [247]. However, despite these studies, systematic studies on the bioactive effects of microbial produced terpenes in inflammatory processes, particularly in LPS-induced human *in vitro* models remain lacking. To date, most studies conducted focused on terpenes of plant or synthetic origin. Consequently, while pharmacological efficacy and immunomodulatory properties of microbial produced terpenes remain insufficiently evaluated, their comparability remains unconfirmed.

This research gap is relevant, as targeted evaluation of microbial produced terpenes validates their therapeutic potential and focuses on sustainable biotechnological production and regulatory acceptance. Considering that stereochemistry [248], purity [249], and potential by-products, such as the toxic farnesyl acetate [249, 250] have exhibited substantial differences in microbial produced terpenes compared to their plant-derived counterparts, therefore targeted comparative studies assessing these parameters with the corresponding plant reference compounds should be conducted from a scientific and an application perspective. This is particularly important for α-humulene, to ensure its safe establishment for future pharmaceutical applications in humans. Furthermore, the THP-1 cell findings presented provide preliminary evidence of the anti-inflammatory effects of α-humulene. However, due to the limitations of the cell model, they can only be limitedly transferred to the human

organism, thereby necessitating conducting further validation of its effects on humans using human peripheral blood, for example [251].

Based on this work's findings, integrating biotechnology and functional pharmacology further, thus presents a promising direction for future studies and applications of terpenoids and terpenes such as α-humulene. In conclusion, the results analysis obtained in this work provides an important foundation for further development of microbial-based terpenes/oids production processes. Furthermore, the presented optimization strategy demonstrates that the complex interplay of several parameters is crucial for the overall process's efficiency and should increasingly be the subject of research rather than always considering individual factors and optimizing them separately.

Robustness, both microbially and process-related, should consequently be considered and evaluated as it demonstrated a robust *C. necator* production strain in this work. This strain maintained consistent performance even under simulated process disturbance, thereby highlighting the suitability of the presented process for industrial scale. Therefore, future study should focus on scaling up the process to bioreactor scale. To this end, the upscaling from laboratory scale to industrial production can be validated and tested, and the knowledge gained can be verified on a bioreactor scale. Here, the process parameters and their interactions with each other can be more comprehensively explored and refined in a controlled bioreactor environment, alongside the potential of fed-batch or alternative cultivation systems. Furthermore, the discovered anti-inflammatory effects of α-humulene offer promising potential for future medical-pharmaceutical applications. Future *in vitro* and *in vivo* studies could therefore help in explicitly understanding the molecular mechanisms of action and the therapeutic potential of α-humulene in treating inflammatory diseases, infections or cancer.

In addition to the optimization of different process parameters described here, future studies should focus on optimizing existing metabolic pathways and implementing innovative genes for terpene production. To this end, the plasmid-based production system could also be further optimized or completely replaced by genome integration of the relevant enzymes. However, despite these approaches, microbial and process robustness should be maintained.

Finally, the application of *C. necator* as a production organism combined with this work's insights can be further transferred to other terpenes/oids or bioactive molecules of interest, especially during sustainable bio-based production processes. Consequently, the presented strategies for process optimization and robustness evaluation offer valuable methodological approaches in the future.

7. Appendix

Parts of this appendix have been published as a supplementary information document in the paper:

Becker L, Dietz E, Holtmann D. Individual process steps optimization of *Cupriavidus necator*-catalyzed production of α-humulene. Biochemical Engineering Journal. 2024; 215:109617. doi:10.1016/j.bej.2024.109617. *

* Author contributions: E.D.: Investigation. L.B.: Writing – review & editing, Writing – original draft, Visualization, Methodology, Investigation, Data curation. D.H.: Writing – review & editing, Supervision, Project administration, Funding acquisition, Conceptualization.

7.1. Plasmid map pKR-hum

Fig. 27 below illustrates the expression plasmid used in this work for the production of α-humulene.

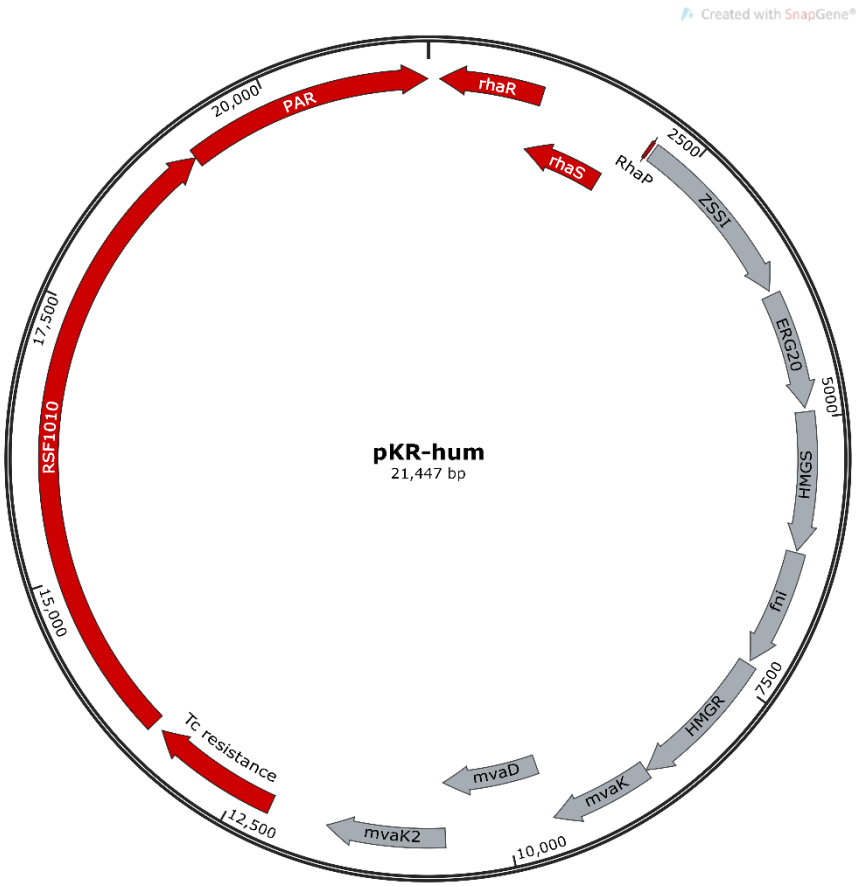

Fig. 27: Plasmid map of the α-humulene production plasmid pKR-hum, based on [5] and adapted using SnapGene®.

The plasmid map (Fig. 27) shows the expression plasmid used, pKR-hum, which was transformed into *C. necator* H16 PHB-4 for α-humulene production. It contains a tetracycline resistance, α-humulene synthase (*zzsI*) as well as a farnesyl pyrophosphate synthase (*erg20*) and the MVA pathway enzymes: *hmgs*, *fni*, *hmgr*, *mvaK*, *mvaD* and *mvaK2.*

7.2. Calibration curves for HPLC and GC-MS analysis

The following Figures, Fig. 28 and 29, show the calibration curves, linearity ranges, as well as the chromatograms and retention times for the D-fructose and α-humulene analysis, respectively.

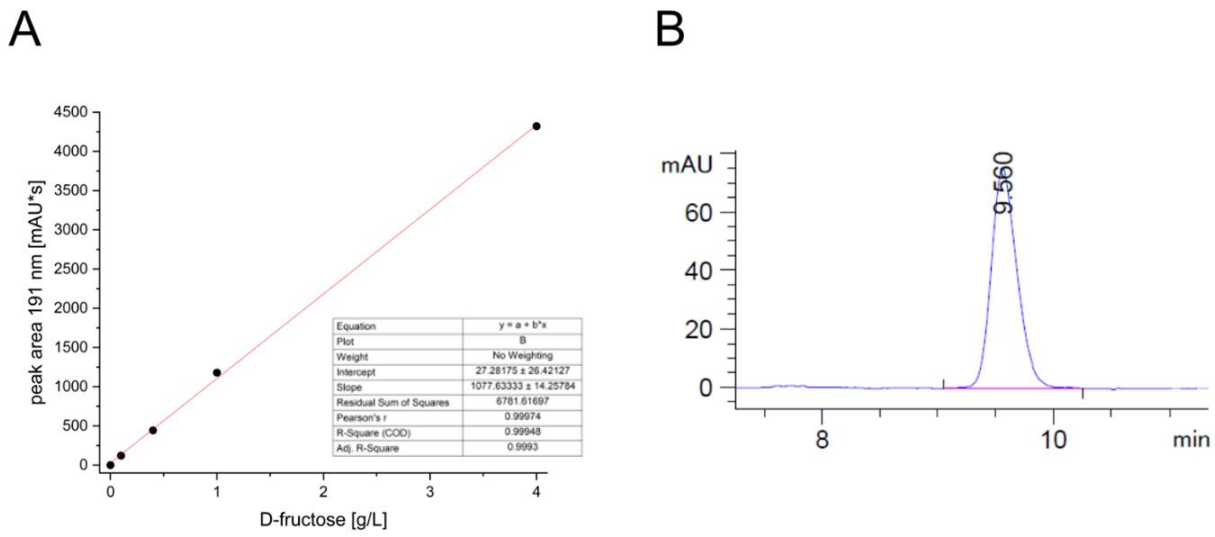

Fig. 28: (A) Calibration curve obtained from HPLC analysis of D-fructose, showing the relationship between D-fructose concentration and peak area; (B) HPLC chromatogram of D-fructose with retention time of 9.560 min; detection using multiple wavelength detector (MWD) at 191 nm.

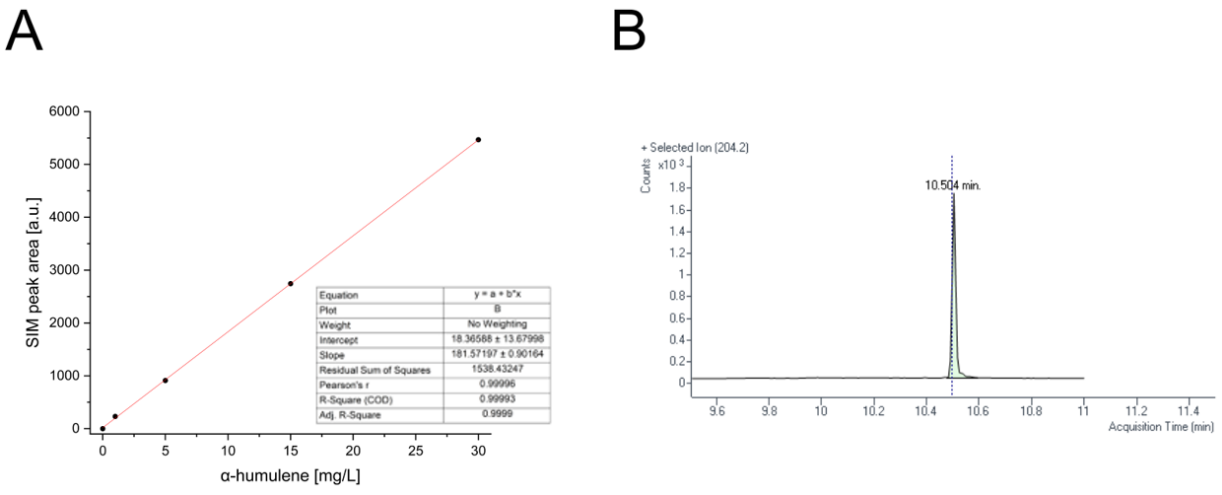

Fig. 29: (A) Calibration curve obtained from GC-MS analysis of α-humulene, showing the relationship between α-humulene concentration and peak area; (B) GC-MS chromatogram of α-humulene with retention time of 10.504 min; detection using single ion monitoring (SIM) corresponding to m/z 204.2.

7.3. Growth rate and yield coefficients formulas

The growth rate (μ) was calculated for each data point using the Cell Growth Quantifier® device (CGQ) software 1.2.2, in accordance with formula 3. Subsequently, the maximum growth rate (μ_{max}) was determined during the exponential phase. Yield coefficients $Y_{X/S}$ (g biomass per g substrate), $Y_{P/S}$ (mg α-humulene per g substrate), and $Y_{P/X}$ (mg α-humulene per g biomass) were calculated using the following formulas 4 to 6.

$$\mu = \frac{\ln(X_2) - \ln(X_1)}{(t_2 - t_1)} \quad (3)$$

$$Y_{X/S} = \frac{\text{biomass formed } (\frac{g}{L})}{\text{substrate consumed } (\frac{g}{L})} \quad (4)$$

$$Y_{P/S} = \frac{\text{α-humulene produced } (\frac{mg}{L})}{\text{substrate consumed } (\frac{g}{L})} \quad (5)$$

$$Y_{P/X} = \frac{\text{α-humulene produced } (\frac{mg}{L})}{\text{biomass formed } (\frac{g}{L})} \quad (6)$$

7.4. 3D response surface modelling

The DoE approach with the individual factor combinations from chapter 2.3.10 was planned and tested, see Tab. 8 in chapter 2.4.4. In addition, the corresponding response values were determined for each run. In the following Fig. 30, the 3D response surface plots of the model are illustrated. A detailed description of the 3D response surface plots can be found in chapter 2.4.4.

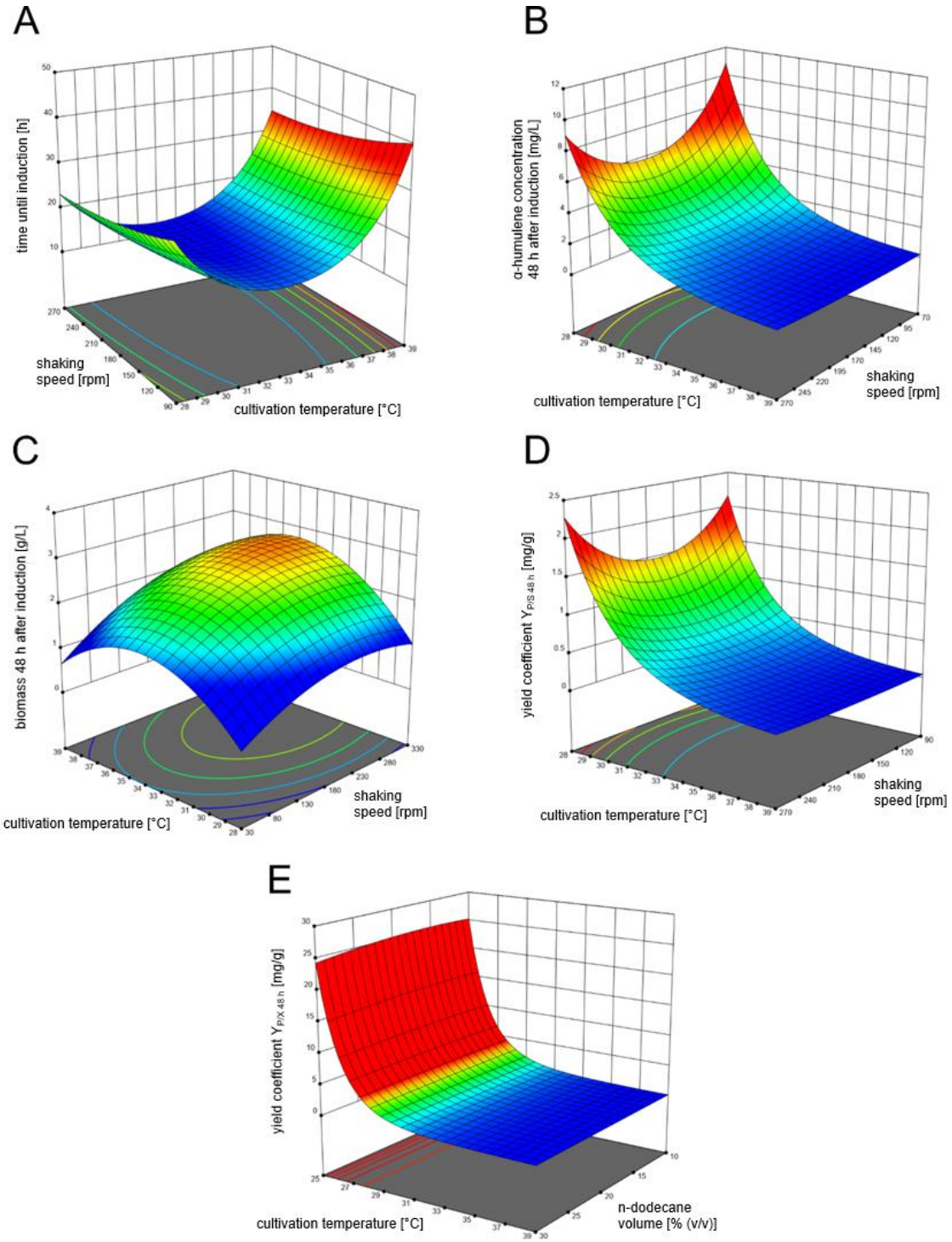

Fig. 30: 3D response surface modelling of the cultivation time until induction (A), α-humulene concentration (B) and biomass (C) as well as $Y_{P/S}$ (D) and $Y_{P/X}$ (E) 48 h after induction, in relation to model factors of *C. necator* pKR-hum: shaking speed and cultivation temperature (A - D, at 20 % (v/v) n-dodecane solvent volume), solvent volume and cultivation temperature (E, at 180 rpm shaking speed). Only significant factors were visualized for modelling purposes.

7.5. Composition of the SOB medium

The following table lists the standard compositions of the super optimal broth (SOB) preculture media used in this work.

Tab. 11: Composition of the super optimal broth (SOB) preculture medium.

Medium component	Concentration [g/L]
Yeast extract	5
Tryptone	20
NaCl	0.5
KCl	0.186
$MgSO_4 * 7 H_2O$	2.4

7.6. Optimization of the L-rhamnose inducer concentration and dosage time

To confirm the influence of L-rhamnose concentration on α-humulene production, time-dependent α-humulene formation by *C. necator* pKR-hum was analyzed after the addition of 0.2, 1 and 2 % (w/v) L-rhamnose (Fig. 31 - A, C and D). Additionally, different inducer concentrations were added to the main culture to assess time-dependent L-rhamnose consumption (Fig. 31 - B). The corresponding yield coefficients ($Y_{X/S}$, $Y_{P/S}$, and $Y_{P/X}$) are presented below, along with the results of the L-rhamnose consumption tests.

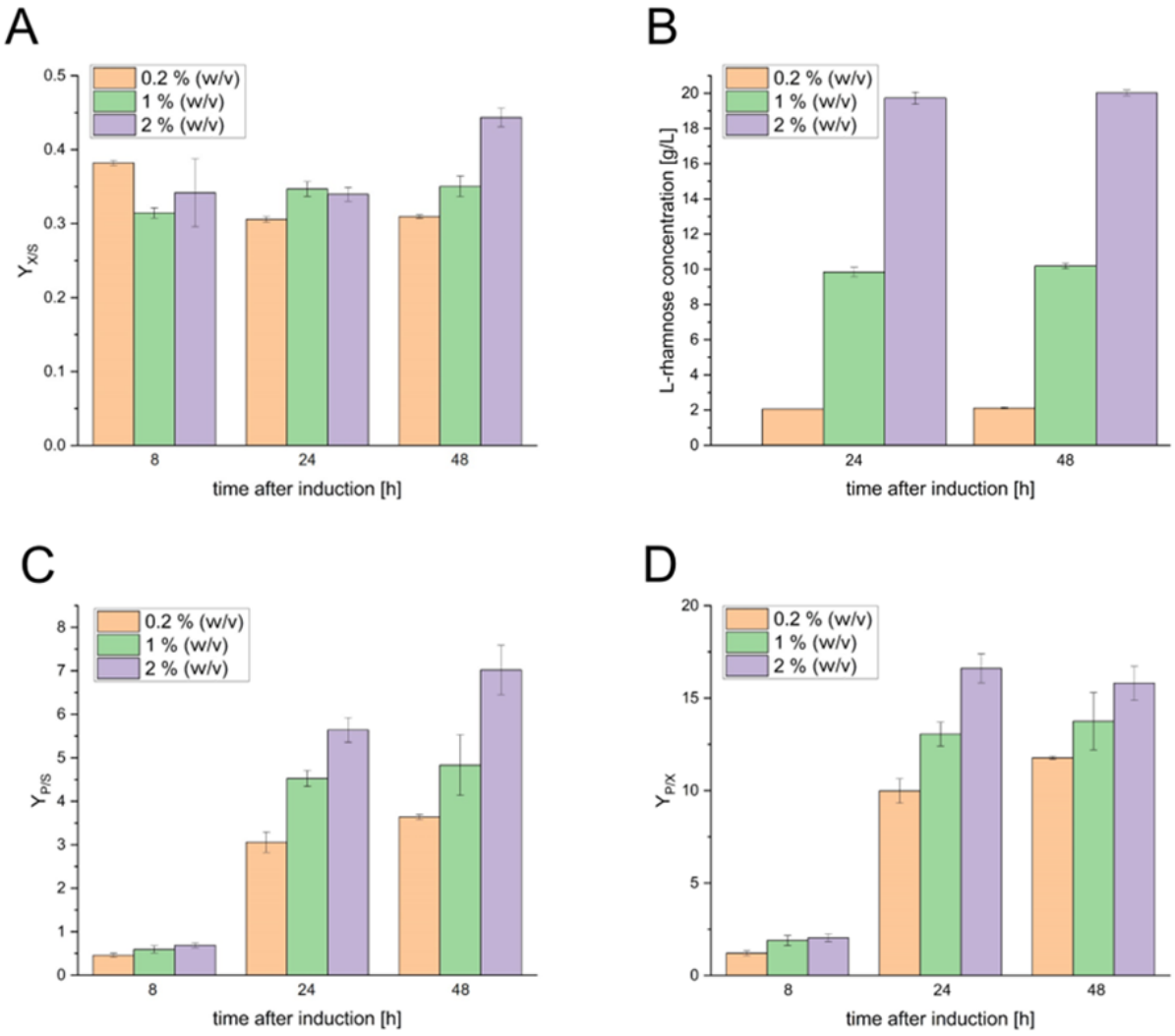

Fig. 31: (A) Biomass/substrate yield coefficients $Y_{X/S}$ of *C. necator* pKR-hum at different L-rhamnose inducer concentrations and times after induction in minimal media (n = 3); (B) Time dependence of L-rhamnose concentrations after induction of *C. necator* pKR-hum in minimal media (n = 3); (C) Product/substrate yield coefficients $Y_{P/S}$ of *C. necator* pKR-hum at different L-rhamnose inducer concentrations and times after induction in minimal media (n = 3); (D) Product/biomass yield coefficients $Y_{P/X}$ of *C. necator* pKR-hum at different L-rhamnose inducer concentrations and times after induction in minimal media (n = 3); all cells were cultivated at 180 rpm and 30 °C, induction at 0.2 - 0.3 g/L biomass.

To test α-humulene production influenced by the time of the L-rhamnose inducer addition, the established standard inducer concentration of 0.2 % (w/v) L-rhamnose was added at different cultivation times between 0 and 21 h after inoculating the main culture. This approach aimed to detect potential growth phase-dependent effects and product formation (Fig. 32 below).

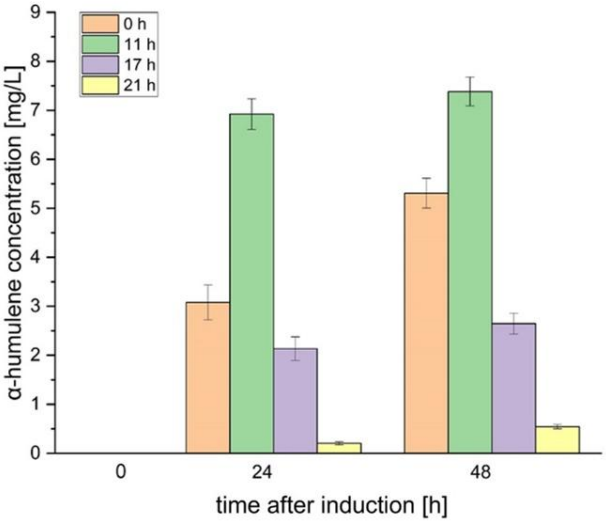

Fig. 32: α-Humulene levels according to different L-rhamnose induction times in minimal media, *C. necator* pKR-hum induced with 0.2 % (w/v) L-rhamnose at biomass 0.043 g/L (0 h), 0.25 g/L biomass (11 h), 0.90 g/L biomass (17 h) and 1.20 g/L biomass (21 h); at 180 rpm and 30 °C (n = 3).

Analysis of the induction time (Fig. 32) revealed that it affects α-humulene product levels. Notably, the addition of L-rhamnose at 0.25 g/L biomass during the exponential growth phase (at 11 h in this experiment - green bar) resulted in the highest α-humulene level among the times tested. The addition directly after the inoculation of the main culture (0 h) reduces the final α-humulene levels (11 h) after 24 and 48 h by 56 and 28 %, respectively. Induction during the early stationary phase (17 h) or the stationary phase (21 h) also led to low α-humulene levels.

7.7. Batch process with different cultivation temperature stages

In order to investigate a possible influence of the cultivation temperature on α-humulene levels, the formation of α-humulene by *C. necator* pKR-hum as a function of process temperature was investigated (Fig. 33). All cells were incubated at 30 °C with 180 rpm until induction in the range of 0.2 - 0.3 g/L biomass using 0.2 % (w/v) L-rhamnose. After the induction step, the cultivation temperature was either changed to 25 and 20 °C, or kept at 30 °C as the control. These temperatures were maintained until the experiment ended. The corresponding yield coefficients $Y_{P/S}$, $Y_{P/X}$ and $Y_{X/S}$ are shown below (Fig. 33 - A, B and C).

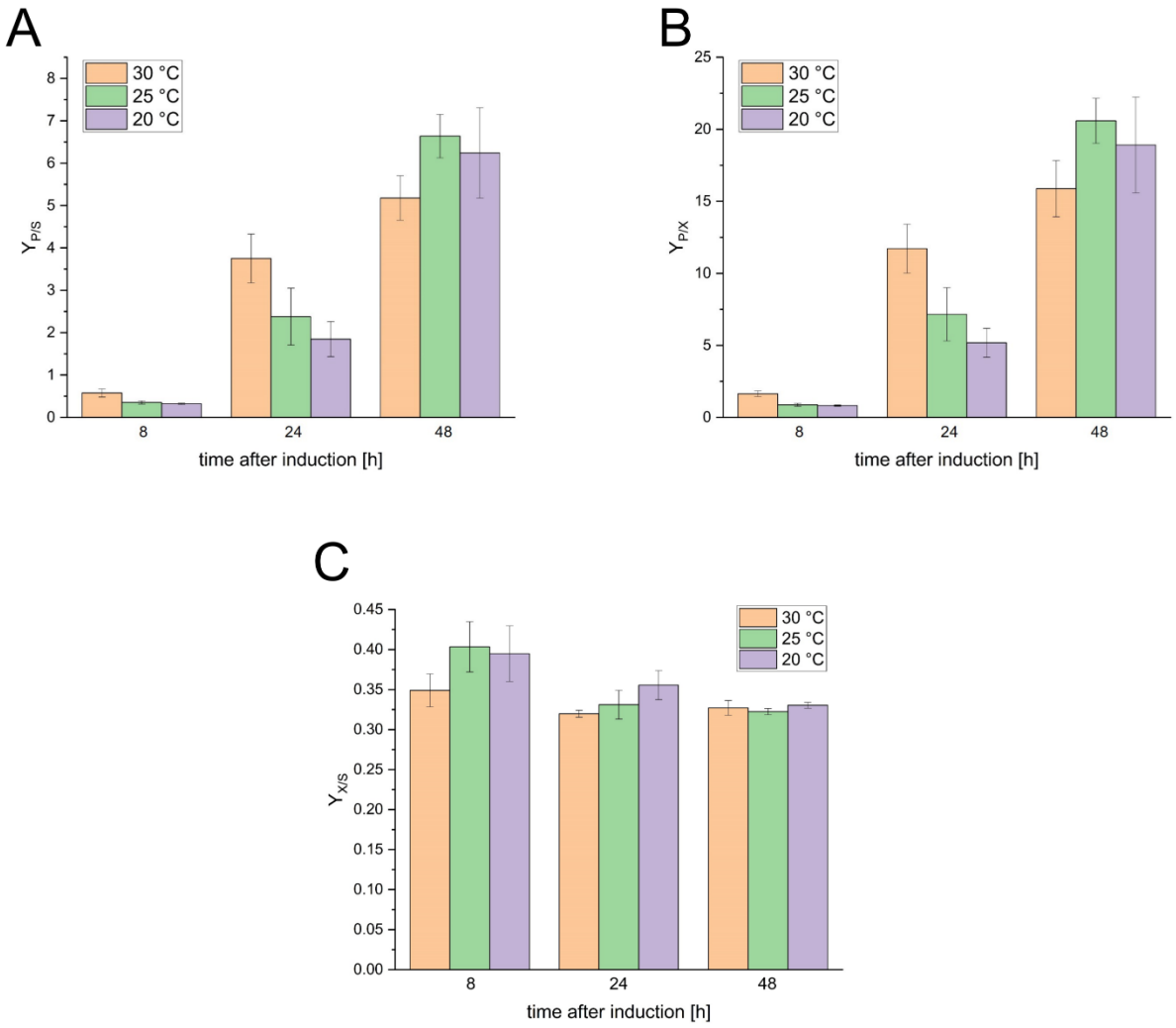

Fig. 33: (A) Product/substrate yield coefficients $Y_{P/S}$ of *C. necator* pKR-hum according to different cultivation temperatures and times after induction in minimal media (n = 3); (B) Product/biomass yield coefficients $Y_{P/X}$ of *C. necator* pKR-hum according to different cultivation temperatures and times after induction in minimal media (n = 3); (C) Biomass/substrate yield coefficients $Y_{X/S}$ of *C. necator* pKR-hum according to different cultivation temperatures and times after induction in minimal media (n = 3); all cells were cultivated at 180 rpm and 30 °C until induction at 0.2 - 0.3 g/L biomass range using 0.2 % (w/v) L-rhamnose and then switched to the corresponding cultivation temperature.

7.8. Combined optimization throughout the whole process vs. standard conditions

After optimizing several single steps throughout the production of α-humulene, the key question was how these combined effects would influence the overall process performance. The standard parameters were extended, based on the following insights. Minimal medium optimizations included (i) an increase of fructose from 4 to 8 g/L and (ii) the addition of 3.75 mg/L iron (II) sulfate heptahydrate. For induction step optimizations, (iii) the concentration of L-rhamnose was increased from 0.2 % to 2 % (w/v), and (iv) the cultivation temperature was reduced from 30 °C to 25 °C, starting 24 h after the induction step. The absolute α-humulene levels, related to the aqueous phase, were compared at 8, 24, and 48 h post-induction under standard and optimized conditions at 25 and 20 °C (Fig. 34).

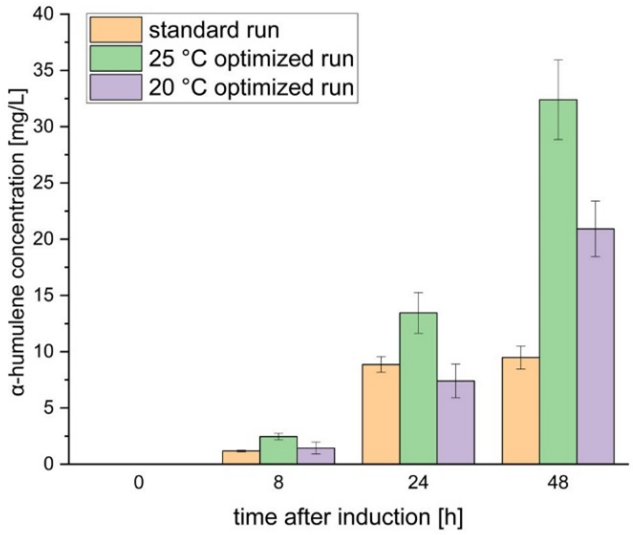

Fig. 34: α-Humulene levels according to standard and optimized conditions and temperatures; *C. necator* pKR-hum cultivated at 180 rpm and 30 °C, standard process induced with 0.2 % (w/v) L-rhamnose at 0.2 - 0.3 g/L biomass, optimized process induced with 2 % (w/v) L-rhamnose at 0.2 - 0.3 g/L biomass, and switched to 25 and 20 °C cultivation temperature 24 h after induction.

Fig. 34 illustrates that maintaining a continuous cultivation temperature of 30 °C, along with established standard parameters (standard run), results in considerably lower α-humulene levels compared to the optimized run at 25 °C, measured at 8, 24, and 48 h post-induction. In order to show a possible effect of the optimized process parameters on the cell growth behavior, *C. necator* pKR-hum cell growth was recorded under both established standard and optimized process conditions (see Fig. 35).

All cells were induced in the range of 0.20 - 0.35 g/L biomass with 0.2 % (w/v) L-rhamnose (established standard condition) or 2 % (w/v) L-rhamnose (optimized condition). For the optimized process, the cultivation temperature was lowered from 30 to 25 °C 24 h after induction. Induction time and the cultivation temperature switch are highlighted in green.

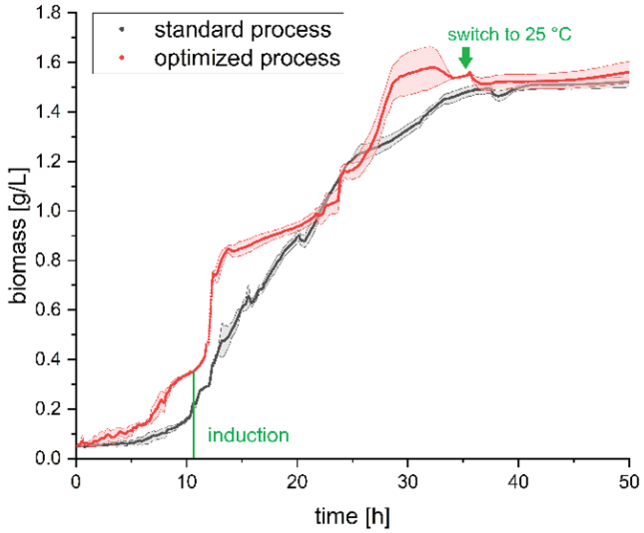

Fig. 35: Main culture growth in minimal medium according to standard and optimized process conditions, *C. necator* pKR-hum cultivated at 180 rpm and 30 °C; standard process induced with 0.2 % (w/v) L-rhamnose at 0.20 - 0.35 g/L biomass and left at 30 °C, optimized process induced with 2 % (w/v) L-rhamnose at 0.20 - 0.35 g/L biomass, and switched to 25 °C 24 h after induction (see green arrow).

Comparing the growth behavior of *C. necator* pKR-hum under established standard and optimized process conditions reveals similar final biomasses of 1.50 - 1.55 g/L, due to the parameter optimizations made or the division of the cultivation process into two temperature stages (Fig. 35). However, it is evident that the lag phase proceeds faster under the optimized process conditions (Fig. 35 - red curve).

8. Bibliography

[1] Pfeifer K, Ergal İ, Koller M, Basen M, Schuster B, Rittmann SK-MR. Archaea Biotechnology. Biotechnology Advances. 2021; 47:107668. doi:10.1016/j.biotechadv.2020.107668.

[2] Market Data Forecast ltd. Global Biotechnology Market Size, Share, Trends, COVID-19 Impact & Growth Analysis Report – Segmented By Technology, Application & Region (North America, Europe, APAC, Latin America, Middle East and Africa) – Industry Forecast (2024 to 2029). https://www.marketdataforecast.com/market-reports/global-biotechnology-market. Accessed Dec. 2, 2024.

[3] Lu J, Brigham CJ, Gai CS, Sinskey AJ. Studies on the production of branched-chain alcohols in engineered *Ralstonia eutropha*. Appl Microbiol Biotechnol. 2012; 96:283-97. doi:10.1007/s00253-012-4320-9.

[4] Kaki SB, Naga Prasad A, Chintagunta AD, Dirisala VR, Sampath Kumar NS, Naidu SJK, Ramesh B. Industrial Scale Production of Recombinant Human Insulin using *Escherichia coli* BL-21. Iran J Sci Technol Trans Sci. 2022; 46:373-83. doi:10.1007/s40995-022-01269-7.

[5] Krieg T, Sydow A, Faust S, Huth I, Holtmann D. CO_2 to Terpenes: Autotrophic and Electroautotrophic α-Humulene Production with *Cupriavidus necator*. Angewandte Chemie International Edition. 2018; 57:1879-82. doi:10.1002/anie.201711302.

[6] De Regil R, Sandoval G. Biocatalysis for biobased chemicals. Biomolecules. 2013; 3:812-47. doi:10.3390/biom3040812.

[7] Wang L, Luo H, Yao B, Yao J, Zhang J. Optimizing Hexose Utilization Pathways of *Cupriavidus necator* for Improving Growth and L-Alanine Production under Heterotrophic and Autotrophic Conditions. International Journal of Molecular Sciences. 2023; 25:548. doi:10.3390/ijms25010548.

[8] Sydow A, Becker L, Lombard E, Ulber R, Guillouet SE, Holtmann D. Autotrophic Production of the Sesquiterpene α-Humulene with *Cupriavidus necator* in a Controlled Bioreactor. Bioengineering. 2023; 10:1194. doi:10.3390/bioengineering10101194.

[9] Kumari S, Nasr M, Kumar S. Technological Advances in Biohydrogen Production from Microalgae. In: Algal biofuels: recent advances and future prospects; Gupta SK, Malik A, Bux F, editors. Springer, Cham. 2017; p. 347-360. doi:10.1007/978-3-319-51010-1_17.

[10] Barros A, Pereira H, Campos J, Marques A, Varela J, Silva J. Heterotrophy as a tool to overcome the long and costly autotrophic scale-up process for large scale production of microalgae. Sci Rep. 2019; 9:13935. doi:10.1038/s41598-019-50206-z.

[11] Vu DH, Mahboubi A, Root A, Heinmaa I, Taherzadeh MJ, Åkesson D. Thorough Investigation of the Effects of Cultivation Factors on Polyhydroalkanoates (PHAs) Production by *Cupriavidus necator* from Food Waste-Derived Volatile Fatty Acids. Fermentation. 2022; 8:605. doi:10.3390/fermentation8110605.

[12] Kamilah H, Al-Gheethi A, Yang TA, Sudesh K. The Use of Palm Oil-Based Waste Cooking Oil to Enhance the Production of Polyhydroxybutyrate [P(3HB)] by *Cupriavidus necator* H16 Strain. Arab J Sci Eng. 2018; 43:3453-63. doi:10.1007/s13369-018-3118-1.

[13] Langsdorf A, Drommershausen A-L, Volkmar M, Ulber R, Holtmann D. Fermentative α-Humulene Production from Homogenized Grass Clippings as a Growth Medium. Molecules. 2022; 27:8684. doi:10.3390/molecules27248684.

[14] Al-Ani S, Kim Y. Carbon preference by *Cupriavidus necator* for growth and accumulation phases: Heterotrophic vs. autotrophic metabolisms. Journal of Power Sources. 2025; 626:235797. doi:10.1016/j.jpowsour.2024.235797.

[15] Christianson DW. Structural and Chemical Biology of Terpenoid Cyclases. Chemical Reviews. 2017; 117:11570-648. doi:10.1021/acs.chemrev.7b00287.

[16] Shrivastava G, Ownley BH, Augé RM, Toler H, Dee M, Vu A, et al. Colonization by arbuscular mycorrhizal and endophytic fungi enhanced terpene production in tomato plants and their defense against a herbivorous insect. Symbiosis. 2015; 65:65-74. doi:10.1007/s13199-015-0319-1.

[17] Wilson EO, Regnier FE. The Evolution of the Alarm-Defense System in the Formicine Ants. The American Naturalist. 1971; 105:279-89. doi:10.1086/282724.

[18] Zhao R, Lu L, Shi Q, Chen J, He Y. Volatile Terpenes and Terpenoids from Workers and Queens of *Monomorium chinense* (Hymenoptera: Formicidae). Molecules. 2018; 23:2838. doi:10.3390/molecules23112838.

[19] Ashour M, Wink M, Gershenzon J. Chapter 5 - Biochemistry of Terpenoids: Monoterpenes, Sesquiterpenes and Diterpenes. In: Annual Plant Reviews Volume 40: Biochemistry of Plant Secondary Metabolism; 2nd edition, Wink M, editor. Wiley-Blackwell, Hoboken. 2010; p. 258-303. doi:10.1002/9781444320503.ch5.

[20] Huibin Z, Liu H, Aboulnaga E, Liu H, Cheng T, Xian M. Chapter 16 - Microbial Production of Isoprene: Opportunities and Challenges. In: Industrial Biotechnology; Wittmann C, Liao JC, editors. Wiley-VCH, Weinheim. 2016; p. 473-504. doi:10.1002/9783527807833.ch16.

[21] Withers ST, Keasling JD. Biosynthesis and engineering of isoprenoid small molecules. Appl Microbiol Biotechnol. 2007; 73:980-90. doi:10.1007/s00253-006-0593-1.

[22] Hartsel JA, Eades J, Hickory B, Makriyannis A. Chapter 53 - *Cannabis sativa* and Hemp. In: Nutraceuticals: Efficacy, safety and toxicity; Gupta RC, editor. Academic Press, San Diego. 2016; p. 735-754. doi:10.1016/B978-0-12-802147-7.00053-X.

[23] Behfar AA, Shushizadeh MR, Far MH, Shoar TS, Farasat M, Ghotrami ER. Gas Chromatography-mass Evaluation of Terpenoids from Persian Gulf *Padina tetrastromatica* sp. AJP. 2018; 12(4) S1515. doi:10.22377/ajp.v12i04.2957.

[24] National Center for Biotechnology Information. PubChem Compound Summary for CID 1195, Isopentenyl pyrophosphate. https://pubchem.ncbi.nlm.nih.gov/compound/Isopentenyl-pyrophosphate. Accessed Dec. 5, 2024.

[25] National Center for Biotechnology Information. PubChem Compound Summary for CID 647, Dimethylallyl diphosphate. https://pubchem.ncbi.nlm.nih.gov/compound/Dimethylallyl-diphosphate. Accessed Dec. 5, 2024.

[26] National Center for Biotechnology Information. PubChem Compound Summary for CID 6557, Isoprene. https://pubchem.ncbi.nlm.nih.gov/compound/Isoprene. Accessed Dec. 5, 2024.

[27] National Center for Biotechnology Information. PubChem Substance Record for SID 348291562, alpha-Humulene, Source: Human Metabolome Database (HMDB). https://pubchem.ncbi.nlm.nih.gov/substance/348291562. Accessed Dec. 5, 2024.

[28] Jang H-I, Rhee K-J, Eom Y-B. Antibacterial and antibiofilm effects of α-humulene against *Bacteroides fragilis*. Can J Microbiol. 2020; 66:389-99. doi:10.1139/cjm-2020-0004.

[29] Niknejad F, Mohammadi M, Khomeiri M, Razavi SH, Alami M. Antifungal and antioxidant effects of hops (*Humulus lupulus* L.) flower extracts. Advances in Environmental Biology. 2014; 395-402. https://www.cabidigitallibrary.org/doi/full/10.5555/20153262331. Accessed Dec. 6, 2024.

[30] Ninkuu V, Zhang L, Yan J, Fu Z, Yang T, Zeng H. Biochemistry of Terpenes and Recent Advances in Plant Protection. International Journal of Molecular Sciences. 2021; 22:5710. doi:10.3390/ijms22115710.

[31] Bouwmeester H, Schuurink RC, Bleeker PM, Schiestl F. The role of volatiles in plant communication. The Plant Journal. 2019; 100:892-907. doi:10.1111/tpj.14496.

[32] Eigenbrode SD, Trumble JT, Millar JG, White KK. Topical Toxicity of Tomato Sesquiterpenes to the Beet Armyworm and the Role of These Compounds in Resistance Derived from an Accession of *Lycopersicon hirsutum* f. *typicum*. J. Agric. Food Chem. 1994; 42:807-10. doi:10.1021/jf00039a042.

[33] Rutnik K, Ocvirk M, Košir IJ. Impact of Hop Freshness on Dry Hopped Beer Quality. Foods. 2022; 11:1310. doi:10.3390/foods11091310.

[34] Sommer S, Lang LM, Drummond L, Buchhaupt M, Fraatz MA, Zorn H. Odor characteristics of novel non-canonical terpenes. Molecules. 2022; 27(12) 3827. doi:10.3390/molecules27123827.

[35] Perini JA, Angeli-Gamba T, Alessandra-Perini J, Ferreira LC, Nasciutti LE, Machado DE. Topical application of Acheflan on rat skin injury accelerates wound healing: a histopathological, immunohistochemical and biochemical study. BMC Complement Altern Med. 2015; 15:203. doi:10.1186/s12906-015-0745-x.

[36] Sylvestre M, Pichette A, Longtin A, Nagau F, Legault J. Essential oil analysis and anticancer activity of leaf essential oil of *Croton flavens* L. from Guadeloupe. Journal of Ethnopharmacology. 2006; 103:99-102. doi:10.1016/j.jep.2005.07.011.

[37] Putra IMH, Pratama IPAAC, Putra KDA, Pradnyaswari GAD, Laksmiani NPL. The potency of alpha-humulene as HER-2 inhibitor by molecular docking. Pharmacy reports. 2022; 2:19. doi:10.51511/pr.19.

[38] De Lacerda Leite GM, De Oliveira Barbosa M, Lopes MJP, De Araújo Delmondes G, Bezerra DS, Araújo IM, et al. Pharmacological and toxicological activities of α-humulene and its isomers: A systematic review. Trends in Food Science & Technology. 2021; 115:255-74. doi:10.1016/j.tifs.2021.06.049.

[39] Fernandes ES, Passos GF, Medeiros R, Da Cunha FM, Ferreira J, Campos MM, et al. Anti-inflammatory effects of compounds alpha-humulene and (-)-trans-caryophyllene isolated from the essential oil of *Cordia verbenacea*. European Journal of Pharmacology. 2007; 569:228-36. doi:10.1016/j.ejphar.2007.04.059.

[40] Becker L, Holtmann D. Anti-inflammatory effects of α-humulene on the release of pro-inflammatory cytokines in lipopolysaccharide-induced THP-1 cells. Cell Biochem Biophys. 2024; 82:839-47. doi:10.1007/s12013-024-01235-7.

[41] Govindarajan M, Benelli G. α-Humulene and β-elemene from *Syzygium zeylanicum* (Myrtaceae) essential oil: highly effective and eco-friendly larvicides against *Anopheles subpictus*, *Aedes albopictus*, and *Culex tritaeniorhynchus* (Diptera: Culicidae). Parasitol Res. 2016; 115:2771-8. doi:10.1007/s00436-016-5025-2.

[42] Jeliazkova E, Zheljazkov VD, Kačániová M, Astatkie T, Tekwani BL. Sequential Elution of Essential Oil Constituents during Steam Distillation of Hops (*Humulus lupulus* L.) and Influence on Oil Yield and Antimicrobial Activity. Journal of oleo science. 2018; 67(7) 871-883. doi:10.5650/jos.ess17216.

[43] Wei M-C, Xiao J, Yang Y-C. Extraction of α-humulene-enriched oil from clove using ultrasound-assisted supercritical carbon dioxide extraction and studies of its fictitious solubility. Food Chemistry. 2016; 210:172-81. doi:10.1016/j.foodchem.2016.04.076.

[44] Zhang L, Yang H, Xia Y, Shen W, Liu L, Li Q, Chen X. Engineering the oleaginous yeast *Candida tropicalis* for α-humulene overproduction. Biotechnol Biofuels. 2022; 15:59. doi:10.1186/s13068-022-02160-8.

[45] Ingle KP, Deshmukh AG, Padole DA, Dudhare MS, Moharil MP, Khelurkar VC. Phytochemicals: Extraction methods, identification and detection of bioactive compounds from plant extracts. J Pharmacogn Phytochem. 2017; 6(1) 32-36. https://www.phytojournal.com/archives/2017/vol6issue1/PartA/6-1-23-924.pdf. Accessed Dec. 8, 2024.

[46] Abdollahi M, Sefidkon F, Calagari M, Mousavi A, Mahomoodally MF. Impact of four hemp (*Cannabis sativa* L.) varieties and stage of plant growth on yield and composition of essential oils. Industrial Crops and Products. 2020; 155:112793. doi:10.1016/j.indcrop.2020.112793.

[47] Ghasemy-Piranloo F, Kavousi F, Kazemi-Abharian M. Comparison for the production of essential oil by conventional, novel and biotechnology methods. Journal of Essential Oil Research. 2022; 34:455-78. doi:10.1080/10412905.2022.2120557.

[48] Orhan IE. Biotechnological Production of Plant Secondary Metabolites. Bentham Science Publishers, Sharjah. 2012; ISBN: 9781608051144.

[49] Hu T, Corey EJ. Short syntheses of (+/-)-delta-araneosene and humulene utilizing a combination of four-component assembly and palladium-mediated cyclization. Org Lett. 2002; 4:2441-3. doi:10.1021/ol026205p.

[50] Hatti-Kaul R, Törnvall U, Gustafsson L, Börjesson P. Industrial biotechnology for the production of bio-based chemicals - a cradle-to-grave perspective. Trends in Biotechnology. 2007; 25:119-24. doi:10.1016/j.tibtech.2007.01.001.

[51] Celińska E, Grajek W. Biotechnological production of 2,3-butanediol--current state and prospects. Biotechnology Advances. 2009; 27:715-25. doi:10.1016/j.biotechadv.2009.05.002.

[52] Parmaki S, Ferreira FC, Esteves T, Afonso CA, Koutinas M. Chapter 12 - Sustainable chemical and biological technologies for the production of enantiopure added-value molecules in biorefineries. In: Biomass, Biofuels, Biochemicals; Varjani S, Pandey A, Bhaskar T, Mohan SV, Tsang DC, editors. Elsevier, Amsterdam. 2022; p. 295-335. doi:10.1016/B978-0-323-89855-3.00006-6.

[53] Stoll IK, Boukis N, Neumann A, Ochsenreither K, Zevaco TA, Sauer J. The Complex Way to Sustainability: Petroleum-Based Processes versus Biosynthetic Pathways in the Formation of C4 Chemicals from Syngas. Ind. Eng. Chem. Res. 2019; 58:15863-71. doi:10.1021/acs.iecr.9b01123.

[54] Lykidis A, Pérez-Pantoja D, Ledger T, Mavromatis K, Anderson IJ, Ivanova NN, et al. The complete multipartite genome sequence of *Cupriavidus necator* JMP134, a versatile pollutant degrader. PLOS ONE. 2010; 5:e9729. doi:10.1371/journal.pone.0009729.

[55] Makkar NS, Casida LE. *Cupriavidus necator* gen. nov., sp. nov.; a Nonobligate Bacterial Predator of Bacteria in Soil. International Journal of Systematic Bacteriology. 1987; 37:323-6. doi:10.1099/00207713-37-4-323.

[56] Swain DM, Yadav SK, Tyagi I, Kumar R, Kumar R, Ghosh S, et al. A prophage tail-like protein is deployed by *Burkholderia* bacteria to feed on fungi. Nat Commun. 2017; 8:404. doi:10.1038/s41467-017-00529-0.

[57] Pfitzner J, Schlegel HG. Denitrifikation bei *Hydrogenomonas eutropha* Stamm H16. Archiv. Mikrobiol. 1973; 90:199-211. doi:10.1007/BF00424972.

[58] Jahn M, Crang N, Gynnå AH, Kabova D, Frielingsdorf S, Lenz O, et al. The energy metabolism of *Cupriavidus necator* in different trophic conditions. Applied and Environmental Microbiology. 2024; 90:e0074824. doi:10.1128/aem.00748-24.

[59] Wohlers H, Assil-Companioni L, Holtmann D. Chapter 11 *Cupriavidus necator* – a broadly applicable aerobic hydrogen-oxidizing bacterium. In: The Autotrophic Biorefinery: Raw Materials from Biotechnology; Kourist R, Schmidt S, editors. De Gruyter, Berlin. 2021; pp. 297-318. doi:10.1515/9783110550603-011.

[60] Jahn M, Crang N, Janasch M, Hober A, Forsström B, Kimler K, et al. Protein allocation and utilization in the versatile chemolithoautotroph *Cupriavidus necator*. Elife. 2021; 10 e69019. doi:10.7554/eLife.69019.

[61] Wixom RL, Sheng Y-B, Becker RS. Utilization of organic nitrogen compounds by *Hydrogenomonas eutropha*. Biotech & Bioengineering. 1972; 14:985-1006. doi:10.1002/bit.260140608.

[62] Verlinden RA, Hill DJ, Kenward MA, Williams CD, Piotrowska-Seget Z, Radecka IK. Production of polyhydroxyalkanoates from waste frying oil by *Cupriavidus necator*. AMB Expr. 2011; 1:11. doi:10.1186/2191-0855-1-11.

[63] Cavalheiro JM, Almeida MCM de, Grandfils C, Da Fonseca M. Poly(3-hydroxybutyrate) production by *Cupriavidus necator* using waste glycerol. Process Biochemistry. 2009; 44:509-15. doi:10.1016/j.procbio.2009.01.008.

[64] Amini M, Yousefi-Massumabad H, Younesi H, Abyar H, Bahramifar N. Production of the polyhydroxyalkanoate biopolymer by *Cupriavidus necator* using beer brewery wastewater containing maltose as a primary carbon source. Journal of Environmental Chemical Engineering. 2020; 8:103588. doi:10.1016/j.jece.2019.103588.

[65] Riedel SL, Jahns S, Koenig S, Bock MCE, Brigham CJ, Bader J, et al. Polyhydroxyalkanoates production with *Ralstonia eutropha* from low quality waste animal fats. Journal of Biotechnology. 2015; 214:119-27. doi:10.1016/j.jbiotec.2015.09.002.

[66] Taga N, Tanaka K, Ishizaki A. Effects of rheological change by addition of carboxymethylcellulose in culture media of an air-lift fermentor on poly-D-3-hydroxybutyric acid productivity in autotrophic culture of hydrogen-oxidizing bacterium, *Alcaligenes eutrophus*. Biotechnology and Bioengineering. 1997; 53:529-33. doi:10.1002/(SICI)1097-0290(19970305)53:5<529:AID-BIT11>3.0.CO;2-B.

[67] Marc J, Grousseau E, Lombard E, Sinskey AJ, Gorret N, Guillouet SE. Over expression of GroESL in *Cupriavidus necator* for heterotrophic and autotrophic isopropanol production. Metabolic Engineering. 2017; 42:74-84. doi:10.1016/j.ymben.2017.05.007.

[68] Crépin L, Lombard E, Guillouet SE. Metabolic engineering of *Cupriavidus necator* for heterotrophic and autotrophic alka(e)ne production. Metabolic Engineering. 2016; 37:92-101. doi:10.1016/j.ymben.2016.05.002.

[69] Milker S, Holtmann D. First time β-farnesene production by the versatile bacterium *Cupriavidus necator*. Microb Cell Fact. 2021; 20:89. doi:10.1186/s12934-021-01562-x.

[70] Milker S, Sydow A, Torres-Monroy I, Jach G, Faust F, Kranz L, et al. Gram-scale production of the sesquiterpene α-humulene with *Cupriavidus necator*. Biotechnology and Bioengineering. 2021; 118:2694-702. doi:10.1002/bit.27788.

[71] Raberg M, Voigt B, Hecker M, Steinbüchel A. A closer look on the polyhydroxybutyrate-(PHB-) negative phenotype of *Ralstonia eutropha* PHB-4. PLOS ONE. 2014; 9:e95907. doi:10.1371/journal.pone.0095907.

[72] Gomes D, Rodrigues LR, Rodrigues JL. Perspectives on the design of microbial cell factories to produce prenylflavonoids. International Journal of Food Microbiology. 2022; 367:109588. doi:10.1016/j.ijfoodmicro.2022.109588.

[73] Sonntag F, Kroner C, Lubuta P, Peyraud R, Horst A, Buchhaupt M, et al. Engineering *Methylobacterium extorquens* for de novo synthesis of the sesquiterpenoid α-humulene from methanol. Metabolic Engineering. 2015; 32:82-94. doi:10.1016/j.ymben.2015.09.004.

[74] Sydow A, Pannek A, Krieg T, Huth I, Guillouet SE, Holtmann D. Expanding the genetic tool box for *Cupriavidus necator* by a stabilized L-rhamnose inducible plasmid system. Journal of Biotechnology. 2017; 263:1-10. doi:10.1016/j.jbiotec.2017.10.002.

[75] Guo Q, Shi T-Q, Peng Q-Q, Sun X-M, Ji X-J, Huang H. Harnessing *Yarrowia lipolytica* Peroxisomes as a Subcellular Factory for α-Humulene Overproduction. J. Agric. Food Chem. 2021; 69:13831-7. doi:10.1021/acs.jafc.1c05897.

[76] Guo Q, Li Y-W, Yan F, Li K, Wang Y-T, Ye C, et al. Dual cytoplasmic-peroxisomal engineering for high-yield production of sesquiterpene α-humulene in *Yarrowia lipolytica*. Biotechnology and Bioengineering. 2022; 119:2819-30. doi:10.1002/bit.28176.

[77] Becker L, Dietz E, Holtmann D. Individual process steps optimization of *Cupriavidus necator*-catalyzed production of α-humulene. Biochemical Engineering Journal. 2024; 215:109617. doi:10.1016/j.bej.2024.109617.

[78] Panich J, Fong B, Singer SW. Metabolic Engineering of *Cupriavidus necator* H16 for Sustainable Biofuels from CO_2. Trends in Biotechnology. 2021; 39:412-24. doi:10.1016/j.tibtech.2021.01.001.

[79] Ronďošová S, Legerská B, Chmelová D, Ondrejovič M, Miertuš S. Optimization of Growth Conditions to Enhance PHA Production by *Cupriavidus necator*. Fermentation. 2022; 8:451. doi:10.3390/fermentation8090451.

[80] Aramvash A, Akbari Shahabi Z, Dashti Aghjeh S, Ghafari MD. Statistical physical and nutrient optimization of bioplastic polyhydroxybutyrate production by *Cupriavidus necator*. Int. J. Environ. Sci. Technol. 2015; 12:2307-16. doi:10.1007/s13762-015-0768-3.

[81] Sydow A, Krieg T, Ulber R, Holtmann D. Growth medium and electrolyte - How to combine the different requirements on the reaction solution in bioelectrochemical systems using *Cupriavidus necator*. Engineering in Life Sciences. 2017; 17(7) 781-791. doi:10.1002/elsc.201600252.

[82] Di Pasqua R, Betts G, Hoskins N, Edwards M, Ercolini D, Mauriello G. Membrane toxicity of antimicrobial compounds from essential oils. J. Agric. Food Chem. 2007; 55:4863-70. doi:10.1021/jf0636465.

[83] Sikkema J, Weber FJ, Heipieper HJ, Bont JAD. Cellular Toxicity of Lipophilic Compounds: Mechanisms, Implications, and Adaptations. Biocatalysis. 1994; 10:113-22. doi:10.3109/10242429409065221.

[84] Aguilar F, Scheper T, Beutel S. Improved Production and *In Situ* Recovery of Sesquiterpene (+)-Zizaene from Metabolically-Engineered *E. coli*. Molecules. 2019; 24:3356. doi:10.3390/molecules24183356.

[85] Woodley JM, Bisschops M, Straathof AJJ, Ottens M. Future directions for *in-situ* product removal (ISPR). J of Chemical Tech & Biotech. 2008; 83:121-3. doi:10.1002/jctb.1790.

[86] Hülsewede D, Meyer L-E, Von Langermann J. Application of *In Situ* Product Crystallization and Related Techniques in Biocatalytic Processes. Chemistry - A European Journal. 2019; 25:4871-84. doi:10.1002/chem.201804970.

[87] Schlegel HG, Lafferty R, Krauss I. The isolation of mutants not accumulating poly-beta-hydroxybutyric acid. Arch Mikrobiol. 1970; 71:283-94. doi:10.1007/BF00410161.

[88] Mifune J, Nakamura S, Fukui T. Targeted engineering of *Cupriavidus necator* chromosome for biosynthesis of poly(3-hydroxybutyrate-co-3-hydroxyhexanoate) from vegetable oil. Can. J. Chem. 2008; 86:621-7. doi:10.1139/v08-047.

[89] Roy S. Quality By design: A Holistic Concept of Building Quality in Pharmaceuticals. IJPBR. 2012; 3(2) 100-108. https://www.oalib.com/research/2733386. Accessed Dec. 12, 2024.

[90] Becker L, Sturm J, Eiden F, Holtmann D. Analyzing and understanding the robustness of bioprocesses. Trends in Biotechnology. 2023; 41:1013-26. doi:10.1016/j.tibtech.2023.03.002.

[91] Phulara SC, Chaturvedi P, Chaurasia D, Diwan B, Gupta P. Modulation of culture medium confers high-specificity production of isopentenol in *Bacillus subtilis*. Journal of Bioscience and Bioengineering. 2019; 127:458-64. doi:10.1016/j.jbiosc.2018.10.002.

[92] Shukla V, Phulara SC. Impact of culture condition modulation on the high-yield, high-specificity and cost-effective production of terpenoids from microbial sources: A review. Applied and Environmental Microbiology. 2021; 87(4) e02369-20. doi:10.1128/AEM.02369-20.

[93] Lambauer V, Kratzer R. Lab-Scale Cultivation of *Cupriavidus necator* on Explosive Gas Mixtures: Carbon Dioxide Fixation into Polyhydroxybutyrate. Bioengineering. 2022; 9:204. doi:10.3390/bioengineering9050204.

[94] Schaible UE, Kaufmann SHE. Iron and microbial infection. Nat Rev Microbiol. 2004; 2:946-53. doi:10.1038/nrmicro1046.

[95] Ribeiro VT, Asevedo EA, De Paiva Vasconcelos LTC, Filho MAO, De Araújo JS, De Macedo GR, et al. Evaluation of induction conditions for plasmid pQE-30 stability and 503 antigen of *Leishmania i. chagasi* expression in *E. coli* M15. Appl Microbiol Biotechnol. 2019; 103:6495-504. doi:10.1007/s00253-019-09948-z.

[96] Egan SM, Schleif RF. A regulatory cascade in the induction of rhaBAD. Journal of Molecular Biology. 1993; 234:87-98. doi:10.1006/jmbi.1993.1565.

[97] Aboutaleb AM, Bian L, Elwany A, Shamsaei N, Thompson SM, Tapia G. Accelerated process optimization for laser-based additive manufacturing by leveraging similar prior studies. IISE Transactions. 2017; 49:31-44. doi:10.1080/0740817X.2016.1189629.

[98] Eriksson L, Johansson E, Kettaneh-Wold N, Wikström C, Wold S. Design of experiments Principles and Applications. Umetrics Academy, Malmö. 2008; pp. 7-16. ISBN 91-973730-0-1

[99] Mandenius C-F, Brundin A. Bioprocess optimization using design-of-experiments methodology. Biotechnology Progress. 2008; 24:1191-203. doi:10.1002/btpr.67.

[100] Soravia S, Orth A. Design of Experiments. In: Ullmann's Encyclopedia of Industrial Chemistry. Wiley-VCH, Weinheim. 2009; ISBN 9783527306732. doi:10.1002/14356007.e08_e01.pub3.

[101] Beg S, Swain S, Rahman M, Hasnain MS, Imam SS. Chapter 3 - Application of Design of Experiments (DoE) in Pharmaceutical Product and Process Optimization. In: Pharmaceutical quality by design: Principles and applications; Beg S, Hasnain MS, editors. Academic Press, San Diego. 2019; p. 43-64. doi:10.1016/B978-0-12-815799-2.00003-4.

[102] Brade H, Opal SM, Vogel SN, Morrison DC, editors. Endotoxin in Health and Disease. Marcel Dekker, New York. 1999; p. 950. ISBN 0824719441.

[103] Amor K, Heinrichs DE, Frirdich E, Ziebell K, Johnson RP, Whitfield C. Distribution of core oligosaccharide types in lipopolysaccharides from *Escherichia coli*. Infect Immun. 2000; 68:1116-24. doi:10.1128/IAI.68.3.1116-1124.2000.

[104] Haase H, Ober-Blöbaum JL, Engelhardt G, Hebel S, Heit A, Heine H, et al. Zinc signals are essential for lipopolysaccharide-induced signal transduction in monocytes. J Immunol. 2008; 181:6491-502. doi:10.4049/jimmunol.181.9.6491.

[105] Grace-Lynn C, Darah I, Chen Y, Latha LY, Jothy SL, Sasidharan S. *In vitro* antioxidant activity potential of lantadene A, a pentacyclic triterpenoid of Lantana plants. Molecules. 2012; 17:11185-98. doi:10.3390/molecules170911185.

[106] Ishii Y, Wang Y, Haziot A, Del Vecchio PJ, Goyert SM, Malik AB. Lipopolysaccharide binding protein and CD14 interaction induces tumor necrosis factor-alpha generation and neutrophil sequestration in lungs after intratracheal endotoxin. Circ Res. 1993; 73:15-23. doi:10.1161/01.res.73.1.15.

[107] Gioannini TL, Teghanemt A, Zhang D, Coussens NP, Dockstader W, Ramaswamy S, Weiss JP. Isolation of an endotoxin-MD-2 complex that produces Toll-like receptor 4-dependent cell activation at picomolar concentrations. Proceedings of the National Academy of Sciences of the United States of America. 2004; 101:4186-91. doi:10.1073/pnas.0306906101.

[108] Hayden MS, West AP, Ghosh S. NF-kappaB and the immune response. Oncogene. 2006; 25:6758-80. doi:10.1038/sj.onc.1209943.

[109] Carmody RJ, Chen YH. Nuclear factor-kappaB: Activation and regulation during toll-like receptor signaling. Cell. Mol. Immunol. 2007; 4 31-41. https://www.cmi.ustc.edu.cn/4/1/31.pdf. Accessed Dec. 15, 2024.

[110] Blackwell TS, Christman JW. The role of nuclear factor-kappa B in cytokine gene regulation. Am J Respir Cell Mol Biol. 1997; 17:3-9. doi:10.1165/ajrcmb.17.1.f132.

[111] Bagheri B, Sohrabi B, Movassaghpour AA, Mashayekhi S, Garjani A, Shokri M, et al. Hydrocortisone reduces Toll-like receptor 4 expression on peripheral CD14+ monocytes in patients undergoing percutaneous coronary intervention. Iranian Biomedical Journal. 2014; 18:76-81. doi:10.6091/ibj.1275.2013.

[112] De Bosscher K, Vanden Berghe W, Haegeman G. The interplay between the glucocorticoid receptor and nuclear factor-kappaB or activator protein-1: molecular mechanisms for gene repression. Endocr Rev. 2003; 24:488-522. doi:10.1210/er.2002-0006.

[113] Mozo L, Suárez A, Gutiérrez C. Glucocorticoids up-regulate constitutive interleukin-10 production by human monocytes. Clinical and experimental allergy: journal of the British Society for Allergy and Clinical Immunology. 2004; 34:406-12. doi:10.1111/j.1365-2222.2004.01824.x.

[114] Dandona P, Aljada A, Garg R, Mohanty P. Increase in plasma interleukin-10 following hydrocortisone injection. J Clin Endocrinol Metab. 1999; 84:1141-4. doi:10.1210/jcem.84.3.5656.

[115] Rao NAS, McCalman MT, Moulos P, Françoijs K-J, Chatziioannou A, Kolisis FN, et al. Coactivation of GR and NFKB alters the repertoire of their binding sites and target genes. Genome Research. 2011; 21(9) 1404-1416. doi:10.1101/gr.118042.110.

[116] Steer JH, Vuong Q, Joyce DA. Suppression of human monocyte tumour necrosis factor-alpha release by glucocorticoid therapy: relationship to systemic monocytopaenia and cortisol suppression. British Journal of Clinical Pharmacology. 1997; 43:383-9. doi:10.1046/j.1365-2125.1997.00586.x.

[117] Aljada A, Ghanim H, Assian E, Mohanty P, Hamouda W, Garg R, et al. Increased IkappaB expression and diminished nuclear NF-kappaB in human mononuclear cells following hydrocortisone injection. J Clin Endocrinol Metab. 1999; 84:3386-9. doi:10.1210/jcem.84.9.6104.

[118] Deroo BJ, Archer TK. Glucocorticoid receptor activation of the I kappa B alpha promoter within chromatin. Mol Biol Cell. 2001; 12:3365-74. doi:10.1091/mbc.12.11.3365.

[119] Leis H, Page A, Ramírez A, Bravo A, Segrelles C, Paramio J, et al. Glucocorticoid Receptor Counteracts Tumorigenic Activity of Akt in Skin through Interference with the Phosphatidylinositol 3-Kinase Signaling Pathway. Mol Endocrinol. 2004; 18:303-11. doi:10.1210/me.2003-0350.

[120] Jain H, Dhingra N, Narsinghani T, Sharma R. Insights into the mechanism of natural terpenoids as NF-κB inhibitors: an overview on their anticancer potential. Experimental oncology. 2016; 38:158-68. https://pubmed.ncbi.nlm.nih.gov/27685522/. Accessed Dec. 17, 2024.

[121] Zhou JY, Tang FD, Mao GG, Bian RL. Effect of alpha-pinene on nuclear translocation of NF-kappa B in THP-1 cells. Acta Pharmacol. Sin. 2004; 25 480-484. http://www.chinaphar.com/article/view/8075/8649. Accessed Dec. 17, 2024.

[122] Ichikawa H, Nair MS, Takada Y, Sheeja DBA, Kumar MAS, Oommen OV, et al. Isodeoxyelephantopin, a novel sesquiterpene lactone, potentiates apoptosis, inhibits invasion, and abolishes osteoclastogenesis through suppression of nuclear factor-kappaB (nf-kappaB) activation and nf-kappaB-regulated gene expression. Clin Cancer Res. 2006; 12:5910-8. doi:10.1158/1078-0432.CCR-06-0916.

[123] Chanput W, Mes JJ, Wichers HJ. THP-1 cell line: an *in vitro* cell model for immune modulation approach. International Immunopharmacology. 2014; 23:37-45. doi:10.1016/j.intimp.2014.08.002.

[124] Kim YK, Hwang JH, Lee HT. Differential susceptibility to lipopolysaccharide affects the activation of toll-like-receptor 4 signaling in THP-1 cells and PMA-differentiated THP-1 cells. Innate Immun. 2022; 28:122-9. doi:10.1177/17534259221100170.

[125] Alagesan S, Minton NP, Malys N. 13C-assisted metabolic flux analysis to investigate heterotrophic and mixotrophic metabolism in *Cupriavidus necator* H16. Metabolomics. 2018; 14:9. doi:10.1007/s11306-017-1302-z.

[126] Almaguer C, Schönberger C, Gastl M, Arendt EK, Becker T. *Humulus lupulus* - a story that begs to be told. A review. J. Inst. Brew. 2014; 120(4) 289-314. doi:10.1002/jib.160.

[127] Legault J, Pichette A. Potentiating effect of beta-caryophyllene on anticancer activity of alpha-humulene, isocaryophyllene and paclitaxel. J Pharm Pharmacol. 2007; 59:1643-7. doi:10.1211/jpp.59.12.0005.

[128] Bocquet L, Rivière C, Dermont C, Samaillie J, Hilbert J-L, Halama P, et al. Antifungal activity of hop extracts and compounds against the wheat pathogen *Zymoseptoria tritici*. Industrial Crops and Products. 2018; 122:290-7. doi:10.1016/j.indcrop.2018.05.061.

[129] Dietz C, Cook D, Huismann M, Wilson C, Ford R. The multisensory perception of hop essential oil: a review. Journal of the Institute of Brewing. 2020; 126:320-42. doi:10.1002/jib.622.

[130] Sköld M, Karlberg A-T, Matura M, Börje A. The fragrance chemical beta-caryophyllene-air oxidation and skin sensitization. Food and Chemical Toxicology. 2006; 44:538-45. doi:10.1016/j.fct.2005.08.028.

[131] Thiry M, Cingolani D. Optimizing scale-up fermentation processes. Trends in Biotechnology. 2002; 20:103-5. doi:10.1016/S0167-7799(02)01913-3.

[132] Nadal-Rey G, McClure DD, Kavanagh JM, Cornelissen S, Fletcher DF, Gernaey KV. Understanding gradients in industrial bioreactors. Biotechnology Advances. 2021; 46:107660. doi:10.1016/j.biotechadv.2020.107660.

[133] Wang Z, Pan H, Ni S, Li Z, Lian J. Establishing CRISPRi for Programmable Gene Repression and Genome Evolution in *Cupriavidus necator*. ACS Synthetic Biology. 2024; 13:851-61. doi:10.1021/acssynbio.3c00664.

[134] Calvey CH, Sànchez i Nogué V, White AM, Kneucker CM, Woodworth SP, Alt HM, et al. Improving growth of *Cupriavidus necator* H16 on formate using adaptive laboratory evolution-informed engineering. Metabolic Engineering. 2023; 75:78-90. doi:10.1016/j.ymben.2022.10.016.

[135] Hilfinger A, Paulsson J. Separating intrinsic from extrinsic fluctuations in dynamic biological systems. Proc Natl Acad Sci USA. 2011; 108:12167-72. doi:10.1073/pnas.1018832108.

[136] Mohd Zahari MAK, Ariffin H, Mokhtar MN, Salihon J, Shirai Y, Hassan MA. Factors affecting poly(3-hydroxybutyrate) production from oil palm frond juice by *Cupriavidus necator* (CCUG52238(T)). J Biomed Biotechnol. 2012; 2012:125865. doi:10.1155/2012/125865.

[137] Singh V, Haque S, Niwas R, Srivastava A, Pasupuleti M, Tripathi CKM. Strategies for Fermentation Medium Optimization: An In-Depth Review. Front. Microbiol. 2016; 7:2087. doi:10.3389/fmicb.2016.02087.

[138] Haaland PD. Experimental design in biotechnology. CRC Press, Boca Raton. 2020; Chapter 5. doi:10.1201/9781003065968. ISBN 978-0824778811.

[139] Triaux Z, Petitjean H, Marchioni E, Boltoeva M, Marcic C. Deep eutectic solvent-based headspace single-drop microextraction for the quantification of terpenes in spices. Anal Bioanal Chem. 2020; 412:933-48. doi:10.1007/s00216-019-02317-9.

[140] Manurung R, Siregar AGA. Performance of menthol based deep eutectic solvents in the extraction of carotenoids from crude palm oil. Int. J. Geomate. 2020; 19, 131-137. https://geomatejournal.com/geomate/article/download/1860/1715. Accessed Dec. 18, 2024.

[141] Sun Y, Liu Z, Wang J, Yang S, Li B, Xu N. Aqueous ionic liquid based ultrasonic assisted extraction of four acetophenones from the Chinese medicinal plant *Cynanchum bungei* Decne. Ultrasonics Sonochemistry. 2013; 20:180-6. doi:10.1016/j.ultsonch.2012.07.002.

[142] De Brabander P, Uitterhaegen E, Verhoeven E, Vander Cruyssen C, De Winter K, Soetaert W. *In Situ* Product Recovery of Bio-Based Industrial Platform Chemicals: A Guideline to Solvent Selection. Fermentation. 2021; 7:26. doi:10.3390/fermentation7010026.

[143] Lima PSS, Lucchese AM, Araújo-Filho HG, Menezes PP, Araújo AAS, Quintans-Júnior LJ, et al. Inclusion of terpenes in cyclodextrins: Preparation, characterization and pharmacological approaches. Carbohydrate Polymers. 2016; 151:965-87. doi:10.1016/j.carbpol.2016.06.040.

[144] Laane C, Boeren S, Vos K. On optimizing organic solvents in multi-liquid-phase biocatalysis. Trends in Biotechnology. 1985; 251-2. doi:10.1016/0167-7799(85)90023-X.

[145] Reslow M, Adlercreutz P, Mattiasson B. Organic solvents for bioorganic synthesis. Appl Microbiol Biotechnol. 1987; 26:1-8. doi:10.1007/BF00282141.

[146] Bruce LJ, Daugulis AJ. Solvent selection strategies for extractive biocatalysis. Biotechnology Progress. 1991; 7:116-24. doi:10.1021/bp00008a006.

[147] Inoue A, Horikoshi K. Estimation of solvent-tolerance of bacteria by the solvent parameter log P. Journal of Fermentation and Bioengineering. 1991; 71:194-6. doi:10.1016/0922-338X(91)90109-T.

[148] Kollerup F, Daugulis AJ. Ethanol production by extractive fermentation – solvent identification and prototype development. Can J Chem Eng. 1986; 64:598-606. doi:10.1002/cjce.5450640410.

[149] Brennan TCR, Turner CD, Krömer JO, Nielsen LK. Alleviating monoterpene toxicity using a two-phase extractive fermentation for the bioproduction of jet fuel mixtures in *Saccharomyces cerevisiae*. Biotechnology and Bioengineering. 2012; 109:2513-22. doi:10.1002/bit.24536.

[150] Cheng T, Zhao Y, Li X, Lin F, Xu Y, Zhang X, et al. Computation of octanol - water partition coefficients by guiding an additive model with knowledge. Journal of chemical information and modeling. 2007; 47.6 2140-2148. doi:10.1021/ci700257y.

[151] Kim S, Chen J, Cheng T, Gindulyte A, He J, He S, et al. PubChem 2023 update. Nucleic Acids Res. 2023; 51(D1) D1373-D1380. doi:10.1093/nar/gkac956.

[152] Nicola L, Bååth E. The effect of temperature and moisture on lag phase length of bacterial growth in soil after substrate addition. Soil Biology and Biochemistry. 2019; 137:107563. doi:10.1016/j.soilbio.2019.107563.

[153] Gasser B, Saloheimo M, Rinas U, Dragosits M, Rodríguez-Carmona E, Baumann K, et al. Protein folding and conformational stress in microbial cells producing recombinant proteins: a host comparative overview. Microb Cell Fact. 2008; 7:11. doi:10.1186/1475-2859-7-11.

[154] Bakkali F, Averbeck S, Averbeck D, Idaomar M. Biological effects of essential oils - a review. Food and Chemical Toxicology. 2008; 46:446-75. doi:10.1016/j.fct.2007.09.106.

[155] Ascrizzi R, Iannone M, Cinque G, Marianelli A, Pistelli L, Flamini G. “Hemping” the drinks: Aromatizing alcoholic beverages with a blend of *Cannabis sativa* L. flowers. Food Chemistry. 2020; 325:126909. doi:10.1016/j.foodchem.2020.126909.

[156] Jiang H, Wang X. Biosynthesis of monoterpenoid and sesquiterpenoid as natural flavors and fragrances. Biotechnology Advances. 2023; 65:108151. doi:10.1016/j.biotechadv.2023.108151.

[157] Rogerio AP, Andrade EL, Leite DFP, Figueiredo CP, Calixto JB. Preventive and therapeutic anti-inflammatory properties of the sesquiterpene alpha-humulene in experimental airways allergic inflammation. British Journal of Pharmacology. 2009; 158:1074-87. doi:10.1111/j.1476-5381.2009.00177.x.

[158] Azubuike CC, Edwards MG, Gatehouse AMR, Howard TP. Applying Statistical Design of Experiments to Understanding the Effect of Growth Medium Components on *Cupriavidus necator* H16 Growth. Appl Environ Microbiol. 2020; 86(17) e00705-20. doi:10.1128/AEM.00705-20.

[159] Boy C, Lesage J, Alfenore S, Gorret N, Guillouet SE. Plasmid expression level heterogeneity monitoring via heterologous eGFP production at the single-cell level in *Cupriavidus necator*. Applied Microbiology and Biotechnology. 2020; 104 5899-5914. doi:10.1007/s00253-020-10616-w.

[160] Janasch M, Crang N, Asplund-Samuelsson J, Sporre E, Bruch M, Gynnå A, et al. Thermodynamic limitations of PHB production from formate and fructose in *Cupriavidus necator*. Metabolic Engineering. 2022; 73:256-69. doi:10.1016/j.ymben.2022.08.005.

[161] Goddeeris C, Cuppo F, Reynaers H, Bouwman WG, Van den Mooter G. Light scattering measurements on microemulsions: estimation of droplet sizes. International Journal of Pharmaceutics. 2006; 312:187-95. doi:10.1016/j.ijpharm.2006.01.037.

[162] Kaplan J. Mechanisms of cellular iron acquisition: another iron in the fire. Cell. 2002; 111:603-6. doi:10.1016/S0092-8674(02)01164-9.

[163] Li C, Zhu L, Pan D, Li S, Xiao H, Zhang Z, et al. Siderophore-Mediated Iron Acquisition Enhances Resistance to Oxidative and Aromatic Compound Stress in *Cupriavidus necator* JMP134. Appl Environ Microbiol. 2019; 85(1) e01938-18. doi:10.1128/AEM.01938-18.

[164] Tindale AE, Mehrotra M, Ottem D, Page WJ. Dual regulation of catecholate siderophore biosynthesis in *Azotobacter vinelandii* by iron and oxidative stress. Microbiology. 2000; 146(7) 1617-1626. doi:10.1099/00221287-146-7-1617.

[165] Weinberg ED. Iron and susceptibility to infectious disease. Science. 1974; 184:952-6. doi:10.1126/science.184.4140.952.

[166] Sivashanmugam A, Murray V, Cui C, Zhang Y, Wang J, Li Q. Practical protocols for production of very high yields of recombinant proteins using *Escherichia coli*. Protein Science. 2009; 18:936-48. doi:10.1002/pro.102.

[167] Strocchi M, Ferrer M, Timmis KN, Golyshin PN. Low temperature-induced systems failure in *Escherichia coli*: insights from rescue by cold-adapted chaperones. PROTEOMICS. 2006; 6:193-206. doi:10.1002/pmic.200500031.

[168] Hartwig S, Frister T, Alemdar S, Li Z, Scheper T, Beutel S. SUMO-fusion, purification, and characterization of a (+)-zizaene synthase from *Chrysopogon zizanioides*. Biochemical and Biophysical Research Communications. 2015; 458:883-9. doi:10.1016/j.bbrc.2015.02.053.

[169] Passanha P, Esteves SR, Kedia G, Dinsdale RM, Guwy AJ. Increasing polyhydroxyalkanoate (PHA) yields from *Cupriavidus necator* by using filtered digestate liquors. Bioresource Technology. 2013; 147:345-52. doi:10.1016/j.biortech.2013.08.050.

[170] Jirovetz L, Bail S, Buchbauer G, Denkova Z, Slavchev A, Stoyanova A, et al. Antimicrobial testings, gas chromatographic analysis and olfactory evaluation of an essential oil of hop cones (*Humulus lupulus* L.) from Bavaria and some of its main compounds. Sci Pharm. 2006; 74:189-201. doi:10.3797/scipharm.2006.74.189.

[171] Chen H, Yuan J, Hao J, Wen Y, Lv Y, Chen L, et al. α-Humulene inhibits hepatocellular carcinoma cell proliferation and induces apoptosis through the inhibition of Akt signaling. Food Chem Toxicol. 2019; 134:110830. doi:10.1016/j.fct.2019.110830.

[172] Olsson L, Rugbjerg P, Torello Pianale L, Trivellin C. Robustness: linking strain design to viable bioprocesses. Trends in Biotechnology. 2022; 40:918-31. doi:10.1016/j.tibtech.2022.01.004.

[173] Gong Z, Nielsen J, Zhou YJ. Engineering Robustness of Microbial Cell Factories. Biotechnology Journal. 2017; 12:1700014. doi:10.1002/biot.201700014.

[174] Trivellin C, Olsson L, Rugbjerg P. Quantification of Microbial Robustness in Yeast. ACS synthetic biology. 2022; 11:1686-91. doi:10.1021/acssynbio.1c00615.

[175] Torello Pianale L, Caputo F, Olsson L. Four ways of implementing robustness quantification in strain characterisation. Biotechnol Biofuels. 2023; 16:195. doi:10.1186/s13068-023-02445-6.

[176] Rao CV, Wolf DM, Arkin AP. Control, exploitation and tolerance of intracellular noise. Nature. 2002; 420:231-7. doi:10.1038/nature01258.

[177] Hoang MD, Riessner S, Oropeza Vargas JE, Von den Eichen N, Heins AL. Influence of varying pre-culture conditions on the level of population heterogeneity in batch cultures with an *Escherichia coli* triple reporter strain. Microorganisms. 2023; 11(7) 1763. doi:10.3390/microorganisms11071763.

[178] Ishii N, Nakahigashi K, Baba T, Robert M, Soga T, Kanai A, et al. Multiple high-throughput analyses monitor the response of *E. coli* to perturbations. Science. 2007; 316(5824) 593-597. doi:10.1126/science.1132067.

[179] Parker DJ, Demetci P, Li GW. Rapid accumulation of motility-activating mutations in resting liquid culture of *Escherichia coli*. Journal of Bacteriology. 2019; 201(19) 10-1128. doi:10.1128/jb.00259-19.

[180] Netea MG, Balkwill F, Chonchol M, Cominelli F, Donath MY, Giamarellos-Bourboulis EJ, et al. A guiding map for inflammation. Nat Immunol. 2017; 18:8 826-831. doi:10.1038/ni.3790.

[181] Peesa JP, Yalavarthi PR, Rasheed A, Mandava VBR. A perspective review on role of novel NSAID prodrugs in the management of acute inflammation. Journal of Acute Disease. 2016; 5:364-381. doi:10.1016/j.joad.2016.08.002.

[182] Lee H-M, Kim J-J, Kim HJ, Shong M, Ku BJ, Jo E-K. Upregulated NLRP3 inflammasome activation in patients with type 2 diabetes. Diabetes. 2013; 62:194-204. doi:10.2337/db12-0420.

[183] Zabłocka A, Kazana W, Sochocka M, Stańczykiewicz B, Janusz M, Leszek J, et al. Inverse Correlation Between Alzheimer's Disease and Cancer: Short Overview. Mol Neurobiol. 2021; 58:6 335-349. doi:10.1007/s12035-021-02544-1.

[184] Furman D, Campisi J, Verdin E, Carrera-Bastos P, Targ S, Franceschi C, et al. Chronic inflammation in the etiology of disease across the life span. Nat Med. 2019; 25:1822-32. doi:10.1038/s41591-019-0675-0.

[185] Roth GA, Abate D, Abate KH, Abay SM, Abbafati C, Abbasi N, et al. Global, regional, and national age-sex-specific mortality for 282 causes of death in 195 countries and territories, 1980-2017: a systematic analysis for the Global Burden of Disease Study 2017. The Lancet. 2018; 392:1736-88. doi:10.1016/S0140-6736(18)32203-7.

[186] Rainsford KD. Anti-Inflammatory Drugs in the 21st Century. In: Inflammation in the Pathogenesis of Chronic Diseases: The COX-2 Controversy; Harris RE, editor. Springer, Dordrecht. 2007; p. 3-27. doi:10.1007/1-4020-5688-5_1.

[187] Aoki T, Narumiya S. Prostaglandins and chronic inflammation. Trends Pharmacol Sci. 2012; 33:304-11. doi:10.1016/j.tips.2012.02.004.

[188] Babu V, Kapkoti DS, Binwal M, Bhakuni RS, Shanker K, Singh M, et al. Liquiritigenin, isoliquiritigenin rich extract of *glycyrrhiza glabra* roots attenuates inflammation in macrophages and collagen-induced arthritis in rats. Inflammopharmacol. 2023; 31:983-96. doi:10.1007/s10787-023-01152-w.

[189] Pandur E, Balatinácz A, Micalizzi G, Mondello L, Horváth A, Sipos K, et al. Anti-inflammatory effect of lavender (*Lavandula angustifolia* Mill.) essential oil prepared during different plant phenophases on THP-1 macrophages. BMC Complement Med Ther. 2021; 21:287. doi:10.1186/s12906-021-03461-5.

[190] Yadav N, Chandra H. Suppression of inflammatory and infection responses in lung macrophages by eucalyptus oil and its constituent 1,8-cineole: Role of pattern recognition receptors TREM-1 and NLRP3, the MAP kinase regulator MKP-1, and NFκB. PLOS ONE. 2017; 12:e0188232. doi:10.1371/journal.pone.0188232.

[191] Horváth G, Horváth A, Reichert G, Böszörményi A, Sipos K, Pandur E. Three chemotypes of thyme (*Thymus vulgaris* L.) essential oil and their main compounds affect differently the IL-6 and TNFα cytokine secretions of BV-2 microglia by modulating the NF-κB and C/EBPβ signalling pathways. BMC Complement Med Ther. 2021; 21:148. doi:10.1186/s12906-021-03319-w.

[192] Poltorak A, Smirnova I, He X, Liu MY, Van Huffel C, McNally O, et al. Genetic and physical mapping of the Lps locus: identification of the toll-4 receptor as a candidate gene in the critical region. Blood Cells, Molecules, and Diseases. 1998; 24:340-55. doi:10.1006/bcmd.1998.0201.

[193] Ntourtoglou G, Tsapou EA, Drosou F, Bozinou E, Lalas S, Tataridis P, et al. Pulsed Electric Field Extraction of α and β-Acids From Pellets of *Humulus lupulus* (Hop). Front. Bioeng. Biotechnol. 2020; 8:297. doi:10.3389/fbioe.2020.00297.

[194] Rettberg N, Biendl M, Garbe L-A. Hop Aroma and Hoppy Beer Flavor: Chemical Backgrounds and Analytical Tools - A Review. Journal of the American Society of Brewing Chemists. 2018; 76:1-20. doi:10.1080/03610470.2017.1402574.

[195] Amira SW, Mohammed MR, Zlatko M, Melissa J, Mahmoud AE. Antifungal Activity of the Volatiles of High Potency *Cannabis sativa* L. Against *Cryptococcus neoformans*. Records of Natural Products. 2015; 10:214-20. https://acgpubs.org/RNP/2016/Volume10/Issue%201/26-RNP-EO_1407-035.pdf. Accessed Dec. 27, 2024.

[196] Coté H, Boucher M-A, Pichette A, Legault J. Anti-inflammatory, antioxidant, antibiotic, and cytotoxic activities of *Tanacetum vulgare* L. essential oil and its constituents. Medicines. 2017; 4(2) 34. doi:10.3390/medicines4020034.

[197] Murao S, Gemmell MA, Callaham MF, Anderson NL, Huberman E. Control of macrophage cell differentiation in human promyelocytic HL-60 leukemia cells by 1,25-dihydroxyvitamin D3 and phorbol-12-myristate-13-acetate. Cancer research. 1983; 43:4989-96. https://aacrjournals.org/cancerres/article/43/10/4989/487047. Accessed Dec. 28, 2024.

[198] Traore K, Trush MA, George M, Spannhake EW, Anderson W, Asseffa A. Signal transduction of phorbol 12-myristate 13-acetate (PMA)-induced growth inhibition of human monocytic leukemia THP-1 cells is reactive oxygen dependent. Leukemia Research. 2005; 29:863-79. doi:10.1016/j.leukres.2004.12.011.

[199] Schwende H, Fitzke E, Ambs P, Dieter P. Differences in the state of differentiation of THP-1 cells induced by phorbol ester and 1,25-dihydroxyvitamin D3. J Leukoc Biol. 1996; 59:555-61. doi:10.1002/jlb.59.4.555.

[200] Sharif O, Bolshakov VN, Raines S, Newham P, Perkins ND. Transcriptional profiling of the LPS induced NF-kappaB response in macrophages. BMC Immunol. 2007; 8:1. doi:10.1186/1471-2172-8-1.

[201] Gioannini TL, Weiss JP. Regulation of interactions of Gram-negative bacterial endotoxins with mammalian cells. Immunol Res. 2007; 39:249-60. doi:10.1007/s12026-007-0069-0.

[202] Kim SJ, Kim HM. Dynamic lipopolysaccharide transfer cascade to TLR4/MD2 complex via LBP and CD14. BMB Reports. 2017; 50:55-7. doi:10.5483/BMBRep.2017.50.2.011.

[203] Ruud TE, Gundersen Y, Krohn CD, Sveen O, Aasen AO. Effects of infliximab and hydrocortisone on *in vitro* cytokine responses after stimulation with lipopolysaccharide. Surg Infect. 2013; 14:30-4. doi:10.1089/sur.2011.093.

[204] Scheinman RI, Cogswell PC, Lofquist AK, Baldwin AS. Role of transcriptional activation of I kappa B alpha in mediation of immunosuppression by glucocorticoids. Science. 1995; 270:283-6. doi:10.1126/science.270.5234.283.

[205] Medeiros R, Passos GF, Vitor CE, Koepp J, Mazzuco TL, Pianowski LF, et al. Effect of two active compounds obtained from the essential oil of *Cordia verbenacea* on the acute inflammatory responses elicited by LPS in the rat paw. British Journal of Pharmacology. 2007; 151:618-27. doi:10.1038/sj.bjp.0707270.

[206] Yeo D, Hwang S-J, Song Y-S, Lee H-J. Humulene Inhibits Acute Gastric Mucosal Injury by Enhancing Mucosal Integrity. Antioxidants. 2021; 10:761. doi:10.3390/antiox10050761.

[207] Zhou L, Tan A, Iasvovskaia S, Li J, Lin A, Hershenson MB. Ras and mitogen-activated protein kinase kinase kinase-1 coregulate activator protein-1- and nuclear factor-kappaB-mediated gene expression in airway epithelial cells. Am J Respir Cell Mol Biol. 2003; 28:762-9. doi:10.1165/rcmb.2002-0261OC.

[208] Chun H-W, Kim S-J, Pham T-H, Bak Y, Oh J, Ryu H-W, et al. Epimagnolin A inhibits IL-6 production by inhibiting p38/NF-κB and AP-1 signaling pathways in PMA-stimulated THP-1 cells. Environmental Toxicology. 2019; 34:796-803. doi:10.1002/tox.22746.

[209] Mommert S, Hüer M, Schaper-Gerhardt K, Gutzmer R, Werfel T. Histamine up-regulates oncostatin M expression in human M1 macrophages. British Journal of Pharmacology. 2020; 177:600-13. doi:10.1111/bph.14796.

[210] Wang P, Zhu F, Konstantopoulos K. Prostaglandin E2 induces interleukin-6 expression in human chondrocytes via cAMP/protein kinase A- and phosphatidylinositol 3-kinase-dependent NF-kappaB activation. American journal of physiology - cell physiology. 2010; 298:C1445-56. doi:10.1152/ajpcell.00508.2009.

[211] Tsuge K, Inazumi T, Shimamoto A, Sugimoto Y. Molecular mechanisms underlying prostaglandin E2-exacerbated inflammation and immune diseases. Int Immunol. 2019; 31:597-606. doi:10.1093/intimm/dxz021.

[212] Kim M-J, Yun J-M. Molecular Mechanism of the Protective Effect of Zerumbone on Lipopolysaccharide-Induced Inflammation of THP-1 Cell-Derived Macrophages. J Med Food. 2019; 22:62-73. doi:10.1089/jmf.2018.4253.

[213] Li J, Wu W, Yang F, Liu L, Wang S-P, Jiao W-H, et al. Popolohuanones G - I, Dimeric Sesquiterpene Quinones with IL-6 Inhibitory Activity from the Marine Sponge *Dactylospongia elegans*. Chemistry & Biodiversity. 2018; 15:e1800078. doi:10.1002/cbdv.201800078.

[214] Saklani A, Hegde B, Mishra P, Singh R, Mendon M, Chakrabarty D, et al. NF-κB dependent anti-inflammatory activity of chlorojanerin isolated from *Saussurea heteromalla*. Phytomedicine. 2012; 19:988-97. doi:10.1016/j.phymed.2012.05.016.

[215] Ahn J-H, Song E-J, Jung D-H, Kim Y-J, Seo I-S, Park S-C, et al. The sesquiterpene lactone estafiatin exerts anti-inflammatory effects on macrophages and protects mice from sepsis induced by LPS and cecal ligation puncture. Phytomedicine. 2022; 99:153934. doi:10.1016/j.phymed.2022.153934.

[216] Pries R, Jeschke S, Leichtle A, Bruchhage K-L. Modes of Action of 1,8-Cineol in Infections and Inflammation. Metabolites. 2023; 13:751. doi:10.3390/metabo13060751.

[217] Juergens UR, Engelen T, Racké K, Stöber M, Gillissen A, Vetter H. Inhibitory activity of 1,8-cineol (eucalyptol) on cytokine production in cultured human lymphocytes and monocytes. Pulmonary Pharmacology & Therapeutics. 2004; 17:281-7. doi:10.1016/j.pupt.2004.06.002.

[218] Yoon W-J, Lee NH, Hyun C-G. Limonene suppresses lipopolysaccharide-induced production of nitric oxide, prostaglandin E2, and pro-inflammatory cytokines in RAW 264.7 macrophages. Journal of Oleo Science. 2010; 59:415-21. doi:10.5650/jos.59.415.

[219] Arranz E, Jaime L, La Lopez de Hazas MC, Vicente G, Reglero G, Santoyo S. Supercritical sage extracts as anti-inflammatory food ingredients. Industrial Crops and Products. 2014; 54:159-66. doi:10.1016/j.indcrop.2014.01.021.

[220] Da Silva SL, Figueiredo PM, Yano T. Cytotoxic evaluation of essential oil from *Zanthoxylum rhoifolium* Lam. leaves. Acta Amaz. 2007; 37:281-6. doi:10.1590/S0044-59672007000200015.

[221] Wewers MD, Dare HA, Winnard AV, Parker JM, Miller DK. IL-1 beta-converting enzyme (ICE) is present and functional in human alveolar macrophages: macrophage IL-1 beta release limitation is ICE independent. J Immunol. 1997; 159:5964-72. doi:10.4049/jimmunol.159.12.5964.

[222] Caicedo MS, Desai R, McAllister K, Reddy A, Jacobs JJ, Hallab NJ. Soluble and particulate Co-Cr-Mo alloy implant metals activate the inflammasome danger signaling pathway in human macrophages: a novel mechanism for implant debris reactivity. Journal of Orthopaedic Research. 2009; 27:847-54. doi:10.1002/jor.20826.

[223] Ferrari D, Chiozzi P, Falzoni S, Dal Susino M, Melchiorri L, Baricordi OR, et al. Extracellular ATP triggers IL-1 beta release by activating the purinergic P2Z receptor of human macrophages. J Immunol. 1997; 159:1451-8. doi:10.4049/jimmunol.159.3.1451.

[224] Drutskaya MS, Nosenko MA, Atretkhany K-SN, Efimov GA, Nedospasov SA. Interleukin-6: From molecular mechanisms of signal transduction to physiological properties and therapeutic targeting. Mol Biol. 2015; 49:837-42. doi:10.1134/S0026893315060060.

[225] Sabaka P, Koščálová A, Straka I, Hodosy J, Lipták R, Kmotorková B, et al. Role of interleukin 6 as a predictive factor for a severe course of Covid-19: retrospective data analysis of patients from a long-term care facility during Covid-19 outbreak. BMC Infectious Diseases. 2021; 21:308. doi:10.1186/s12879-021-05945-8.

[226] Ma Y, Ren Y, Dai Z-J, Wu C-J, Ji Y-H, Xu J. IL-6, IL-8 and TNF-α levels correlate with disease stage in breast cancer patients. Advances in Clinical and Experimental Medicine. 2017; 26:421-6. doi:10.17219/acem/62120.

[227] Tsai M-S, Chen W-C, Lu C-H, Chen M-F. The prognosis of head and neck squamous cell carcinoma related to immunosuppressive tumor microenvironment regulated by IL-6 signaling. Oral Oncology. 2019; 91:47-55. doi:10.1016/j.oraloncology.2019.02.027.

[228] Weber R, Groth C, Lasser S, Arkhypov I, Petrova V, Altevogt P, et al. IL-6 as a major regulator of MDSC activity and possible target for cancer immunotherapy. Cellular Immunology. 2021; 359:104254. doi:10.1016/j.cellimm.2020.104254.

[229] Qin L, Ma D, Lin G, Sun W, Li C. Low temperature promotes the production and efflux of terpenoids in yeast. Bioresource Technology. 2024; 395:130376. doi:10.1016/j.biortech.2024.130376.

[230] Phulara SC, Chaurasia D, Diwan B, Chaturvedi P, Gupta P. *In-situ* isopentenol production from *Bacillus subtilis* through genetic and culture condition modulation. Process Biochemistry. 2018; 72:47-54. doi:10.1016/j.procbio.2018.06.019.

[231] Wright LP, Rohwer JM, Ghirardo A, Hammerbacher A, Ortiz-Alcaide M, Raguschke B, et al. Deoxyxylulose 5-Phosphate Synthase Controls Flux through the Methylerythritol 4-Phosphate Pathway in Arabidopsis. Plant Physiol. 2014; 165:1488-504. doi:10.1104/pp.114.245191.

[232] Zhou K, Zou R, Stephanopoulos G, Too H-P. Enhancing solubility of deoxyxylulose phosphate pathway enzymes for microbial isoprenoid production. Microb Cell Fact. 2012; 11:148. doi:10.1186/1475-2859-11-148.

[233] Kim S-W, Kim J-B, Jung W-H, Kim J-H, Jung J-K. Over-production of beta-carotene from metabolically engineered *Escherichia coli*. Biotechnol Lett. 2006; 28:897–904. doi:10.1007/s10529-006-9023-9.

[234] Lee PC, Mijts BN, Schmidt-Dannert C. Investigation of factors influencing production of the monocyclic carotenoid torulene in metabolically engineered *Escherichia coli*. Appl Microbiol Biotechnol. 2004; 65:538-46. doi:10.1007/s00253-004-1619-1.

[235] Kim S-W, Kim J-B, Ryu J-M, Jung J-K, Kim J-H. High-level production of lycopene in metabolically engineered *E. coli*. Process Biochemistry. 2009; 44:899–905. doi:10.1016/j.procbio.2009.04.018.

[236] Roche B, Aussel L, Ezraty B, Mandin P, Py B, Barras F. Reprint of: Iron/sulfur proteins biogenesis in prokaryotes: formation, regulation and diversity. Biochim Biophys Acta. 2013; 1827:923-37. doi:10.1016/j.bbabio.2013.05.001.

[237] Kirby J, Dietzel KL, Wichmann G, Chan R, Antipov E, Moss N, et al. Engineering a functional 1-deoxy-D-xylulose 5-phosphate (DXP) pathway in *Saccharomyces cerevisiae*. Metabolic Engineering. 2016; 38:494-503. doi:10.1016/j.ymben.2016.10.017.

[238] Kim NM, Peng D, Sandoval NR. Nucleotide-level characterization and improvement of l-arabinose- and l-rhamnose-inducible systems in *E. coli* using a high-throughput approach. Nucleic Acids Res. 2025; 53.7. doi:10.1093/nar/gkaf224.

[239] Zhang C, Seow VY, Chen X, Too H-P. Multidimensional heuristic process for high-yield production of astaxanthin and fragrance molecules in *Escherichia coli*. Nat Commun. 2018; 9:1858. doi:10.1038/s41467-018-04211-x.

[240] Yang J, Nie Q, Ren M, Feng H, Jiang X, Zheng Y, et al. Metabolic engineering of *Escherichia coli* for the biosynthesis of alpha-pinene. Biotechnol Biofuels. 2013; 6:60. doi:10.1186/1754-6834-6-60.

[241] Kitano H. Biological robustness. Nat Rev Genet. 2004; 5:826-37. doi:10.1038/nrg1471.

[242] Zhou Y, Han L-R, He H-W, Sang B, Yu D-L, Feng J-T, et al. Effects of agitation, aeration and temperature on production of a novel glycoprotein GP-1 by *Streptomyces kanasenisi* ZX01 and scale-up based on volumetric oxygen transfer coefficient. Molecules. 2018; 23.1.125. doi:10.3390/molecules23010125.

[243] Elahi S, Tsuchiaka S, Mizutani T, Fujikawa H. Characteristics of Staphylococcal Enterotoxin A Production and Growth of *Staphylococcus aureus* in Shaking and Stationary Cultures. Biocontrol Sci. 2018; 23:207-14. doi:10.4265/bio.23.207.

[244] Chung C-F, Lin S-C, Juang T-Y, Liu Y-C. Shaking Rate during Production Affects the Activity of *Escherichia coli* Surface-Displayed *Candida antarctica* Lipase A. Catalysts. 2020; 10:382. doi:10.3390/catal10040382.

[245] Reinecke F, Steinbüchel A. *Ralstonia eutropha* strain H16 as model organism for PHA metabolism and for biotechnological production of technically interesting biopolymers. Journal of Molecular Microbiology and Biotechnology. 2009; 16:91-108. doi:10.1159/000142897.

[246] Pohlmann A, Fricke WF, Reinecke F, Kusian B, Liesegang H, Cramm R, et al. Genome sequence of the bioplastic-producing "Knallgas" bacterium *Ralstonia eutropha* H16. Nat Biotechnol. 2006; 24:1257-62. doi:10.1038/nbt1244.

[247] Li T-Y, Liang W-L, Zhao Y-M, Chen W-D, Zhu H-X, Duan Y-Y, et al. Alpha-Pinene-encapsulated lipid nanoparticles diminished inflammatory responses in THP-1 cells and imiquimod-induced psoriasis-like skin injury and splenomegaly in mice. Front. Immunol. 2024; 15:1390589. doi:10.3389/fimmu.2024.1390589.

[248] Rabe P, Schmitz T, Dickschat JS. Mechanistic investigations on six bacterial terpene cyclases. Beilstein J. Org. Chem. 2016; 12:1839-50. doi:10.3762/bjoc.12.173.

[249] Tsigoriyna L, Sango C, Batovska D. An update on microbial biosynthesis of β-caryophyllene, a sesquiterpene with multi-pharmacological properties. Fermentation. 2024; 10.1.60. doi:10.3390/fermentation10010060.

[250] Meigs TE, Sherwood SW, Simoni RD. Farnesyl acetate, a derivative of an isoprenoid of the mevalonate pathway, inhibits DNA replication in hamster and human cells. Experimental cell research. 1995; 219.2.461-470. doi:10.1006/excr.1995.1253.

[251] Bosshart H, Heinzelmann M. THP-1 cells as a model for human monocytes. Annals of translational medicine. 2016; 4.21.438. doi:10.21037/atm.2016.08.53.

9. Declaration

I declare that I have completed this dissertation single-handedly without the unauthorized help of a second party and only with the assistance acknowledged therein. I have appropriately acknowledged and cited all text passages that are derived verbatim from or are based on the content of published work of others, and all information relating to verbal communications. I consent to the use of an anti-plagiarism software to check my thesis. I have abided by the principles of good scientific conduct laid down in the regulations of the leading University which were delivered to me in carrying out the investigations described in the dissertation.

Signature:

_____

Lucas Ernst Becker

Date:

_____